

EVALUATION OF THE IMPACTS OF HURRICANE HUGO
ON THE LAND COVER OF FRANCIS MARION NATIONAL
FOREST, SOUTH CAROLINA USING REMOTE SENSING

A Thesis

Submitted to the Graduate Faculty of the
Louisiana State University and
Agricultural and Mechanical College
in partial fulfillment of the
requirements for the degree of
Master of Science

in
The Department of Geography and Anthropology

By
Amit Kulkarni
B.E., University of Pune, 1997
December, 2004

DEDICATION

This thesis is dedicated to my father, and my three grandparents who have all passed into the great void or whatever place you choose to believe. I would have loved to do this while they were here. I am sure all of them would have been proud, but extremely surprised that I came this far.

ACKNOWLEDGMENTS

First, I would like to thank my advisor, Dr. Nina Lam, for her tremendous breadth of knowledge, focus, and for her unstinting support throughout my life here at LSU. She was extremely tolerant of my idiosyncrasies and always found a way to work around them despite her hectic schedule. I will fall sick if I work at her pace, I wonder how she manages to keep her cool juggling so many things. I would also like to thank her for getting the necessary funds from NASA, for the purchase of the Landsat TM satellite images and the reference aerial photographs used in this study. I would like to thank Mr. DeWitt Braud for his sage advice in the processing of the images, his tolerance when I asked newbie questions, and gently guiding me onto the right path. I thank Dr. Michael Leitner for helping me with the GPS portion of the thesis, teaching me cartography, and a few soccer tricks.

I would like to thank the Department of Geography and Anthropology, Louisiana State University for awarding me the 2004 Richard J. Russell field research grant to help fund a field trip to the Francis Marion National Forest, SC. The images and photos were acquired through a NASA Intelligent Systems research grant (NAS-2-37143) to Drs. Charles Emerson, Dale Quattrochi, and Nina Lam.

I would like to thank Umit Cicekli for introducing me to soccer by dragging me to the Edward Gay field on Saturdays, and for the importance of keeping at least the kitchen area clean. For my soccer buddies Suat Namli, Petrica Trifas, Atanas Atanasov, Jeffrey Handel, Oskar Arrequi, Michael Durham, Sameer Raina, and countless others for their patience and for spending quality time on developing my non-existent soccer skills. It is

unfortunate that soccer is also the reason why I got a broken ankle. Even though it is a major source of injuries I still feel is a good sport for getting fit quickly.

I cannot forget my classmate, Srinivas Vinnakota and the gang at Room 70 and 121 for providing me free home cooked food during the hectic period when I was trying to write my thesis, and when I was laid up with a broken ankle. Srinivas also helped by prodding me to finish the thesis and in lending me with books, and in general saving me some money. To classmate, Lawrence Kiage for some soccer tips and hammering of basic facts at the right time. Thanks also to Guiyun Zhou, for providing help with ICAMS, and for letting me borrow his vast collection of fractal related papers. Brian Allen and Derrick Angelloz for some interesting conversations.

A special thanks for Manuel “Manny” Casarez for teaching me a lot about American culture and music. In addition, for trying to teach me the Southern and Californian accents, and overall help in improving my pronunciation. Thanks also for Dilip Bhagwani, who has been an excellent friend. I would like to thank these friends Deepak Rawat, Ajay Phatak (now sadly deceased), Nilesh Vinzanekar, Malory D’Costa, Vishal Nikalje, Prasad Sardeshpande, Anant Kantak, Vivek Misar, Sandeep Sathe, Rajesh Kothari, Shubhanan Bhagwat, Bipin Sawant, and others for their help with free food, easy money, careless advice, and loose morals (at least when some of them were single).

Last but not the least, my younger brother, Ashish, who is a certified genius, for grasping and explaining computing concepts elegantly, when most boys his age have just started reading dime novels. Our analytical skills were honed at these discussions, and permanently helped bury our squabbling. I admire my mother, Vaishali, who is financially independent, for teaching me some commercial skills; and who generously

offers me money and advice whenever I call her, which is rarely. My maternal aunt, Shirish, whose meteoric rise in the dog eat dog world of Corporate India makes me enormously proud. I have learned a lot from all of my grandparents whose support had carried me through my formative years, and especially to my maternal grandmother after all of the other three grandparents have journeyed into the great void.

TABLE OF CONTENTS

DEDICATION.....	ii
ACKNOWLEDGEMENTS	iii
LIST OF TABLES	viii
LIST OF FIGURES	ix
ABSTRACT.....	xii
CHAPTER 1: INTRODUCTION.....	1
1.1 Objectives and Hypothesis.....	3
CHAPTER 2: LITERATURE REVIEW.....	5
2.1 Problems in Change Detection	6
2.2 Land Use, Land Cover and Some Problems	7
2.3 Review of Change Detection Methods	8
2.3.1 Data Preparation, Transformation, and Multiple Image Integration.....	8
2.3.2 Change Detection Analysis.....	10
2.3.2.1 Principal Component Analysis	13
2.3.2.2 Tasseled Cap Transformation	14
2.3.2.3 Fractal Methods	16
2.3.2.4 Post-Classification Comparison.....	20
2.3.3 Accuracy Assessment of Classification.....	21
2.4 Importance of Coastal Wetland Forests.....	24
CHAPTER 3: DATA SOURCES AND METHODOLOGY.....	29
3.1 Data Sources and Software	29
3.1.1 Landsat TM Images	29
3.1.2 Aerial Photography	29
3.1.3 National Land Cover Data: South Carolina.....	30
3.1.4 GPS Points Survey.....	31
3.1.5 Software Used in Study	31
3.2 Study Area	32
3.3 Methodology.....	33
3.3.1 Preparation of Images	33
3.3.2 Hybrid Image Classification and Change Detection.....	40
3.3.3 Digitization of Aerial Photographs	43
3.3.4 Accuracy Assessment of Classification.....	44
3.3.5 Field Trip: GPS Points Collection Procedure and Interviews	46
3.3.6 PCA Change Detection Procedure.....	47
3.3.7 TCT Change Detection Procedure.....	48
3.3.8 Fractal Change Detection Procedure	48

CHAPTER 4: RESULTS AND DISCUSSION	50
4.1 Accuracy Assessment of Classification.....	50
4.1.1 Results for Individual Land Cover Classes.....	50
4.1.2 Results for Errors of Commission (User’s Accuracy) and Omission (Producer’s Accuracy)	57
4.1.3 Kappa Analysis Results	58
4.2 Change Detection Through Classification.....	58
4.3 GPS Point Survey Results.....	62
4.4 Change Detection Using PCA	62
4.5 Change Detection Using TCT.....	66
4.6 Change Detection Using the Local TPSA Fractal Method.....	75
4.6.1 Choice of Moving Window Size.....	76
4.6.2 Analysis for the 1987 and 1989 NDVI Images.....	81
4.6.3 Analysis for the 1987 Local TPSA Image	82
4.6.3.1 Road Network	82
4.6.3.2 Wambaw Swamp	83
4.6.3.3 Little Wambaw Wilderness and Coffee Creek Swamp	83
4.6.3.4 Woody Wetland Patch	84
4.6.3.5 Cultivated Row Crops.....	84
4.6.4 Analysis for 1989 Local TPSA Image.....	84
4.6.4.1 Road Network	85
4.6.4.2 Wambaw Swamp	85
4.6.4.3 Little Wambaw Wilderness and Coffee Creek Swamp	85
4.6.4.4 Woody Wetland Patch	86
4.6.4.5 Cultivated Row Crops.....	86
4.6.5 Change Detection of Local TPSA Image.....	86
4.6.6 Zonal Statistics for Correlation of Classified Land Cover Areas to <i>D</i> Values.....	87
 CHAPTER 5: CONCLUSION.....	 90
 REFERENCES.....	 93
 APPENDIX A: LOCAL FRACTAL OUTPUT FOR DIFFERENT MW SIZES... 	 101
 APPENDIX B : TABLES USED FOR TASSELED CAP TRANSFORM	 111
 APPENDIX C : TASSELED CAP TRANSFORM EQUATIONS.....	 114
 VITA	 115

LIST OF TABLES

Table 1: Possible outcomes of a change detection study	11
Table 2: Wetland functions and associated socioeconomic benefits in the coastal wetlands of Norfolk and Suffolk Broads in eastern UK	28
Table 3: Band statistics for Landsat study area subset for 1987	38
Table 4: Band statistics for Landsat study area subset for 1989	38
Table 5: Classification scheme	42
Table 6: 1987 Classification statistics	54
Table 7: 1989 Classification statistics	54
Table 8: Classified area of land cover classes for 1987 and 1989	55
Table 9: From-to change classes “Summary” with area in hectares	61
Table 10: GPS point locations and class values for 1987, 1989, and 2004	64
Table 11: PC component variance	70
Table 12: Classification to Fractal Dimension Zonal Statistics for 1987	89
Table 13: Classification to Fractal Dimension Zonal Statistics for 1989	89
Table 14: Local fractal dimension D values for the 1987 and 1989 images	110

LIST OF FIGURES

Figure 1: Coordinate structure for triangular prism method.....	19
Figure 2: Error source accumulation process in a remote sensing project	25
Figure 3: Map of SC showing the location of FMNF and the path of Hurricane Hugo ...	34
Figure 4: Storm Track of Hurricane Hugo.....	35
Figure 5: Study area in subsetting FMNF scene displayed using bands 4, 3, 2 (RGB).....	36
Figure 6: Landsat study area subset for 1987 in Bands 3, 4, 5 (RGB)	37
Figure 7: Landsat study area subset for 1989 in Bands 3, 4, 5 (RGB)	37
Figure 8: ArcView printout of the study area	51
Figure 9: A woody wetland scene from the Coffee creek swamp	52
Figure 10: Woody wetland scene from the Wambaw swamp	52
Figure 11: Classified image for 1987.....	53
Figure 12: Classified image for 1989.....	53
Figure 13: Change detection classified image	60
Figure 14: 56 GPS points in yellow overlaid on the 1989 classified image.....	63
Figure 15: PC 1 for 1987	67
Figure 16: PC 1 for 1989	67
Figure 17: PC 2 for 1987	68
Figure 18: PC 2 for 1989	68
Figure 19: PC 3 for 1987	69
Figure 20: PC 3 for 1989	69
Figure 21: TCT brightness for 1987	72
Figure 22: TCT brightness for 1989	72

Figure 23: TCT greenness for 1987	73
Figure 24: TCT greenness for 1989	73
Figure 25: TCT wetness for 1987	74
Figure 26: TCT wetness for 1989	74
Figure 27: NDVI for 1987	77
Figure 28: NDVI for 1989	77
Figure 29: TPSA for 1987 with 17x17 MW with 5 Arithmetic steps.....	78
Figure 30: Same image after a 5x5 convolution low pass filter	78
Figure 31: TPSA for 1989 with 17x17 MW with 5 Arithmetic steps.....	79
Figure 32: Same image after a 5x5 convolution low pass filter	79
Figure 33: Change detection TPSA with 17x17 MW with 5 arithmetic steps.....	80
Figure 34: Same image after a 7x7 focal majority filter.....	80
Figure 35: TPSA for 1987 with 33x33 MW with 5 Geometric steps	101
Figure 36: TPSA for 1989 with 33x33 MW with 5 Geometric steps	101
Figure 37: TPSA for 1987 with 9x9 MW with 5 Arithmetic steps.....	102
Figure 38: TPSA for 1989 with 9x9 MW with 5 Arithmetic steps.....	102
Figure 39: TPSA for 1987 with 11x11 MW with 5 Arithmetic steps.....	103
Figure 40: TPSA for 1989 with 11x11 MW with 5 Arithmetic steps.....	103
Figure 41: TPSA for 1987 with 15x15 MW with 5 Arithmetic steps.....	104
Figure 42: TPSA for 1989 with 15x15 MW with 5 Arithmetic steps.....	104
Figure 43: TPSA for 1987 with 21x21 MW with 5 Arithmetic steps.....	105
Figure 44: TPSA for 1989 with 21x21 MW with 5 Arithmetic steps.....	105
Figure 45: TPSA for 1987 with 25x25 MW with 5 Arithmetic steps.....	106

Figure 46: TPSA for 1989 with 25x25 MW with 5 Arithmetic steps.....	106
Figure 47: Change detection TPSA with 33x33 MW with 5 Geometric steps.....	107
Figure 48: Change detection TPSA with 9x9 MW with 5 Arithmetic steps	107
Figure 49: Change detection TPSA with 11x11 MW with 5 Arithmetic steps	108
Figure 50: Change detection TPSA with 15x15 MW with 5 Arithmetic steps	108
Figure 51: Change detection TPSA with 21x21 MW with 5 Arithmetic steps	109
Figure 52: Change detection TPSA with 25x25 MW with 5 Arithmetic steps	109

ABSTRACT

Hurricane Hugo struck the South Carolina coast on the night of September 21, 1989 at Sullivan's Island, where it was considered a Category 4 on the Saffir-Simpson scale when the hurricane made landfall (Hook *et al.* 1991). It is probably amongst the most studied and documented hurricanes in the United States (USDA Southern Research Station Publication 1996). There has been a Landsat TM based Hugo damage assessment study conducted by Cablk *et al.* (1994) in the Hobcaw barony forest. This study attempted to assess for a different and smaller study area near the Wambaw and Coffee creek swamp. The main objective of this study was to compare the results of the traditional post-classification method and the triangular prism fractal method (TPSA hereafter, a spatial method) for change detection using Landsat TM data for the Francis Marion National Forest (FMNF hereafter) before and after Hurricane Hugo's landfall (in 1987 and 1989). Additional methods considered for comparison were the principal component analysis (PCA hereafter), and tasseled cap transform (TCT hereafter).

Classification accuracy was estimated at 81.44% and 85.71% for the hurricane images with 4 classes: water, woody wetland, forest and a combined cultivated row crops/transitional barren class. Post-classification was successful in identifying the Wambaw swamp, Coffee creek swamp, and the Little Wambaw wilderness as having a gain in homogeneity. It was the only method along with the local fractal method, which gave the percentage of changed land cover areas. Visual comparison of the PCA and TCT images show the dominant land cover changes in the study area with the TCT in general better able to identify the features in all their transformed three bands. The post-classification method, PCA, and the TCT brightness and greenness bands did not report

increase in heterogeneity, but were successful in reporting gain in homogeneity. The local fractal TPSA method of a 17x17 moving window with five arithmetic steps was found to have the best visual representation of the textural patterns in the study area. The local fractal TPSA method was successful in identifying land cover areas as having the largest heterogeneity increase (a positive change in fractal dimension difference values) and largest homogeneity increase (a negative change in fractal dimension difference values). The woody wetland class was found to have the biggest increase in homogeneity and the forest class as having the biggest increase in heterogeneity, in addition to identifying the three swamp areas as having an overall increased homogeneity.

CHAPTER 1: INTRODUCTION

Coastal wetland forests are an important part of the Earth ecosystems. They contribute a disproportionate share of human settlement sites primarily due to transport availability through land and waterways, and easy access to food and water (Michener *et al.* 1997). Wetlands include various types of swamps, marshes, beaches, and shorelines and are shaped amongst other things by severe natural phenomena like the occurrence of hurricanes and tropical storms (Michener *et al.* 1997). Lugo (2000) summarizes the effects and outcomes of hurricanes on Caribbean forests, which can be applicable to coastal wetland forests.

- Sudden and massive tree mortality;
- delayed patterns of tree mortality;
- alternative methods of forest regeneration;
- opportunities for a change in successional direction;
- high species turnover and opportunities for species change in forests;
- diversity of age classes; faster biomass and nutrient turnover;
- species substitutions and changes in turnover time of biomass and nutrients;
- lower aboveground biomass in mature vegetation;
- carbon sinks;
- selective pressure on organisms; and
- convergence of community structure and organization.

Coch (1994) states that hurricane wind damage occurs on different spatial scales: microscale, mesoscale, and megascale. While it is generally accepted that catastrophic wind damage due to hurricanes is a major cause of forest damage (Coch 1994, Michener *et al.* 1997, Peterson 2000), secondary damage like insect infestation and/or forest wildfires can often exceed the forest damage due to high winds in a hurricane Cablk *et al.* (1994). Studying the past spatial effects of hurricane damages like its extent, intensity, and identification of vulnerable secondary areas, planners and strategists try to figure out

new ways to predict the future spatial effects, which can be done quite effectively by satellite data analysis (Cablak *et al.* 1994). Recognizing this need there have been many studies on the impact of hurricanes on coastal forests and wetlands using remote sensing (Hayes and Sader 2001, Ramsey *et al.* 1997, Ramsey *et al.* 1998, Ramsey *et al.* 2001a). Various approaches of automated classification have been used, including the use of neural networks by Dai and Khorram (1999), using Bi-directional Reflectance Distribution Function by Roy *et al.* (2002), decision trees in Chan *et al.* (2001), Friedl and Brodley (1997), fractals by De Cola (1989), Lam (1990), Lam *et al.* (1998) and others. Automated identification of change detection patterns are the holy grail of remote sensing and there exists a need for development of basic algorithms, which provide reliable and rapid identification of time series imagery over large areas. Read and Lam (2002) gave an excellent summary of the need for automated change detection: due to development of finer spatial and spectral resolution of satellite data, fast identification of 'hot spots', and the need for reproducibility with minimized work for analysts.

If fractal methods, which are spatial methods founded on the spatial complexity principle, are in use for classification or identification of land cover, then they can also be used for automated change detection. There has been interest in the application of fractals to identify land use-land cover change patterns in remotely sensed data since fractals were first conceived by Mandelbrot in 1975 (De Cola 1989, De Jong and Burrough 1995, Emerson *et al.* 1999, Lam and De Cola 1993, Lam *et al.* 1998, Rees 1992). All the studies cited above have considered fractals directly to describe land use-land cover classification for remote sensing images. Mesev *et al.* (1995) used Maximum Likelihood classifier derived output as input to a fractal classification algorithm as a

means of urban land-use density analysis. Yet, there is a lack of a study for direct comparison of the performance of fractals with various spectral methods for change detection. Hence, this study compares the effectiveness of selected fractal method and traditional spectral techniques to differentiate change in Landsat TM data for change detection in the coastal forest region of South Carolina.

In trying to analyze a subset of the Landsat TM image for change detection using spectral methods, the effect of scale should be considered. According to Tobler's first law of Geography (Tobler 1970) "*Everything is related to everything else, but near things are more related than distant things*", and Goodchild's corollary (Goodchild 2003) that "*objects at a coarse resolution are more identifiable than those at a fine resolution*". Since the basic concept of fractals is its self-similarity, so the analysis done at different scales should be theoretically equivalent (Goodchild and Mark 1987). However, practically, most natural things captured in remote sensing images are not self-similar (Read and Lam 2002). This issue of scale will affect the methods used in change detection (i.e., the local fractal TPSA method), and hence the change detection results.

1.1 Objectives and Hypothesis

The study investigates the performance of fractal dimension in change detection and compares its performance with traditional techniques like post-classification comparison using hybrid classification, PCA, and TCT. This will be achieved through development of change impact analysis for a study site in coastal South Carolina, the Francis Marion national forest. The objectives for this study are:

- 1) Identify the impacts on land cover changes for the study area from 1987 to 1989.
- 2) Identify the spatial patterns of the impacts.

- 3) Deduce which remote sensing method amongst the one chosen is better for change detection, and can the fractal method capture the changes effectively?

The research hypothesis is that the fractal method will successfully identify the land cover changes due to the hurricane.

The selection of the classification and the two image differencing techniques, PCA and TCT, for change detection comparison with fractals is because they have been widely used in the remote sensing literature (Crist and Cicone 1984a, 1984b, Fung and Ledrew 1987, Li and Yeh 1998, Mas 1999, Singh 1989). The post-classification comparison was selected to be the reference and its accuracy is verified by large-scale aerial photographs and GPS points from ground truthing. The TCT, which is good at vegetative discrimination, was selected because of the vegetative nature of the study area, while the PCA was chosen to highlight the dominant changes (Read 1999).

CHAPTER 2: LITERATURE REVIEW

The most efficient, predictable, and economical way of monitoring changes on the earth surface as compared to field data collection or aerial photography, is by using satellite remote sensing (Hayes and Sader 2001, Maeder *et al.* 2002). Land use-land cover (LULC hereafter) classification and change detection has been one of the first and most critical applications of remote sensing to produce thematic maps (Foody 2002). Some of the many methods of analysis encountered in remote sensing literature are as follows:

- 1) Spectral based e.g. Image ratioing, Image differencing, Image classification
- 2) Statistical e.g. PCA and Tasseled Cap
- 3) Spatial/textural e.g. lacunarity, fractal, variogram, spatial autocorrelation

During this process of environment change, typically a fixed scale of measurement is used at discrete intervals to build a series of time series images. The predecessor of remote sensing for environmental characterization and monitoring are the aerial photographs, whose origins can be traced back to World War I and are documented in many historical articles/novels. Satellite remote sensing began in earnest in the 1970's with the advent of the Landsat program (Lillesand and Kiefer 2004). A major reason for the widespread use of satellite images is that the scale of the analysis can be varied easily by manipulation and leads itself naturally to automation with computers. Initially, due to the resolution of the satellite images, the scale was restricted to regional or higher scale, for e.g. in AVHRR, Landsat MSS etc. Now due to the advent of 1-meter panchromatic and 4-meter multispectral IKONOS satellite imagery, it is easier to do analysis on a city block scale (Space Imaging 2004).

2.1 Problems in Change Detection

Remote sensing change detection suffers from several problems. The accuracy of results obtained using multiple methods is highly dependent on the image processing technique being used, for example, unsupervised classification was found to be superior to PCA and image differencing by Mas (1999), whereas Dai and Khorram (1999) found supervised classification inferior to neural network. Lam and Quattrochi (1992) mention that inappropriate application of a method can lead to a meaningless study. As geographic data is present in several different scales, the scale of analysis also causes problems, i.e. spatial and spectral scales. The same area when analyzed on different scales will result in different spatial pattern interpretation (Lam and Quattrochi 1992). Lam and Quattrochi (1992) summarize the problem well when they state that the *“best choice of scale depends on the study objectives, the type of environment, and kind of information desired”*.

There also exists the problem of subjective interpretation of results, for example in a PCA analysis two different people with varying experience and knowledge of the area under analysis, may produce different conclusions given the same inputs. Read (1999) and Xiao (2000) state that the environment of analysis for e.g. the cloud cover, influences the performance of different change detection methods. A typical remote sensing image contains a tremendous amount of information and spatial complexity. Added to this fact is that the finished products for a designated area can be obtained every 3 days for the 1-meter panchromatic and 4-meter multispectral IKONOS products (Space Imaging 2004). This causes a skewed information overload, as there is a lot of information retrieval. Moreover, the addition of the hyperspectral satellites, which has

many bands, makes it impossible for manual analysis (Lillesand and Kiefer 2004, Xiao 2000). Currently a given area is selected with manageable discrete time slices to build the time-series imagery for manual change detection. Typically, the full range of the stored images is unutilized as it is unsuitable for consistent human analysis, which leads to the case for automation in remote sensing. The automation process will lead to lower costs, and lead to a widespread usage of remote sensing products, much as GPS has taken the world by storm by moving into the mainstream usage.

2.2 Land Use, Land Cover and Some Problems

Land use and land cover are interrelated and often used in the remote sensing literature, though sometimes the terms cause confusion. Land cover is defined as the feature type present on the surface of the earth, for example vegetation, water, different soils, rock, barren land etc; while land use is defined as a piece of land associated with some anthropogenic activity, which can be socioeconomic or cultural, and can be classified as land cover too (Dobson *et al.* 1995, Lillesand and Kiefer 2004). Lillesand and Kiefer (2004) give an excellent example when they state that an urban tract of land can be described as residential use, while the land cover would consist of rooftop, pavement, vegetation etc. The USGS derived Anderson classification system with Level 1 classification scheme is used for this study (Anderson *et al.* 1976). The problem with land use analysis with the higher LULC levels like Levels 3 and 4 is that it is restricted to aerial photographs and commercial high-resolution satellites with resolutions better than 4 meters (Lillesand and Kiefer 2004). Another problem with deriving accurate land use data for most purposes is that as yet it cannot be done independently through remote

sensing, it needs socioeconomic inputs like census, municipal, police survey etc, and in the absence of such data a in-situ interpretation is necessary (Lillesand and Kiefer 2004).

2.3 Review of Change Detection Methods

Change detection is a comparison of multi-temporal remotely sensed images, sometimes for pre-event and post-event, to map and analyze the spatial patterns of the changes in land cover or land use over time. Lillesand and Kiefer (2004) and Read (1999) states that change detection techniques broadly involve four steps:

1. data preparation by accurate registration, transformation, and multiple image mosaicking
2. the actual change detection analysis
3. production of change detection maps and statistics
4. accuracy assessment of the change maps (only for classification)

2.3.1 Data Preparation, Transformation, and Multiple Image Integration

A typical change detection study involves the analysis of remote sensing images, which are sampled at different times, and acquired sometimes from different satellite sensors with differing spatial, spectral, and radiometric resolutions (Read 1999). The basic premise of a change detection study is that the land cover changes will result in more variation in the Digital Number (DN hereafter) radiance than all other secondary changes combined, for e.g. atmospheric, noise, geometric and radiometric errors (Mas 1999). Therefore, for meaningful analysis, the image data must be converted into a common format i.e. normalization, to resolve all the differences during the image acquisition process to guarantee accuracy of results for the study. The images acquired

from the satellite providers all undergo a common set of procedures termed image pre-processing, to create a precise representation of the original scene (Lillesand and Kiefer 2004). The pre-processing includes corrections such as radiometric, geometric, and noise removal. Lillesand and Kiefer (2004) define a basic minimum set of corrections for a multiple images change detection study as

1. geometric correction to account for the satellite sensor idiosyncrasies of systematic and random distortions
2. radiometric calibration of the radiance values from different sensors to account for seasonal changes in position and distance of sun relative to earth, and atmospheric effects.
3. resampling for registration/overlay of multiple dates, resolutions and a eventual merge into a GIS.

Ideally, the problem would be reduced if the data were obtained from a single sensor, say Landsat 5 or Landsat 7, which would have the same spectral, spatial, and radiometric resolution (Read 1999). However, in most cases, appropriate time-series images from a single sensor are not available. In addition, the properties of the satellite or the sensor itself change over time, as in the recent case with Landsat 7 where its Scan Line Corrector (SLC) system failed due to a mechanical failure (USGS 2004). Precise resampling of multiple images with ground control points using either independent ground truth registration or co-registration is very important before proceeding further for analysis (Singh 1989). The general rule for accurate change-detection is to ensure pixel co-registration is within 1/2 pixel of the satellite spatial resolution as an acceptable error (Lillesand and Kiefer 2004). Read (1999) highlights the importance of choosing of a

suitable temporal scale by observing that any change detection technique identifies changes between discrete checkpoints in time, and any intermediate though still valid changes occurring in between those checkpoints will be undocumented. Many researchers state the importance of maintaining the soil moisture conditions in tropical forests and lagoons by stating that changes in dry and wet conditions can cause interpretation problems (Grover *et al.* 1999, Mas 1999, Townsend and Walsh 1998).

To summarize, for change detection using remote sensing, several factors must be taken into consideration, including the temporal resolution, spatial resolution, spectral resolution, radiometric resolution, the atmospheric conditions, and the seasonal effects. Since it is practically impossible to ensure the above, the person conducting change detection contrives to make it as similar as possible, hence the need for various corrections in the pre-processing stage.

2.3.2 Change Detection Analysis

A typical set of spectral change-detection techniques used in a change detection study are chosen including image ratioing, image classification, and image differencing (Read 1999). A threshold value for change using gray level thresholding or thresholds derived from histogram of the image is generated in order to separate the areas of land cover change from the secondary changes (Singh 1989). The most commonly used method for change detection usually is the independent post-classification comparison (Li and Yeh 1998). Read (1999) states that the choice of a method depends on the study objectives and data availability. The results of a change detection study will produce the possible outcomes as outlined in Table 1.

Table 1: Possible outcomes of a change detection study

Study objective	Knowledge required	Remote sensing technique
from-to change classes	a priori or a posteriori	Classification
Change/no change classes	No	Fractals, Image differencing, Image ratioing
Change/no change classes with direction of change information	No	change vector analysis

(Modified from: Read 1999)

Li and Yeh (1998) state that the pixel based change detection methods have two variations: image differencing and image ratioing. These spectral techniques need no prior or subsequent knowledge for general comparison and hot spot detection, but suffer from the disadvantage that they can provide only a change/no change result, with no information of the nature of change (Li and Yeh 1998, Read 1999). Some of the advantages with the image ratioing techniques are that different bands can sense different land cover features to get a complete picture of the changes occurring in the area; variations in sun angle, shadows, and reflectance between images are minimized because of the absolute magnitude reduction due to the ratio operation (Lillesand and Kiefer 2004, Read 1999). This leads to the development of various indexes based on combinations of satellite bands for different applications: NDVI, Time NDVI, several indexes for mineral detection etc. (ERDAS Imagine 8.7 Field Guide). Read (1999) mentions that with both the pixel based approaches, the change summary depends on the chosen thresholds, which are sometimes chosen arbitrarily but generally based on band statistics.

Another technique, PCA, is more complicated than the classification or the differencing methods. Fung and Ledrew (1987) and Read (1999) state that the results from PCA is a transformed dataset and is image dependent, the proportion of change in study area should be small relative to the no-change area. The classification method is suitable for cases where radiometric calibration is not possible (Read 1999). However, classification suffers from the disadvantage that individual image errors may be multiplied (Mas 1999). Of special interest in this study is the observation of the study by Houhoulis and Michener (2000), where they state that the spectral similarities among many land cover classes for such as wetlands, agricultural fields, and forests make

satellite image classification based solely on spectral properties very difficult. The following sections review the remote sensing literature for the different methods used for change detection in this study.

2.3.2.1 Principal Component Analysis

PCA is a multivariate statistical technique often used as a data reduction technique in remote sensing (Lillesand and Kiefer 2004, Singh 1989). In a dataset with n number of variables, two or more variables are often linked together and if that dataset is reduced to the new transformed variables (principal components), the changes are easier to spot and explain. The set of new images representing the number of desired principal components are derived from linear combinations of an original set of multi-spectral and/or multi-temporal images. PCA can be applied by either using the covariance matrix or the correlation matrix extracted from the images, depending on whether the dataset consists of raw/unstandardized or standardized variables (Krzanowski 1984). The eigenvalues and eigenvectors are then computed from either the covariance or the correlation matrix. The eigenvalues refer to either the covariance or the correlation of the n^{th} principal component (Krzanowski 1984). The eigenvectors contain the transformation coefficients, which represent the direction and contribution of each band on the components. The new components are the addition of the product of the DN's of individual bands and the coefficient of the band on the components (Lillesand and Kiefer 2004).

The new matrix formed by the principal components has the following properties (Mather and Openshaw 1974, Shaw and Wheeler 1994):

- The principal components are uncorrelated (orthogonal) to each other.

- The successive principal components account for the remaining maximum variance after extraction of previous principal components.

The PCA transformation is constrained such that the total variance of the input dataset should equal the total variance of the PCA output. The content of the principal component images are themselves not fixed, as it is highly dependent on the input information content, and the output is derived statistically. Typically, the first component will depict the dominant variance of the image with low noise and high signal content, while the second is a bipolar component with high values from some bands and low values from other bands. The third and possibly the fourth and higher components generally depict the subtle details obscured by the first two components with correspondingly lower signal to noise ratio i.e. low signal strength with high noise values (Fung and Ledrew 1987, Singh 1989). PCA has a major limitation that interpretation of the derived dataset is difficult between different dates or different scenes due to this image specific nature of the technique itself (Crist and Cicone 1984a). To overcome the limitation, Li and Yeh (1998) proposed using PCA with stacked multiple temporal images so that all the classification signatures produced are the same leading to reduced errors since all the images are classified simultaneously.

2.3.2.2 Tasseled Cap Transformation

TCT is a variation of PCA, but with fixed coefficients for a given sensor of a satellite (Crist and Cicone 1984a). The TC Transform is sensor dependent, since the reflectance curves for different types of classes are different for every sensor and so has fixed coefficients for different satellite sensors (Crist and Kauth 1986). The transformation leads to the establishment of new spectral axes due to rotation so that the

original image is projected into three new components: brightness, greenness, and wetness (Crist and Cicone 1984a). It is important to note that TCT does not require that the data transformation of new axes to be orthogonal, instead the data plane is oriented so that there is direct relation to physical scene characteristics (Crist and Cicone 1984a). Read (1999) terms the TCT as a “*vegetative transform differencing*”. Crist and Cicone (1984a) also demonstrate that the variability of the six reflective bands of TM data can be effectively reduced to three dimensions by defining a plane of soils, a plane of vegetation, and a transition zone between the two planes. Crist and Cicone (1984a) define the three TCT bands:

- **Brightness:** Weighted sum of all reflectance bands for the sensor so it is more responsive to changes in total reflectance. It is sensitive to the measurement of soils or bare surfaces, i.e. TM bands 3, 4, and 5, but increase in vegetation density particularly in TM band 1 and 2 have no effect on this component.
- **Greenness:** Contrast between the sum of the visible bands and the near-infrared (NIR hereafter) bands. It is useful as a measure for green vegetation density as this band responds to both high visible absorption, and high NIR reflectance.
- **Wetness:** Contrast between the sum of the visible and the near-infrared bands with the sum of longer-infrared bands. It is sensitive to both soil moisture and plant moisture as it has high visible reflectance and high NIR absorption and shows the interrelationship between soil and canopy moisture. It is mostly depicting soil moisture, and to a lesser extent the plant moisture.

While PCA tries to reduce total image variance into several principal components, TCT tries to delineate into three distinct bands preserving the information in each data

structure (clusters of data points in the 6 dimensional TM plane) and the geometric relationships between the data structures. TCT is an invariant transformation and is sensor dependent, whereas PCA is sensor independent (Crist and Kauth 1986). TCT is a useful tool in land-cover change detection of forest over large study areas and long time periods (Collins and Woodcock 1996, Franklin *et al.* 2002).

2.3.2.3 Fractal Methods

The concepts of fractals and fractal dimension were first introduced by Mandelbrot in 1977 (Lam 1990). Lam (1990) gives a succinct review of the fractal concepts. Read and Lam (2002) observe that the fractal dimension D has been used to characterize land use/land cover changes in remote sensing, but not much research for change detection has taken place using fractals. Nath and Dewangan (2002), Read and Lam (2002), and Weishampel *et al.* (2001) are some of the very few examples who have used fractals for change detection for seismic reflection and LULC change.

Fractals are based on the concept of self-similarity, which means that theoretically, the structure remains consistent at a reduced scale recursively, and scale independent comparisons are possible (Goodchild and Mark 1987, Lam and Quattrochi 1992). Fractals as used in remote sensing tend to emphasize the spatial relationships between adjacent cells (Lam and De Cola 1993). They are different from the traditional spectral methods, which either perform a direct pixel-by-pixel comparison between two images or matrix of from-to classes during classification. Ridd *et al.* (forthcoming) state that instead of finding micro-level changes in pixel comparison and then trying to interpret change, a comparison of the analysis of spatial relationships between images in

a time-series will reflect significant differences much faster simply by an indication of a large change in the fractal dimension D .

Read and Lam (2002) state that the more spatially complex the area under question the higher is the fractal dimension. Since most natural phenomena are not pure fractals they will have varying fractal dimensions D at different scales, for remote sensing images D varies between 2 and 3 for different land-cover types and different spectral bands. Some studies have found D value close to 1.0 for water surfaces and for convective and supercell storms (Angeles *et al.* 2004, Feral and Sauvageot 2002). Other studies working with Landsat TM and AVIRIS images found significantly high D values for urban areas (Lam 1990, Qiu *et al.* 1999).

Fractal dimensions calculated for remote sensing images can be used theoretically to link/extrapolate local changes to regional and global scale changes because of its scale independent property. However, in practice it is not possible to always extrapolate changes when the scale of analysis is changed (Emerson *et al.* 1999, Lam 1990, Lam and Quattrochi 1992, Read and Lam 2002). A major caveat pointed out by Lam (1990) is that for the same surface, the D values for different fractal algorithms are different. Finally, Read and Lam (2002) and Ridd *et al.* (forthcoming) highlight the main problems prohibiting the widespread use of fractals in remote sensing as the lack of standardized tools and lack of algorithm details in research papers while comparing the same fractal algorithms.

Many methods have been developed to measure the fractal dimension of natural phenomena. In geography, various fractal algorithms like isarithm, triangular prism, and variogram have been described (Goodchild 1980, Jaggi *et al.* 1993, Kolibal and Monde

1998, Lam and De Cola 1993, Qiu *et al.* 1999). All the above fractal methods, along with other spatial methods, are included in ICAMS (Image Characterization and Modeling Systems) described in and developed by Lam *et al.* (1997), Lam *et al.* (1998), and Quattrochi *et al.* (1997). Lam *et al.* (2002) found that in comparison with the isarithm and variogram methods, the triangular prism method is more accurate for estimation of fractal dimension of surfaces with high spatial complexity, which is a characteristic of remote sensing imagery. The modified triangular prism method was therefore chosen for this study.

The triangular prism method implemented in ICAMS is described below (Read and Lam 2002, Ridd *et al.* forthcoming). It considers a 3D pixel square formed by four pixels which are neighbors to the centered original pixel and which are projected vertically to form four triangles with the original pixel at center of this virtual “triangular prism”. The pixels per side represent step size, and length of the vertically extended lines is their z values. The area for the four individual triangles at the top of prism thus formed is calculated individually and then summed up until all of the total surface area for the image is also calculated for increasing step sizes. Then the log-log plot between the total surface areas and the step sizes is used to calculate the regression slope B using the least squares regression on the selected points. The fractal dimension D is then $D = 2 - B$. See Figure 1 for explanation.

The difference between the original triangular prism method implementation and the modified ICAMS implementation is in the nature of calculation of the fractal dimension values (Lam *et al.* 2002). The original method uses a square of step size to regress the triangular prism areas whereas the modified method uses only the step size to

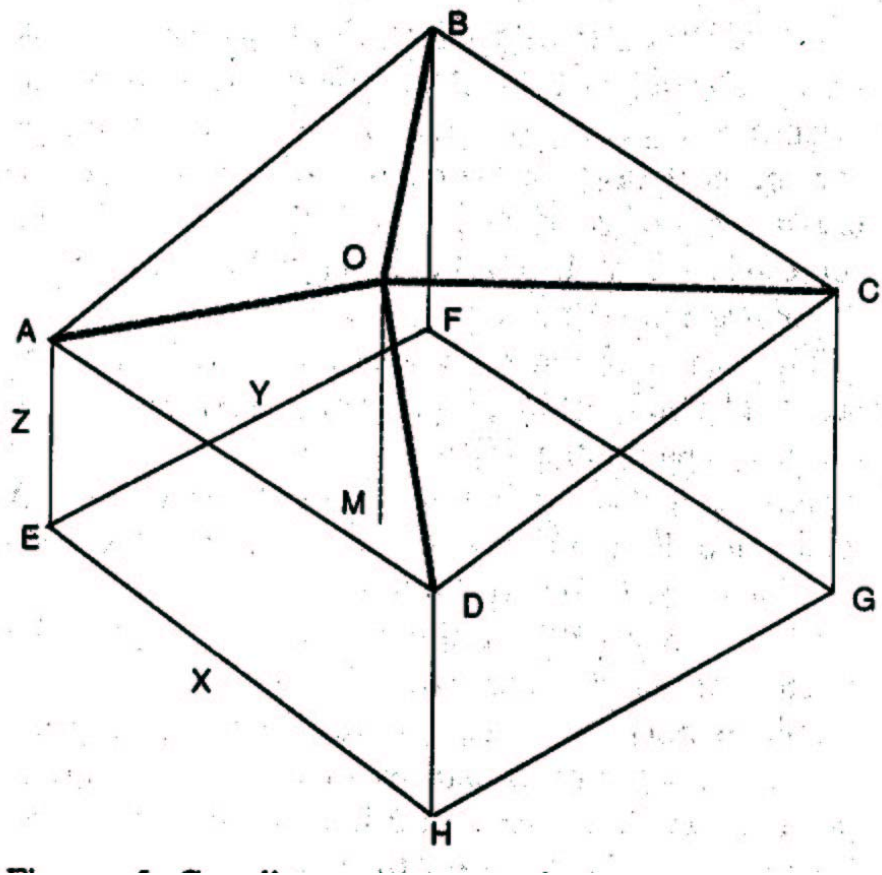


Figure 1: Coordinate structure for triangular prism method

(Source: Jaggi *et al.* 1993)

derive the correct fractal dimension values.

2.3.2.4 Post-Classification Comparison

This is perhaps widely used because of its ease in manipulation in spite of its many inherent disadvantages. The analyst can lump many change classes into a single thematic class because of their irrelevance to the study, conversely the analyst can also study a particular land cover class with more detail, for example, by conducting analysis of Level 2, 3 or 4 in the USGS-Anderson classification system (Read 1999). Generally, unsupervised classification is preferred in a typical scene when the amount of spectrally separable land cover classes is unknown and the total spectral variation is assumed wide, that is, the land cover class reflectances represent a diverse study area (Thomson *et al.* 1998). Supervised classification, on the other hand, is preferred where the land cover classes are more homogeneous. The choice is determined by the nature of the land cover classes in the study area.

One problem of this procedure is the occurrence of the edge effects, which may occur at various stages in the classification process. Read (1999) states that the edge effects occur from image misregistration during geometric correction process, fuzzy boundaries in the reference data, and misclassification of doubtful pixels. The seriousness of edge effects depends on the spatial resolution and the number of different bands of the satellite sensor, i.e. the spectral resolution. The edge effects will decrease if we increase the spatial resolution and the number of bands of satellite, on the other hand it will lead to more data, and more usage of computational resources, which is difficult to handle with current generation of desktop machines. It is ultimately a tradeoff between too much and too less information for spectral techniques. Serra *et al.* (2003) state that

combination of data from different sensors can contain a significant proportion of boundary errors.

In unsupervised classification, it is difficult to choose the correct number of spectrally separable classes such that there are no bands with mixed information. During classification it is sometimes apparent that what has been classed as one land cover class (e.g. water) in one part of the image appears to be another land cover class (e.g. wetland) in another part of the same image. Read (1999) summarizes the problems succinctly:

- 1) Edge transitions across different vegetation types.
- 2) Edge transitions between different classes within the same image.
- 3) Boundary uncertainties due to fragmentation.

Mertens *et al.* (2003), who use a genetic algorithm for sub-pixel mapping in their paper, state that in a remote sensing image, mixed pixels are a reality. That is the reason for the advent of the soft classification and sub-pixel techniques in recent years. Mertens *et al.* (2003) define soft classification as using the degree of membership of pixels belonging to different land cover classes and sub-pixel mapping as a procedure used to sharpen classified image using mixed pixels.

2.3.3 Accuracy Assessment of Classification

In remote sensing studies, which use any sort of classification technique for change detection, either supervised, unsupervised, or hybrid, finally have to undertake an accuracy assessment procedure to ensure the accuracy of interpretation of the matrix of from-to classes. Arzandeh and Wang (2003) state that change-detection accuracy is highly dependent on the accuracy of the individual classifications of the images involved in the process. Lillesand and Kiefer (2004) state, “*A classification is not complete until*

its accuracy is assessed". Congalton (2001) further elaborates the reasons for accuracy assessment as

1. The need to know the truthfulness of our analysis and to learn from mistakes
2. Quantitative comparison of classification methods
3. Use the accuracy assessment in execution of policy decisions

Congalton (2001) explains why accuracy assessment is needed by giving an example of disagreeing wetland maps of the same area created by different agencies; and without a reliable and valid accuracy assessment, nobody will know which wetland map to use.

Lillesand and Kiefer (2004) describe the accuracy measures in the generation of an error matrix (also called confusion matrix or contingency table): producer, user, overall accuracy, and the Kappa statistics. They state that the classification errors are of either commission (inclusion) or omission (exclusion). They define the following terms:

- The overall accuracy is defined as the sum of all correctly classified pixels divided by total number of pixels.
- Producer's accuracy indicates the performance of the analyst in performing the classification of any given cover type. It is the ratio of correctly classified pixels for each land cover class to the total number of pixels used in reference dataset.
- User's accuracy informs the user of the reliability of the classification procedure. It is defined as the ratio of correctly classified pixels for a given land cover class to the total number of pixels in that class.

Lillesand and Kiefer (2004) define the Kappa (khat) statistic as a ratio of the measure of the difference of agreement between reference data and classifier to the chance agreement

between reference and random classifier. It serves as an indicator that if Kappa approaches 1.0, it is more true agreement as opposed to it approaching 0, which is more of a chance agreement with accuracy of classification (Cablak *et al.* 1994).

Congalton (2001) in Figure 2 illustrates the gradual building up of the errors in a change detection study. In general, to increase the accuracy of the classification process the following considerations have to be followed:

1. Sampling scheme: Compares the classified data to the ground truth or reference data in either of two ways: either by construction of random points or integration of user defined field plot data usually through use of GPS (ERDAS Imagine 8.7 Field Guide). Congalton (2001) states that in most change detection studies stratified random sampling is sufficient.
2. Sample size: A minimum of 50 samples per map class are required to ensure a good classification estimate Congalton (2001). Therefore, for five different classes, a minimum of 250 samples need to be taken.
3. Sampling unit: Congalton (2001) defines three sampling units. (a) pixel (b) a 3x3 pixel group and (c) a polygon, but stating the need for avoiding a single pixel for sampling due to the difficulty of correlation on the surface even with GPS.
4. Use of post-classification contextual filter: Zukowskyj *et al.* (2001) state that choosing a simple filter may increase classification accuracy.
5. Combination of map classes: Ramsey *et al.* (2001b), Zhu *et al.* (2000) state that the proper combination of homogeneous classes during classification will reduce misclassification errors.

Read (1999) states that the accuracy assessment procedure depends heavily on the quality of the reference data; ideally, the accuracy should be very high, but practically it may be outdated or very low quality. Foody (2002) states that there are lots of problems associated with accuracy assessment which are impossible to achieve in practice, such as the assumption of perfect coregistration of data sets. He further states that one of the major problems of the confusion matrix and the kappa coefficient is the absence of information of the spatial distribution of the classification errors. Reference data used can range from diaries, historic maps, USGS Quads, aerial photography, DOQQ's, to GPS.

2.4 Importance of Coastal Wetland Forests

Cox and Peron (2002) define wetlands as

“an area where the soil is saturated with or covered with water, supporting hydrophytic plants – plants that can grow in water or very wet soil – for a good portion of the year”.

Most studies in hurricane damaged coastal wetland forests (referred to as wetlands interchangeably in this study), and in general for southeastern coastal forests, note dramatic losses in the acreage of the wetlands (Cablak *et al.* 1994, Michener *et al.* 1997, Ramsey *et al.* 1997, Ramsey and Laine 1997, Ramsey *et al.* 1998, Ramsey *et al.* 2001b). To understand these losses and to help in assessment of long-term changes in coastal wetland forest landscapes, more remote sensing based studies are being conducted. The choice of remote sensing is generally made due to the inaccessibility of the wetlands, which are composed of marshes and swamps.

For much of modern history wetlands have been misunderstood and misused, we hear of evidence of drainage of wetlands for commercial reclamation in coastal cities, for

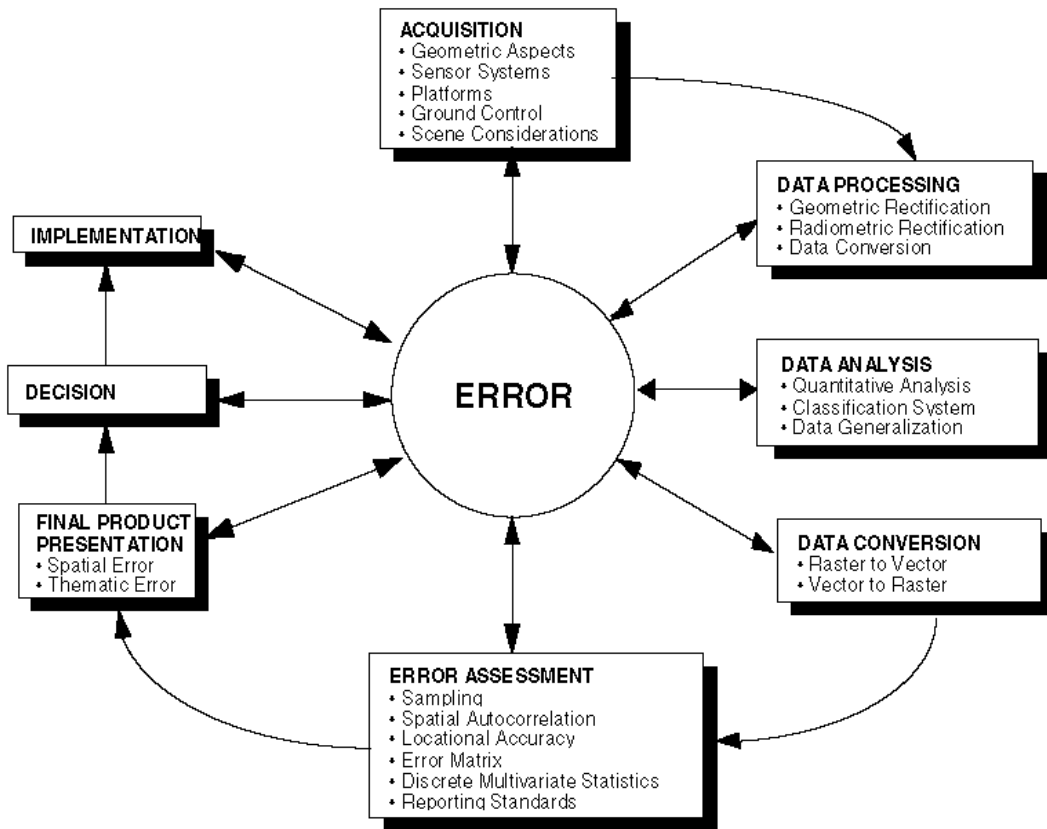


Figure 2: Error source accumulation process in a remote sensing project

(Source: Congalton 2001)

agriculture in Israel, building of dikes/levees etc. Cox and Peron (2002) state that before the 1960's wetlands were viewed as wastelands, unfit for any useful purpose. Turner *et al.* (2003) in Table 2 summarizes the wetland functions and its innumerable socioeconomic benefits in the coastal wetlands of Norfolk and Suffolk Broads in eastern UK, which can be applied to similar places around the world. In the city of Kolkatta (formerly Calcutta) in West Bengal state in India, massive coastal wetlands act as natural sewage treatment facilities, protect it from the inevitable Himalayan floods, and provide a rich habitat for migratory birds. Drained or devastated coastal wetlands are a source of greenhouse gases including Carbon dioxide and Methane, caused by aerobic degradation (Van Den Bos 2003). Brinson and Malvarez (2002) note that countries with lost wetlands have a hard time in trying to maintain and subsequently increase the area and bio-diversity of its wetlands. Due to the anecdotal and well-known evidence of global warming, it is predicted that the oceans will rise over the next few decades flooding many parts of the world. In such a scenario, humans can learn a lot from wetlands, which harbor extensive flora and fauna, highly adapted to living in seawater. Halophytes, which are salt tolerant plants, thrive in coastal wetlands; Schmalzer (1995) outlines the tremendous bio-diversity of saline and brackish marshes.

Conner (1998) states that the mangrove forests of the southeastern United States are the most studied for the impact of hurricanes. Conner (1998) further states that hurricanes cause upto 90% mortality of mangroves in south Florida, the mangrove forests reach maturity in 20-25 years which coincides with the mean frequency of major Gulf hurricanes; and so the hurricanes to some extent control the species composition within mangrove dominated areas by keeping them in a perpetually formative state to keep the

net biomass production higher. Day *et al.* (1995) speculate that the delta regions of the world can be the first line of defense against a sea level rise due to global warming, simply by ensuring that the wetlands get enough sediment input needed for sustenance and to prevent flooding by seawater level increase. Conner (1998) states that high winds and storm surge waves roll up portions of mangrove swamps into ridges of trees, grasses, aquatic plants, and algae; these with the help of the trapped silt/sediments imprison large areas of freshwater which acts as a buffer against saltwater intrusion. Conner (1998) also states that the hurricanes also create conditions for regeneration of wetlands by the creation of newly exposed 'flats'.

An emerging field called phytoremediation uses various wetland trees, grasses, and plants to clean polluted urban and industrial environments by utilizing artificially constructed wetlands, which mimic their natural counterparts. Research is still going on for the search of species, which can clean different pollution infected sites, without the biodiversity within the wetland forests, it will be impossible to harness these ecological cleaning machines in the service of humanity.

Table 2: Wetland functions and associated socioeconomic benefits in the coastal wetlands of Norfolk and Suffolk Broads in eastern UK

Function	Biophysical structure or process maintaining function	Socio-economic use and benefits	Threats
<i>Hydrological functions</i>			
Flood water retention	Short- and long-term storage of overbank flood water and retention of surface water runoff from surrounding slopes	Natural flood protection alternative, reduced damage to infrastructure (road network etc.), property and crops	Conversion, drainage, filling and reduction of storage capacity, removal of vegetation
Groundwater recharge	Infiltration of flood water in wetland surface followed by percolation to aquifer	Water supply, habitat maintenance	Reduction of recharge rates, overpumping, pollution
Groundwater discharge	Upward seepage of ground water through wetland surface	Effluent dilution	Drainage, filling
Sediment retention and deposition	Net storage of fine sediments carried in suspension by river water during overbank flooding or by surface runoff from other wetland units or contributory area	Improved water quality downstream, soil fertility	Channelization, excess reduction of sediment throughput
<i>Biogeochemical functions</i>			
Nutrient retention	Uptake of nutrients by plants (N and P), storage in soil organic matter, absorption of N as ammonium, absorption of P in soil	Improved water quality	Drainage, water abstraction, removal of vegetation, pollution, dredging
Nutrient export	Flushing through water system and gaseous export of N	Improved water quality, waste disposal	Drainage, water abstraction, removal of vegetation, pollution, flow barriers
Peat accumulation	<i>In situ</i> retention of C	Fuel, Paleo-environmental data source	Overexploitation, drainage
<i>Ecological functions</i>			
Habitat for (migratory) species (biodiversity)	Provision of microsites for macro-invertebrates, fish, reptiles, birds, mammals and landscape structural diversity	Fishing, wildfowl hunting, recreational amenities, tourism	Overexploitation, overcrowding and congestion, wildlife disturbance, pollution, interruption of migration routes, management neglect
Nursery for plants, animals, micro-organisms	Provision of microsites for macro-invertebrates, fish, reptiles, birds, mammals	Fishing, reed harvest	Overexploitation, overcrowding and wildlife disturbance, management neglect
Food web support	Biomass production, biomass import and export via physical and biological processes	Farming, fen biomass as alternative energy source	Conversion, extensive use of inputs (pollution), market failures

(Source: Turner *et al.* 2003)

CHAPTER 3: DATA SOURCES AND METHODOLOGY

3.1 Data Sources and Software

This study evaluates the impact of Hurricane Hugo on the land cover in a part of the Francis Marion National Forest. This study will supplement the change detection study published in Cablk *et al.* (1994) for the Hobcaw forest, with the same WRS Path/Row coordinates but a different study area. It also attempts to explore a new method, namely local fractals, for change detection.

3.1.1 Landsat TM Images

Three Landsat TM images were purchased for the purpose of the study: pre-event image in 1987, post-event image in 1989, and a recovery event image in 2001. They were obtained for WRS path 16 row 37 on 14 October 1987, 11 October 1989, and 18 September 2001 respectively. They represented the best possible scenes in the USGS Landsat TM archive in the months of September and October for which the selected area was relatively cloud free. The reason for the selection of the pre-event image of 1987 is that the available 1988 images consist of clouds over the study area. The few areas of cloud and cloud shadow in the obtained images are mostly present outside the study area, but are classified as 'cloud' in post-classification comparison, if present, and ignored in all other analyses. The recovery image is excluded from the present analysis due to time constraints and unavailability of a suitable reference image.

3.1.2 Aerial Photography

Two reference aerial photographs were obtained from the USGS. They are dated 02/09/1989 for the pre-event image and 01/27/1990 for the post event image. They are of

a scale of 1:20,000 with actual paper size of 18' by 18' with 1 inch equaling 1666 feet, Color IR images obtained from the NAPP archive with a Flight line – Station number of 0795W-293 near the Wambaw swamp and Coffee creek area in FMNF lying between coordinates of latitude N 33°10' - N 33°5' and longitude W 79°39' - W 79°33'. The available aerial photographs for the study area for ground truth were not available in the same year and month for both the pre-hurricane and post-hurricane images, so it is hoped that the images will suffice for classification accuracy.

3.1.3 National Land Cover Data: South Carolina

The South Carolina NLCD dataset obtained from the USGS was used during classification. The dataset was produced over a course of several years from 1992 – 2000, and consists of a standardized land cover data for the conterminous US using mosaicked Landsat TM data. From the USGS Readme file, the projection is Albers Conical Equal Area, with NAD83 Datum and a Spheroid of GRS1980. The latitudes of the two standard parallels are 29.5 degrees North Latitude and 45.5 degrees North Latitude. The longitude of the Central Meridian is 96 degrees West Longitude. The latitude of the Origin of the Projection is 23 degrees North Latitude. The False Easting at central meridian is 0 meters, and the False Northing at origin is 0 meters. Number of rows are 11915 and number of columns are 15620 with a pixel size of 30 X 30 meters. The upper left projection coordinates are 1138290 and 1458540 meters, while the lower right projection coordinates are 1606860 and 1101120 meters respectively.

3.1.4 GPS Points Survey

A Trimble GeoExplorer 3 GPS data logger was used for the collection of GPS points used in the study. GPS points were acquired on the field trip undertaken during the period of June 15 – June 19 2004 to validate the classification procedure and acquire any relevant information from the USDA Forest Service, Wambaw Ranger District, FMNF office. Even though the field trip was undertaken after such a long time after the hurricane occurrence, it proved to be immensely helpful in the classification procedure.

3.1.5 Software Used in Study

The image pre-processing which included file manipulation, rectification, classification, change detection using PCA, TCT and various GIS functions, and the accuracy assessment procedures used in the study were performed in ERDAS Imagine 8.6 / 8.7 image processing software.

ICAMS is a package, which contains selected spatial analysis functions for the analysis and characterization of remote sensing data (Lam *et al.* 1998). The ICAMS package is used in this study to calculate the fractal dimensions using the triangular prism method in a local fashion using a moving window, and to produce the change difference image.

GPS Pathfinder Office 2.9 was used for the post-processing of the GPS point data features like GPS point upload to the software, and for differential correction of the acquired data.

ArcView 3.3 was used to merge the GPS Point Id vs. Feature class table, and the GPS Point Id vs. UTM coordinates table into a shapefile, which would be used in ERDAS Imagine for an overlay over the classified images.

3.2 Study Area

Hurricane Hugo made landfall just north of Charleston, SC on September 22, 1989 while it hit the South Carolina coast in the early morning hours of September 22, 1989, it was classified as a Category 4 hurricane on the Saffir-Simpson scale (Conner 1998, Hook *et al.* 1991). Hook *et al.* (1991) states that the center of the eye of Hurricane Hugo passed within 8 km of the FMNF. Cablk *et al.* (1994) state that approximately \$6 billion in hurricane induced damage was attributable to Hugo, which makes it #2 on the top ten costliest hurricanes in the 20th century (NOAA 2004). Cablk *et al.* (1994) state that 23 of 46 counties in South Carolina were affected with 1.8 million hectares of varying forest damage. Figure 3 shows the path of Hurricane Hugo (Conner 1998), and Figure 4 shows the storm track (USDC-NWS, North Atlantic Hurricane Tracking Chart. 2003). Figure 5 shows the study area in relation to the subset of the FMNF while, Figures 6 and 7 are the subsetted study area in the FMNF for 1987 and 1989.

The FMNF contains roughly 252,840 acres and is located in the coastal plains of South Carolina (Monitoring and Evaluation Annual Reports 2002). It is a multiple-use resource with plenty of forest based recreation activities including hunting, hiking, camping and picnicking (Hammit *et al.* 1990). Coch (1994) states that coast-normal hurricane tracks (perpendicular to the coast) tend to produce a wide swath of destruction, and Hook *et al.* (1991) state that most of the Hurricane Hugo's damage occurred due to short duration gusts formed in and near the eyewall covering nearly the entire area of FMNF. FMNF was formed in 1936 due to creation of barren land by extensive railroad logging of large, old-growth longleaf pine, loblolly pine, and cypress timber, and is very

diverse in land cover. (Monitoring and Evaluation Annual Reports: Francis Marion National Forest 2002, Cablk *et al.* 1994).

3.3 Methodology

3.3.1 Preparation of Images

The pre-event image dated October 14, 1987 and the post-event image dated October 11, 1989 were received from USGS in the form of raw Landsat TM bands in BSQ Format. These were each transformed into a single Generic binary unsigned 8-bit image with the seven layers using the Import Function in ERDAS Imagine 8.7; the images were then projected to UTM Zone 17 North with spheroid of GRS 1980 and datum of NAD 83, using the 'Layer Info' option in the currently selected Image Viewer. A subset consisting of the FMNF, which is just north of Columbia, SC where Hurricane Hugo first hit the South Carolina coast, was selected. This was then subsetted again to include the study area closely corresponding to the aerial photos for both the 1987 and 1989 Landsat images. The images were subsetted such that the rows and columns were the same and covered a little more area than the reference aerial photographs. A major reason was that the larger spatial extent of the Landsat TM images allowed moving window computations for the local TPSA method to run throughout the area covered by the reference aerial photographs. Moving window computations produce an edge where there is no information output.

It should be noted that wherever possible, the option "Ignore zero in Output stats" is always chosen in ERDAS Imagine when calculating statistics for output file for all parts in the analysis. Using the 'Swipe' tool, which can be considered as a crude change detection tool, swiping one image on top of another both horizontally and vertically I

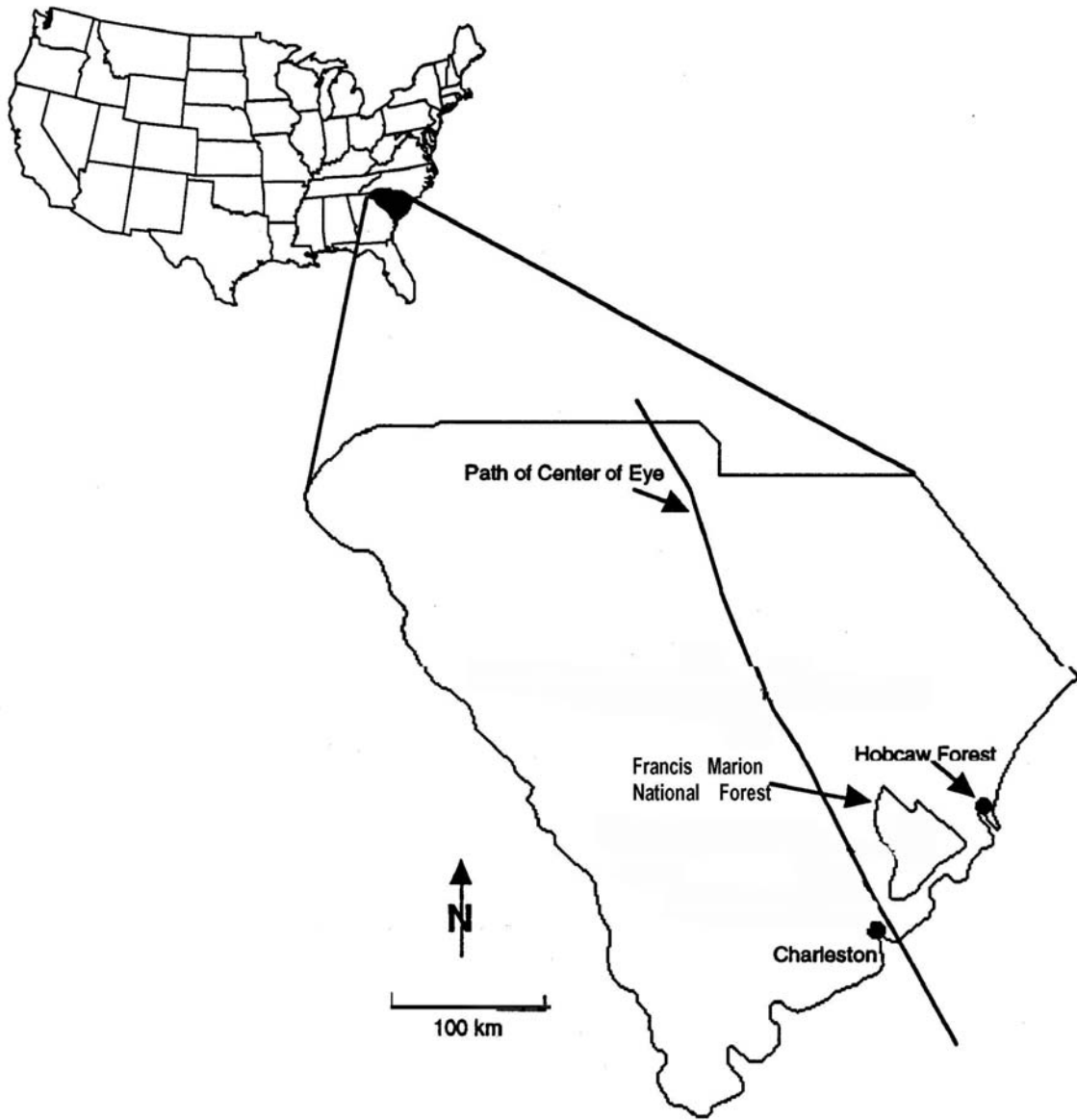


Figure 3: Map of SC showing the location of FMNF and the path of Hurricane Hugo

(Modified from: Conner 1998)

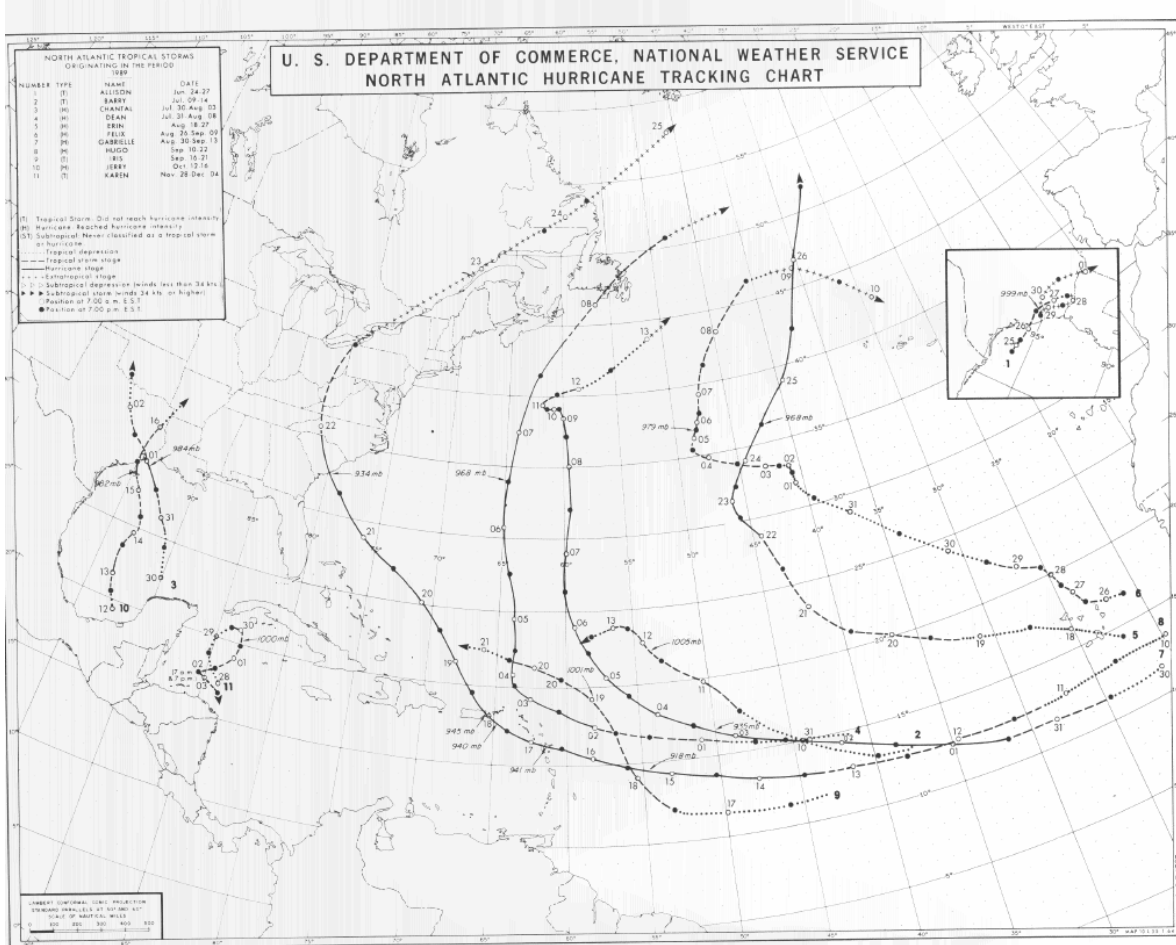


Figure 4: Storm track of Hurricane Hugo

(Source: NOAA 2004)

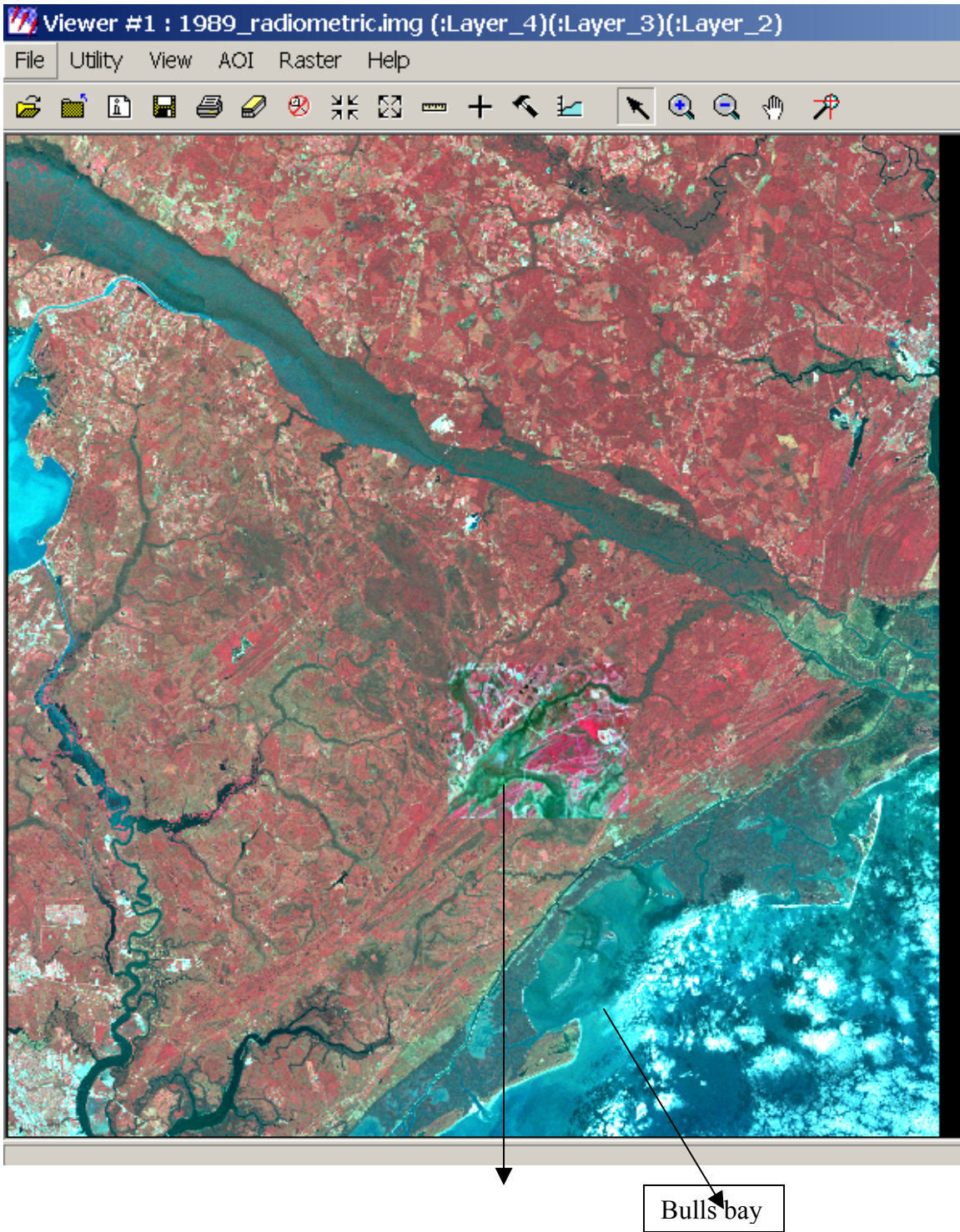


Figure 5: Study area in subsetting FMNF scene displayed using bands 4, 3, 2 (RGB)

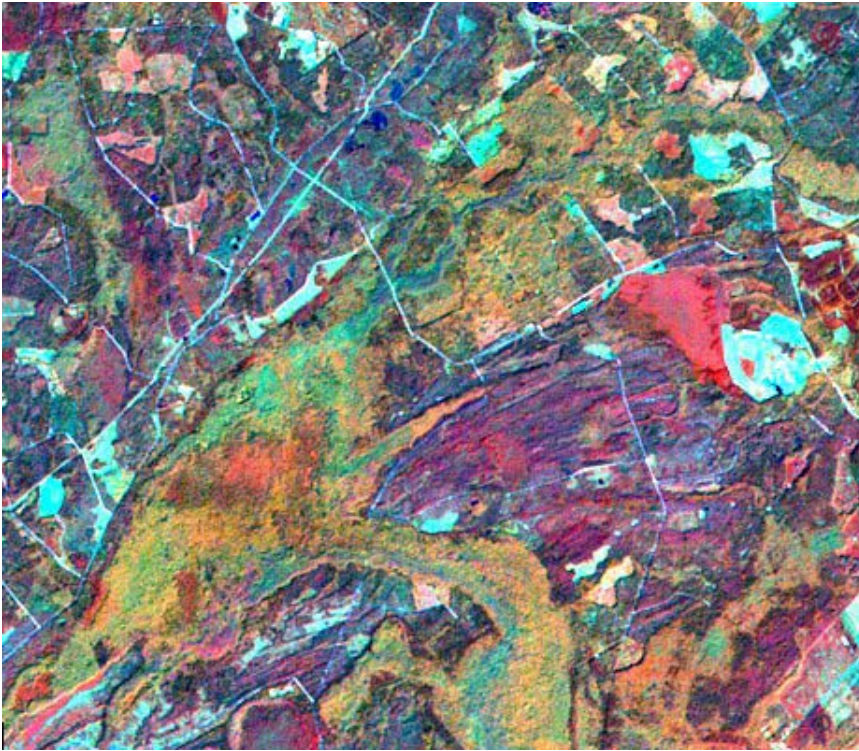


Figure 6: Landsat study area subset for 1987 in Bands 4, 5, 3 (RGB)

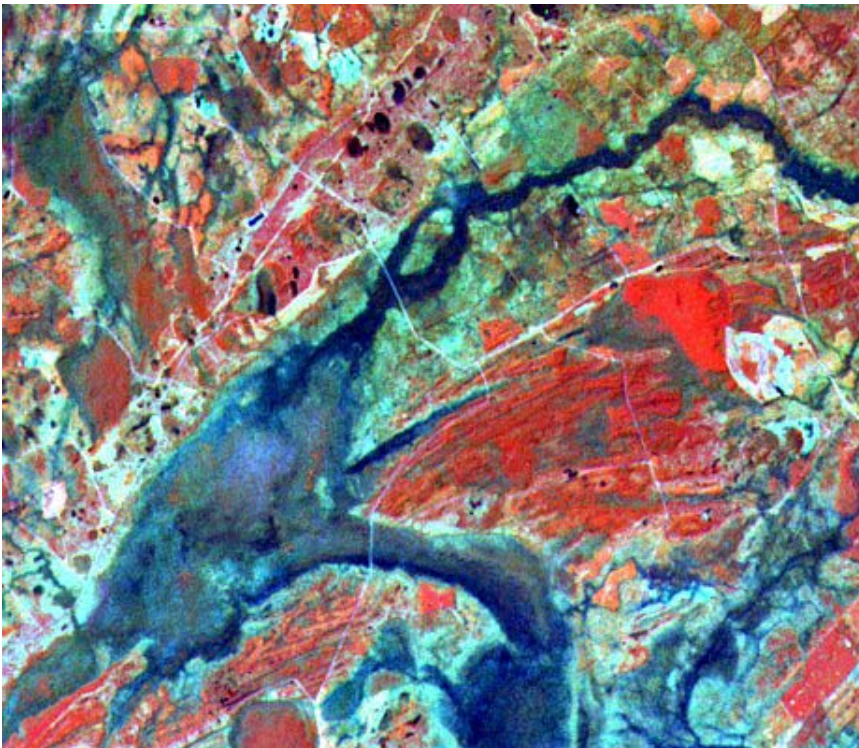


Figure 7: Landsat study area subset for 1989 in Bands 4, 5, 3 (RGB)

Table 3: Band statistics for Landsat study area subset for 1987

Band statistics for subsetting 1987 image

Band #	Min	Max	Mean	Median	Mode	Std. Dev.
1	44	128	56.04	56	56	2.24
2	16	68	21.5	21	21	1.56
3	11	80	16.82	16	16	2.39
4	7	92	54.61	54	53	5.43
5	6	173	42.98	42	39	8.76
7	4	109	13.53	13	12	4.19

Table 4: Band statistics for Landsat study area subset for 1989

Band statistics for subsetting 1989 image

Band #	Min	Max	Mean	Median	Mode	Std. Dev.
1	43	161	62.5	62	62	2.43
2	10	84	23.93	24	23	1.59
3	5	142	25.34	25	24	2.97
4	7	175	50.63	51	56	10.43
5	2	153	57.73	56	53	10.43
7	2	168	23.92	23	23	4.85

visually compared the images to see if the land cover features matched. This made it clear that the images were not geo-referenced to each other. Accurate geo-referencing is very important for change detection so that the pre-event and post-event images match each other as closely as possible spatially, otherwise relative locations of all objects will be shifted in the images giving erroneous change detection results. The only differences detected by our methods should be the actual land cover changes.

Geometric correction using Polynomial transform was selected with the goal of attaining a resultant RMS error of less than 1 pixel by 1 pixel. The post-event image of 1989 was treated as reference and the 1987 image was the input image. A pixel for Landsat TM represents a 28.5-meter by 28.5-meter square (USGS Image header file). Twelve ground control points (GCP's) were selected such that there would be roughly three rows of four GCP's each, so that the images could be geo-referenced to each other. The nearest neighbor resampling method is preferred for rectification because it preserves the original values of the input pixels (ERDAS Imagine 8.7 field guide). The actual RMS error obtained was 13.0057 meters, which is slightly less than one-half of a pixel, which is acceptable. The rows and columns were again subsetted to make sure of exact match. The final images had 400 rows and 462 columns denoting height and width respectively. The upper left UTM coordinates are 625071.50 and 3672934.00 while the lower right UTM coordinates are 638210.00 and 3661562.50 respectively.

The resulting geometrically corrected images were then processed for radiometric correction. For the USGS radiometric correction procedure the thermal band six should be stripped out from the images, which was accomplished for both the unsigned 8-bit images. Mr. DeWitt Braud supplied the necessary radiometric model files for conversion

of Landsat 4 and 5 image files into a Landsat 7 image file, and an Excel spreadsheet, which included a Julian date model, for the calculation of Earth-Sun distance. The tables used in conversion are listed in Appendix B (Chander and Markham 2003). The radiometric models needed an eccentricity model and solar elevation as input, which was obtained from the USGS supplied header files for both the images.

The output of the reflectance procedure is a floating-point image, which was used for analysis for Tasseled Cap transform only. The DN input images were used for all other analysis. The DN input images were then subsetted to have only Bands 4, 5, and 3, the band statistics are shown in Tables 3 and 4.

3.3.2 Hybrid Image Classification and Change Detection

The unsupervised method was used initially because the study area is small and it was better to discover spectral classes for the more complicated 1987 image. However, due to low accuracy of the initial classification and problems in proper discrimination between some land cover classes, hybrid classification approach was used. Only bands 3, 4, and 5 were used for classification. The unsupervised method was used to generate a signature file with 100 classes. Each spectral class was then checked individually to ensure that univariate standard deviation was less than 10 % of the mean value for all the three bands under consideration. Histograms for the three bands were also checked to ensure that they had a normal appearance. Spectral classes, which failed both these checks, were eliminated from further analysis. Afterwards the pixel count column was copied to the probability column, and this final signature file was used for generation of a supervised classification.

With the help of the USGS National Land Cover Data (NLCD) image for South Carolina, reference aerial photos, and GPS field data I then lumped these classes into four classes following USGS NLCD scheme. Table 5 shows the classification scheme used in the study. The roads present in the study area belong to the transport category in the urban land cover class, but since the roads are sometimes spectrally obscured by the cultivated row crops, and the percentage of roads in the study area is minuscule, so they are combined into a single land cover class called cultivated row crops / transitional barren (C.R.C / T.B). A major reason for lumping classes together is avoid the difficulty of finding truly random reference points for such a small land cover class.

Both the images were then recoded (Interpreter ==> GIS Analysis ==> Recode) with the same class values to ensure that it contained only the following four classes: water, woody wetland, forest, and cultivated row crops/transitional barren. The recoded images were then fed to the clump function for clumping a contiguous group of pixels in a single thematic class, (Interpreter ==> GIS Analysis ==> Clump) with 4 connected neighbors to smoothen out the image and reduce the output image's grainy appearance. It assigns an isolated pixel surrounded by pixels of a dominating land cover class to be merged into the surrounding class (ERDAS Imagine 8.7 field guide). Finally, the clumped pixels were then fed to the Eliminate GIS function (Interpreter ==> GIS Analysis ==> Eliminate) to eliminate clumps smaller than 2 hectares. Initially a 1 hectare eliminate filter was used, which produced a grainier appearance but after comparing with a 2 hectare eliminate filter I felt that the visual appearance of the final change detection image would be slightly improved with a 2 hectare eliminate filter.

Table 5: Classification scheme

Land cover class	Description (Land use)	Recoded value
Water	Streams, Lakes, and Rivers.	1
Woody Wetland	Forested wetland or shrubland vegetation and where either soil or substrate is saturated with water.	2
Forest	Deciduous, Evergreen, Mixed forest with logging and including downed trees.	3
Cultivated row crops / transitional barren	Herbaceous vegetation and crops. Clear-cut forests in various stages of regrowth.	4

(Modified and adapted from: Anderson *et al.* 1976, Cablk *et al.* 1994, Lillesand and Kiefer 2004, Read and Lam 2002, USGS NLCD 2000)

After the individual images were classified, to generate a change detection image, a GIS matrix analysis was performed (Interpreter ==> GIS Analysis ==> Matrix). The default “Intersection” operation was selected with an 8-bit unsigned output. The result was an image with from-to change classes. A from-to class with more than 5000 pixel count was color coded in the change detection image. The rest of the from-to change classes were ignored to reduce the complexity of interpretation due to presence of many different colors. An Interpreter ==> GIS Analysis ==> Summary command was also run on the individual classifications, with the zone file as the 1989 classification and the input file as the 1987 classification.

3.3.3 Digitization of Aerial Photographs

Two aerial photographs were scanned in the CADGIS Lab of Louisiana State University using an Advent Colortrac 52” Color scanner with a maximum resolution of 800 dpi. The 20” by 20” images, with 1-inch margins on all sides, were scanned with three cameras corresponding to RGB into TIFF format. They were digitized with a 0.66-meter pixel resolution. These were then imported to ERDAS Imagine 8.7 as a native .img file, and geometrically corrected using polynomial transform individually to the 1989 Landsat image for easier pixel-to-pixel comparison of the input and reference data for accuracy assessment. A difficulty found during the geometric correction procedure was the absence of quality GCP’s. Geometric correction was more time consuming for the aerial photographs to the reference 1989 image compared to the registration of Landsat scene of 1987 to the reference of 1989. The actual number of GCP’s was chosen such that they were not obscured by vegetation or wetland in each air photo image. GCP’s were chosen at visible road intersections, or corner areas, which were unchanged

in the input and reference images. The number of GCP's for the 1987 air photo to 1989 Landsat image registration were 10 with a 14.08 meter RMS error, and for the 1989 air photo to the 1989 Landsat reference was 11 GCP's with a 12.92 meter RMS error. It should be noted that the digitized aerial photographs were set to the exact same projection/spheroid as the Landsat images. The aerial photographs were also resampled to the lower resolution of the Landsat TM images of 28.5 meters by 28.5 meters. Resampling allowed me to do a Geo link between the two viewers, and make it easier to find land cover features, but the scanned aerial photograph was used for classification accuracy. This resulted in a grainier looking output photos with hard edge transitions, which does not totally correspond to the original due to the mismatched spatial scales.

3.3.4 Accuracy Assessment of Classification

The accuracy assessment for the study used a stratified random sampling scheme with a 3x3 window size pixel majority filter (Congalton 2001). The class values were assigned based on a window size of 3, with a 'Clear Majority' window majority rule, and a 'Discard Window' action in absence of a majority. Initially, a total of 256 points for accuracy assessment per image were generated using stratified random sampling and selecting only the classified land cover classes and excluding the default unclassified class. This number of accuracy assessment points ensured that all of the land cover categories would contain the recommended 50 points (Congalton 2001). Since the study area in the air photo is approximately 8.8 km by 8.8 km, this translates to about 308x308 pixels, which yields 94,864 pixels available for reference. However, the subsetted Landsat scenes contained 400 rows and 462 columns, which yield 184,800 pixels. The

additional area was covered in this study because the hurricane damage was noticeable in the Wambaw swamp and the Coffee creek swamp.

Initially, I selected stratified random sampling with the default 10 minimum points, but since the water class with a very small area covered in the 1987 image was also elevated to 10 points, the overall accuracy was reduced, so minimum points was discarded from further analysis, just a regular stratified sampling was used. The random points were sometimes generated on the edge of the aerial photographs where there was no data, or outside of the spatial extent of the air photos; such points were deleted from further analysis. Since more than a third of points were deleted due to these reasons in both the 1987 and 1989 accuracy assessment, additional random points were added in increments of 30 for selected land cover classes to make sure each land cover class would be covered with at least 50 points. Due to this, about 194 and 266 random points were finally selected for accuracy assessment in the 1987 and 1989 images respectively. The water class was not represented with the required 50 sample points, because it had an area representing less than 1 % area for the 1987 classification. The points would not have been truly random but would have been highly clustered.

Classified points were finally compared to the digitized aerial photographs to determine the land cover class of the input data within a given area; and not as a true pixel-by-pixel comparison, to partially overcome the mismatch in the spatial scales between the Landsat 28.5 meter resolution and the down sampled reference air photos. After the completion of the reference and input points matrix a report was generated, which consisted of the user's accuracy, producer's accuracy, overall accuracy, the confusion matrix, and the Kappa statistics.

3.3.5 Field Trip: GPS Points Collection Procedure and Interviews

Initially, before the field trip the cultivated row crops class was classified as barren. After a meeting with Ms. Antoinette “Tonee” Davis, Forester, USDA Forest Service, FMNF Wambaw Ranger District, I got the information that there is no barren class inside the FMNF, it was therefore necessary to redo the classification procedure. She further told me that the cultivated row crops class is usually where the shrubs and grasses like Bahia grass, rye grass, sunflower etc. are planted, specifically for sustaining the quail and turkey population in the FMNF. A couple of landowners, James A. Matthews and Gloria Smock, informed me that the abundant sand encountered in the study area on the dirt roads, near road intersections, and adjacent clearings was due to past hurricanes including Hugo. This process dumped many sediments into the Wambaw and Coffee creek swamps, and Little Wambaw wilderness allowing for their regeneration due to the creation of short lived barren areas of sandy flats (Conner 1998).

The GPS points were chosen to be collected as distinct point features for the four land cover classes in the study: water, woody wetland, forest, and cultivated row crops/transitional barren. Unfortunately, most of the cultivated row crops class inside the study area is privately managed and for the “Thompson Corner” and “Mechaw” areas, which are the biggest cultivated row crops areas, no GPS points could be taken since permission was not acquired. GPS positions were taken along roads and wilderness trails identifiable in the 1987 and 1989 image hard copies. GPS positions were taken for a maximum of 300 meters distance on either side of the roads and wilderness trails to avoid being lost in the dense vegetation. GPS points were recorded in the UTM, GRS 1980, NAD 83, with Zone 17 North setting with a minimum number of satellites set as four.

Positions were automatically discarded when insufficient satellites were present or there was poor geometry for the satellites.

Post-processing was performed in Baton Rouge; the data was uploaded into a PC, and then differentially corrected using the default “Smart Code and Carrier Phase Processing”. The reference station of CORS, Florence Darlington Technical College, South Carolina, which was 130 km from the study area where the points were logged was selected. The data for 53 GPS points, which was differentially corrected, was then exported to the “Sample Arc/INFO (NT) Generate Setup” which produced two files: a GPS Point Id vs. Feature class and the GPS Point Id vs. UTM coordinates. Seven more positions were added manually, all from the Wambaw swamp area, which could not be logged due to poor geometry problems. These positions were recorded in a scrapbook, by noting down adjacent GPS positions with the approximate offsets in meters where recording was possible.

ArcView was used to join these two tables and create a combined shapefile with an “Add Event theme” option, and was then used in ERDAS Imagine for an overlay over the classified images for validation.

3.3.6 PCA Change Detection Procedure

For PCA, only the geometrically rectified 3 band DN images are used as input. The thermal band is not used in the analysis to maintain consistency with hybrid classification. Output is chosen to be stretched to 8-bit unsigned, with the desired principal components as six. The eigen matrix and eigenvalues are written to separate files. This procedure is repeated for both the 1987 and 1989 images.

3.3.7 TCT Change Detection Procedure

For TCT, the radiometric pre-processed images with floating point is used as input, with the output stretched to 8-bit unsigned, and the selection of the coefficients for either Landsat 4 or 5 according to the inputs from the header files. The thermal band is not used in the analysis because of the need for radiometric correction, which assumed an absent thermal band. This procedure was repeated for both the 1987 and 1989 images. The TCT equations for the Landsat 4 and Landsat 5 for the generation of the brightness, greenness, and wetness are listed in Appendix C.

3.3.8 Fractal Change Detection Procedure

For fractal analysis, the same subsets as that for the PCA and hybrid classification are used as input. To maintain consistency with the other analyses, the thermal band is stripped out for analysis. Moreover, NDVI derived from the two images, instead of individual bands were used for change detection. Therefore, the NDVI .img files are imported to the ERDAS 7.X LAN format, and fed to the ICAMS (Image Characterization and Modeling Systems) software, which produces separate NDVI .BSQ file for further analysis.

A “Local Triangular Prism” with varying moving window sizes of 9x9 pixels to 33x33 pixels, with a fixed five steps increasing arithmetically and geometrically, with the floating point images stretched to 8 bits with 2 standard deviations, was run on the two 1987 and 1989 NDVI files to produce a local fractal representation of the NDVI images. The moving window is experimented because a large number of methods for spatial analysis in a wide range of scientific fields are conceptually based on the moving window for discerning spatial patterns (Dale *et al.* 2002, StOnge and Cavayas 1997).

Finally, the resulting fractal transformed image files, which are in .BSQ file format, are fed to the difference function in ICAMS to produce a corresponding change detection output image.

To examine whether land cover change can be measured by the change in fractal dimension values. A fractal dimension to land cover classification Zonal Statistics for both 1987 and 1989 was performed using the Interpreter ==> GIS Analysis ==> Summary command with the fractal image file used as the input file and the classified file used as the zone file. The summary command requires a thematic integer image so the floating point local fractal file had to be converted. The file was imported into Imagine with the 'Generic Binary' option as an IEEE 32-bit float data type, an image record length of 1848, with the rows and columns equal to 400 and 462 respectively. The 'Map Info' and the projection information for this imported file were then set equal to the classified file. Model Maker was then used to multiply the D values by 100 and round them out to produce a 16 bit unsigned thematic file. A D value of 2.81 would thus be represented as 281 in the file.

CHAPTER 4: RESULTS AND DISCUSSION

This chapter will present the results of the study with the following sequence: accuracy assessment of classification, change detection through classification, GPS results, PCA analysis, TCT analysis, and finally the Fractal analysis using the modified triangular prism method as implemented in ICAMS.

4.1 Accuracy Assessment of Classification

Figure 8 shows the study area as acquired from a scanned hard copy printout of FMNF from the USDA Forest Service, Wambaw Ranger District. Figures 9 and 10 show a photo of a typical woody wetland area. Figure 11 and 12 show the resultant classified images, and Figure 13 shows the changes. The full error matrix, the user's and producer's accuracy tables, Kappa statistics are presented in Tables 6 and 7 for the 1987 and 1989 classified images. A look at the pre-event image error matrix dated October 14, 1987 yields us an overall image classification accuracy of 81.44 % and for the October 11, 1989 post-event image is 85.71%. The overall Kappa statistic for the 1987 image is 0.7183, and for the 1989 image is 0.8004. The relative area of each individual land cover class for the October 14, 1987 and the October 11, 1989 classifications is as follows in Table 8. Overall classification accuracy for the 1987 is lower than the 1989 image, and it is due to the fragmented nature of the 1987 image during the classification process.

4.1.1 Results for Individual Land Cover Classes

The most significant finding is that the percentage of water in the post event image is 4.07% (607 hectares), which clearly substantiates the findings of Cablk *et al.* (1994), that the hurricane caused an increase in water due to the storm surge. The

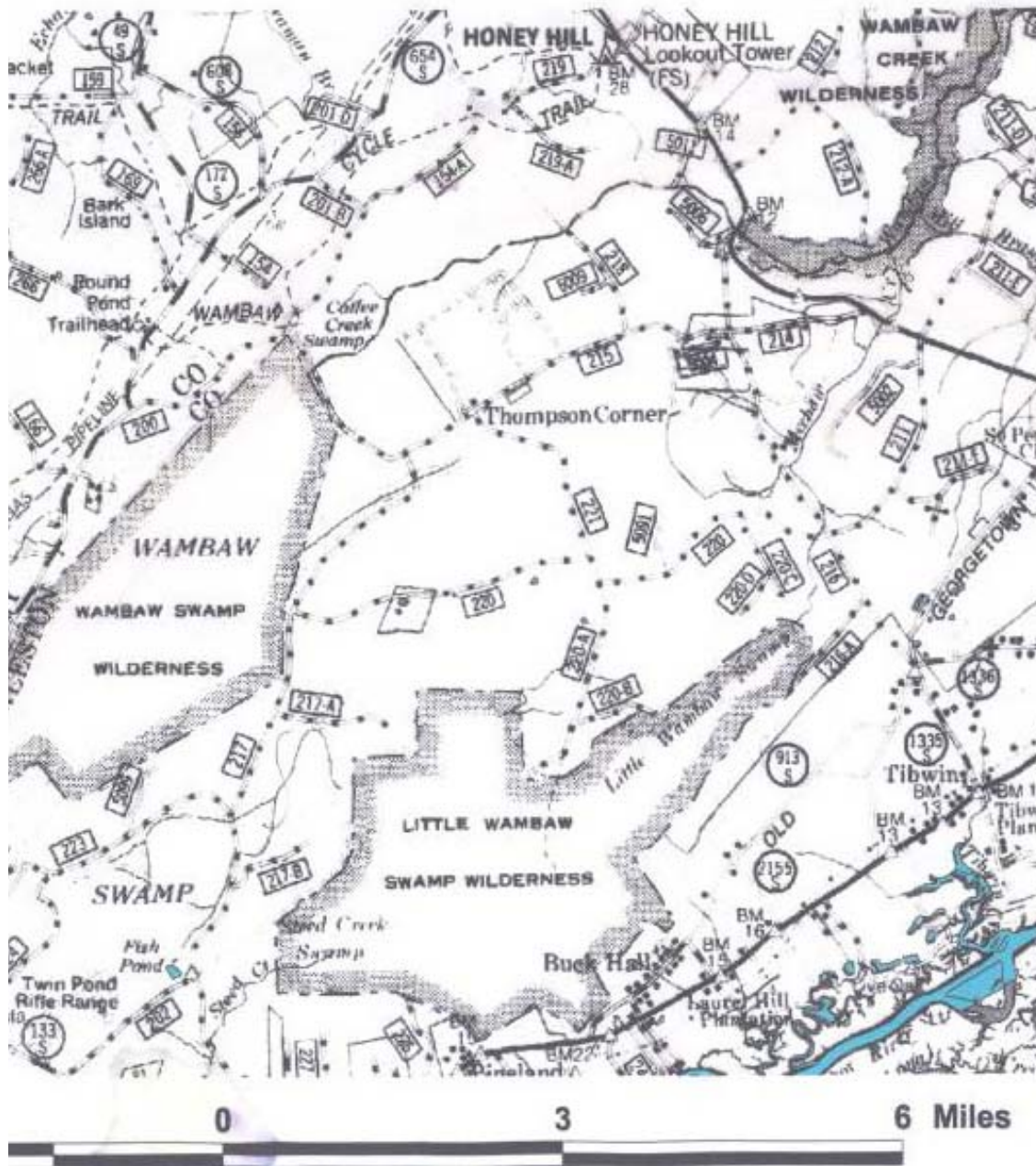


Figure 8: ArcView printout of the study area

(Source: USDA Forest Service, Francis Marion National Forest, Wambaw Ranger District, 2004)

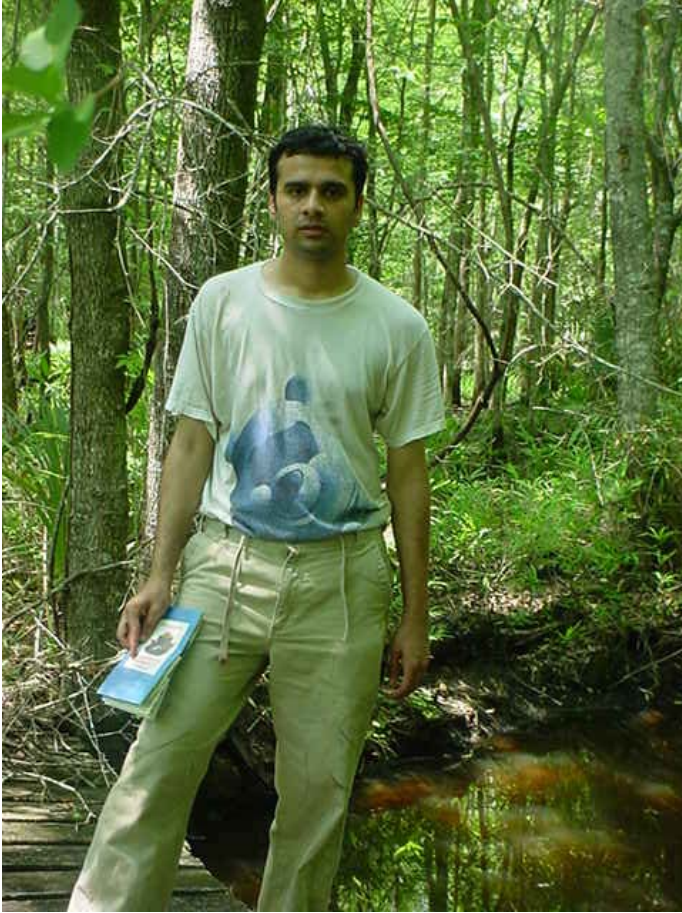
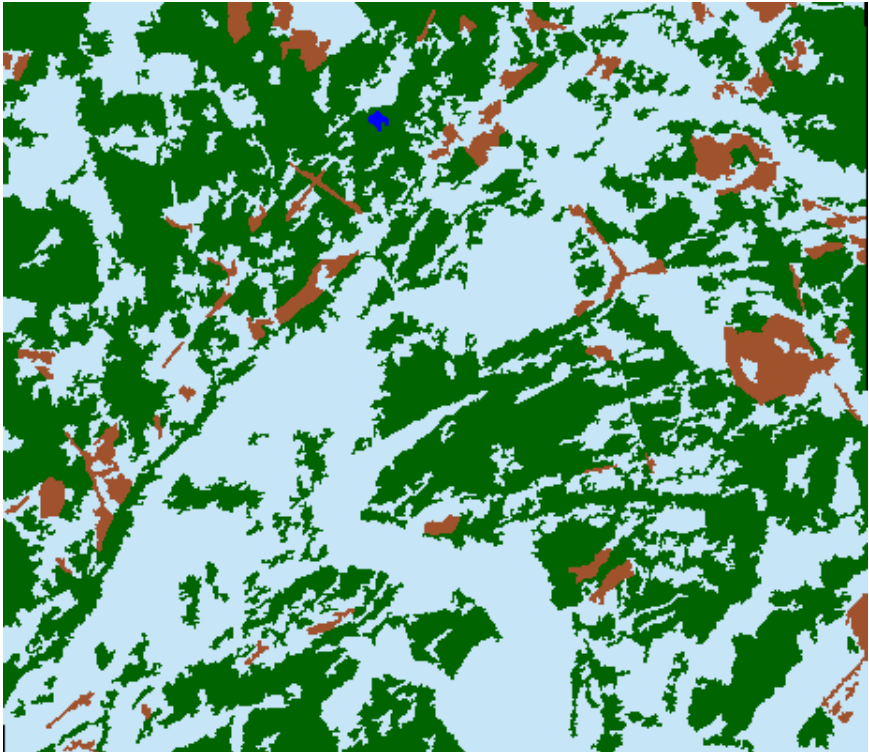


Figure 9: A woody wetland scene from the Coffee creek swamp



Figure 10: Woody wetland scene from the Wambaw swamp



- Water
- Woody Wetland
- Forest
- Cult. row crops/ trans. barren

Figure 11: Classified image for 1987

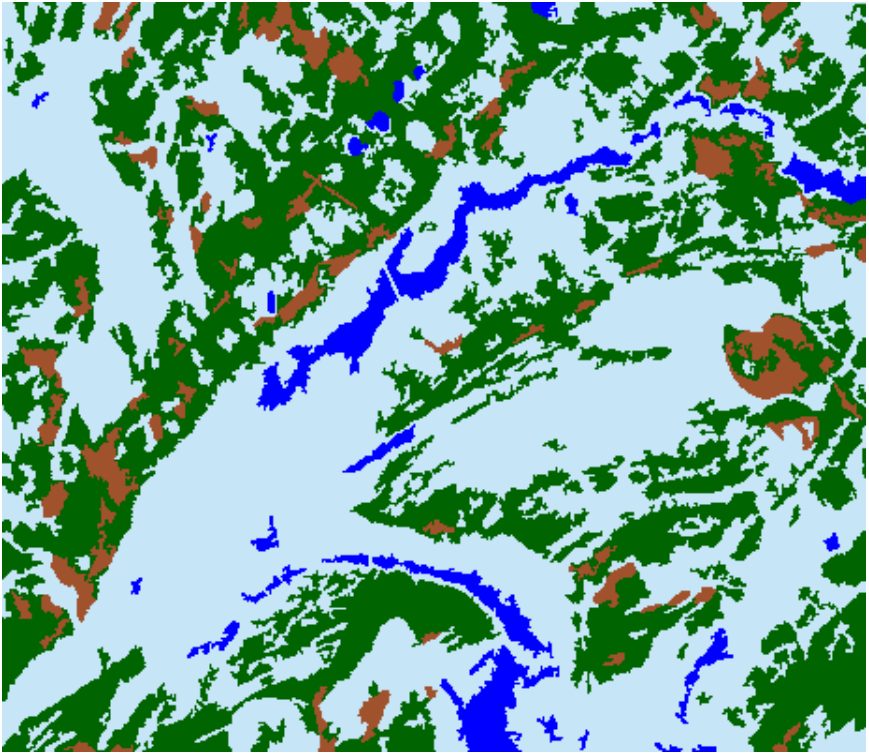


Figure 12: Classified image for 1989

Table 6: 1987 Classification statistics

Classified landcover data	Reference landcover data				Classified Totals	Number Correct	Producers Accuracy	Users Accuracy	Kappa
	Water	Woody wetland	Forest	Cult. row crops/ trans. barren					
Water	0	0	0	0	0	0	0.00 %	0.00 %	0.0
Woody Wetland	0	65	5	1	71	65	74.71 %	91.55 %	0.8468
Forest	0	13	51	3	67	51	83.61 %	76.12 %	0.6517
Cult. row crops/trans. barren	0	9	5	42	56	42	91.3 %	75.00 %	0.6723
Reference Totals	0	87	61	46	194	158			

Overall Classification Accuracy = 81.44%
 Overall Kappa Statistics = 0.7183

Table 7: 1989 Classification statistics

Classified landcover data	Reference landcover data				Classified Totals	Number Correct	Producers Accuracy	Users Accuracy	Kappa
	Water	Woody wetland	Forest	Cult. row crops/ trans. barren					
Water	44	7	0	0	51	44	100 %	86.27 %	0.8355
Woody Wetland	0	95	7	0	102	95	82.61 %	93.14 %	0.8791
Forest	0	10	49	2	61	49	75.38 %	80.33 %	0.7397
Cult. row crops/trans. barren	0	3	9	40	52	40	95.24 %	76.92 %	0.7260
Reference Totals	44	115	65	42	266	228			

Overall Classification Accuracy = 85.71%
 Overall Kappa Statistics = 0.8004

Table 8: Classified area of land cover classes for 1987 and 1989

Land cover class	Area in hectares 1987	Percent area (%) 1987	Area in hectares 1989	Percent area (%) 1989
Water	5.35	0.04	607	4.07
Woody wetland	7455.16	50.01	8214.2	55.1
Forest	6739.48	45.21	5362.15	35.97
C.R.C/T.B	706.83	4.74	723.47	4.85
Total area	14906.82		14906.82	

distribution of the woody wetland areas has become more widespread connecting a contiguous area over the Wambaw, Coffee creek swamps, and the Little Wambaw wilderness. Woody wetland area has been lost outside the contiguous swamps mostly to the forest class; this is confirmed from Figure 13.

The forest class has declined from 45.21% (6739.48 hectares) to 35.97% (5362.15 hectares) from 1987 to 1989. Figure 13 visually confirms that a major portion of the 1987 forest area has been lost to woody wetland, water, and cultivated row crops classes in decreasing order of area outside the three designated swamps.

The total area of cultivated row crops/transitional barren class has increased slightly from 4.74% (706.83 hectares) to 4.85% (723.47 hectares) due to the hurricane. But the maximum gain has been recorded by the water and woody wetland classes at the expense of the forest class, which is interesting. Looking at the Landsat TM subset of the study area by overlaying it on top of the original Landsat scene acquired from USGS as shown in Figure 5 it is clear that the storm surge would have come in from the Bulls Bay, which protrudes landwards. The path of the hurricane was to the west of the study area on 21-24 September 1989 (Hook *et al.* 1991), and the storm surge from the hurricane would have penetrated the study area. During the intervening period from the end of the hurricane and the Landsat scene acquisition date of 11 October 1989, the surge might have caused the increase in moisture content, which show up in the post-event classification. Cablk *et al.* (1994) state that the storm surge, which was approximately 4 meters above the mean sea level, traversed the barrier islands adjacent to the Bulls Bay on the coast, and temporarily caused salt water flooding. From the NCDC website (NCDC 2004) the month of October 1989 caused 4.18 inches of precipitation with a rank

of 84 in the period of record from 1895 to 2004. This proves that the classification was not biased towards enhanced moisture classes.

4.1.2 Results for Errors of Commission (User's Accuracy) and Omission (Producer's Accuracy)

It should be recalled from the literature review that user's accuracy represents reliability of classified pixels and producer's accuracy measures the performance of the analyst in taking samples for each class.

The errors of omission (producer's accuracy) for the woody wetland and forest classes, and error of commission (user's accuracy) for the forest and cultivated row crops/transitional barren class were the major limiting factor affecting overall accuracy for the 1987 image. A possible reason for the poor user's accuracy for the forest and the cultivated row crops/transitional barren class in the 1987 classification is due to the fragmented occurrence of the classes in the original image. This is possibly the same reason why it was hard to classify the woody wetland and forest classes by the analyst in 1987 resulting in low producer's accuracy for the woody wetland and forest classes in 1987.

The major factor limiting the overall accuracy of the 1989 image was the low user's accuracy (error of commission) and the low producer's accuracy (error of omission) for the forest class. A possible reason for the low user's accuracy in the 1989 classification for the forest class is due to the homogeneous nature of the study area after the hurricane, which made it difficult to represent small forested areas. A probable reason for the low producer's accuracy for the forest class for 1989 is due to a possible misclassification around the Wambaw swamp and Little Wambaw wilderness.

4.1.3 Kappa Analysis Results

As can be recalled from the literature review section, as Kappa approaches 1.0, the classification is accurate, and as it approaches 0, it indicates the classification is not better than the random agreement between the reference and the classified pixels.

Overall, the conditional kappa was better for the 1989 image at 0.8004 as compared to 0.7183 for the pre-hurricane image. For the 1987 image, the conditional kappa values for the forest and the cultivated row crops/transitional barren class were the lowest at 0.6517 and 0.6723 respectively, and the highest values was recorded for the woody wetland class at 0.8468. For the 1989 image, the conditional kappa values for the forest and C.R.C/T.B class were the lowest at 0.7397 and 0.7260 respectively and the values for the woody wetland class the highest at 0.8791.

In both the image classifications the combined woody wetland class was the most accurately represented as their class conditional kappa was the highest compared to the other classes of water, forest, and C.R.C/T.B classes. The forest conditional kappa was low for the 1989 image at 0.7397, much better than the 0.6517 for the 1987 image, indicating that the classification for the 1989 image for forest class was more accurate.

4.2 Change Detection Through Classification

Figure 13 is the change detection output produced by the matrix intersection of the 1987 and 1989 images of the study area. Table 9 gives us the from-to change classes for the change detection classification. It is clear that the forest area that has been ‘lost’, a total of 1377.33 hectares due to the hurricane and has become transformed into water and woody wetland classes. The most interesting finding from Table 9 is the conversion

of the woody wetland class into forest class to the extent of 2206.56 hectares. From looking at the change detection output image, the light green color denotes this finding.

This conversion can be explained possibly due to the storm surge, which inundated the Wambaw creek, Little Wambaw wilderness, and the Coffee creek swamps. Some of the heavily flooded area has remained as water, the low-lying areas saturated with water are classed as woody wetlands, while the receding areas close to the edge of the swamps has been classified as forest. The post-event scanned aerial photograph before geometric correction contains visible uprooted and/or broken trees, known as blowdown/standing dead, which are evident when we zoom into the study area, but which are missing in the Landsat TM scenes (Cablak *et al.* 1994).

The 'lost' forest area actually contributes to make it evident that the Wambaw creek, Little Wambaw wilderness, and the Coffee creek swamps is contiguous. On the other hand, the change detection image depicts the regenerated forest totally outside the three swamp areas, and in places where contiguous patches of forest were present before the hurricane struck the study area. The major area which was regenerated into woody wetland was the forest – woody wetland class, which has an overall area of 3640.83 hectares, mostly located inside of the Wambaw swamp, Coffee creek swamp, and the Little Wambaw wilderness, denoted by the Magenta color. As a result, the hurricane makes the woody wetland and the forest boundary easier to distinguish in the post-hurricane image, and finally in the change detection image. The unchanged woody wetland area is represented by a light blue color, the unchanged forest area is denoted by a dark green color. Blue color represents the conversion of the woody wetland area into water class.

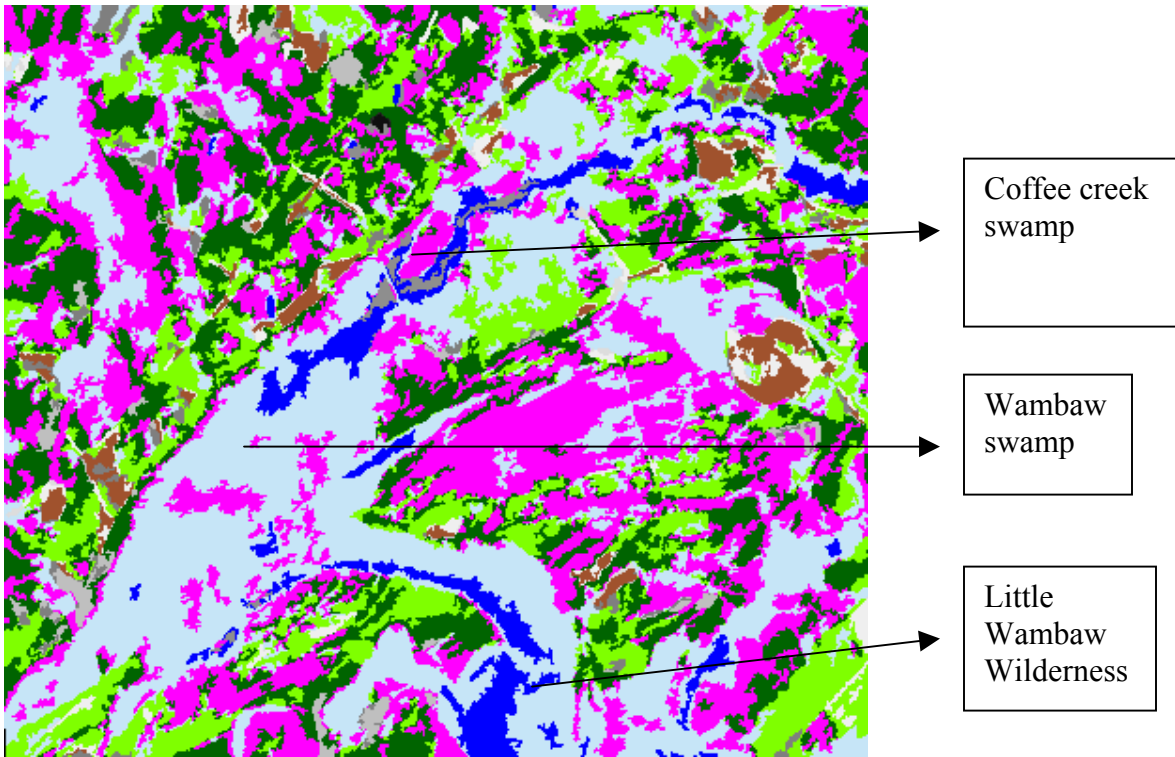


Figure 13: Change detection classified image

	Wetland to water conversion
	Woody wetland
	Wetland to Forest conversion
	Forest to wetland conversion
	Forest
	Cult. row crops / trans. barren

Table 9: From-to change classes “Summary” with area in hectares

1989	Water	1987 Woody wetland	Forest	Cult. row crops/ trans. barren	Total
Water	4.22 (0.7 %)	0.24 (0 %)	0.89 (0.02 %)	0.00 (0 %)	5.35
Woody wetland	526.18 (86.69 %)	4536.01 (55.22 %)	2206.56 (41.15 %)	186.41 (25.77 %)	7455.16
Forest	74.89 (12.34 %)	3640.83 (44.32 %)	2842.63 (53.01 %)	181.13 (25.04 %)	6739.48
Cult. row crops/ trans. barren	1.71 (0.28 %)	37.12 (0.45 %)	312.07 (5.82 %)	355.93 (49.20 %)	706.83
Total	607 (100 %)	8214.2 (100 %)	5362.15 (100 %)	723.47 (100 %)	14906.82

N.B – The zone file was the 1989 classification while the input classified file was the 1987 classification.

4.3 GPS Point Survey Results

An example overlay of the GPS points plotted in yellow on the 1989 classified image is shown in Figure 14. The points are all clustered in areas, which are accessible from the roads and wilderness trails, and are not truly random. The road names are the internal FMNF designated roads and are marked in Figure 14.

Table 10 shows the GPS id's with their UTM X and Y locations and the mappings for the 2004 using GPS, recoded 1987, and recoded 1989 images. GPS locations were used to check for major classification problems and not for accuracy assessment due to the gap of almost 15 years after the hurricane occurred in 1989 and the current year of analysis of 2004.

4.4 Change Detection Using PCA

Only the first three components were chosen for analysis because they have variances $> 1\%$. For easier visual comparison, the individual principal components are displayed together for 1987 and 1989 in Figures 15 through 20. The principal component variance for the two images is shown in Table 11. For PC1 component, the 1987 image contains 74.43% variance whereas the 1989 image contains about 62.5% variance. Both images show clearly the existence of the swamp of Wambaw creek, which was not revealed clearly during the classification procedure. The 1989 PC1 image also displays a clear separation of the swamp from the surrounding feature classes with its high moisture content due to the hurricane. The Cultivated row crops/transitional barren feature class is displayed clearly in PC1 for the 1987 image, but due to the increased area of the flats due to the hurricane, there is an increased albedo associated with the 1989 image. The Cultivated row crops/transitional barren feature for 1987 PC1 is also the brightest

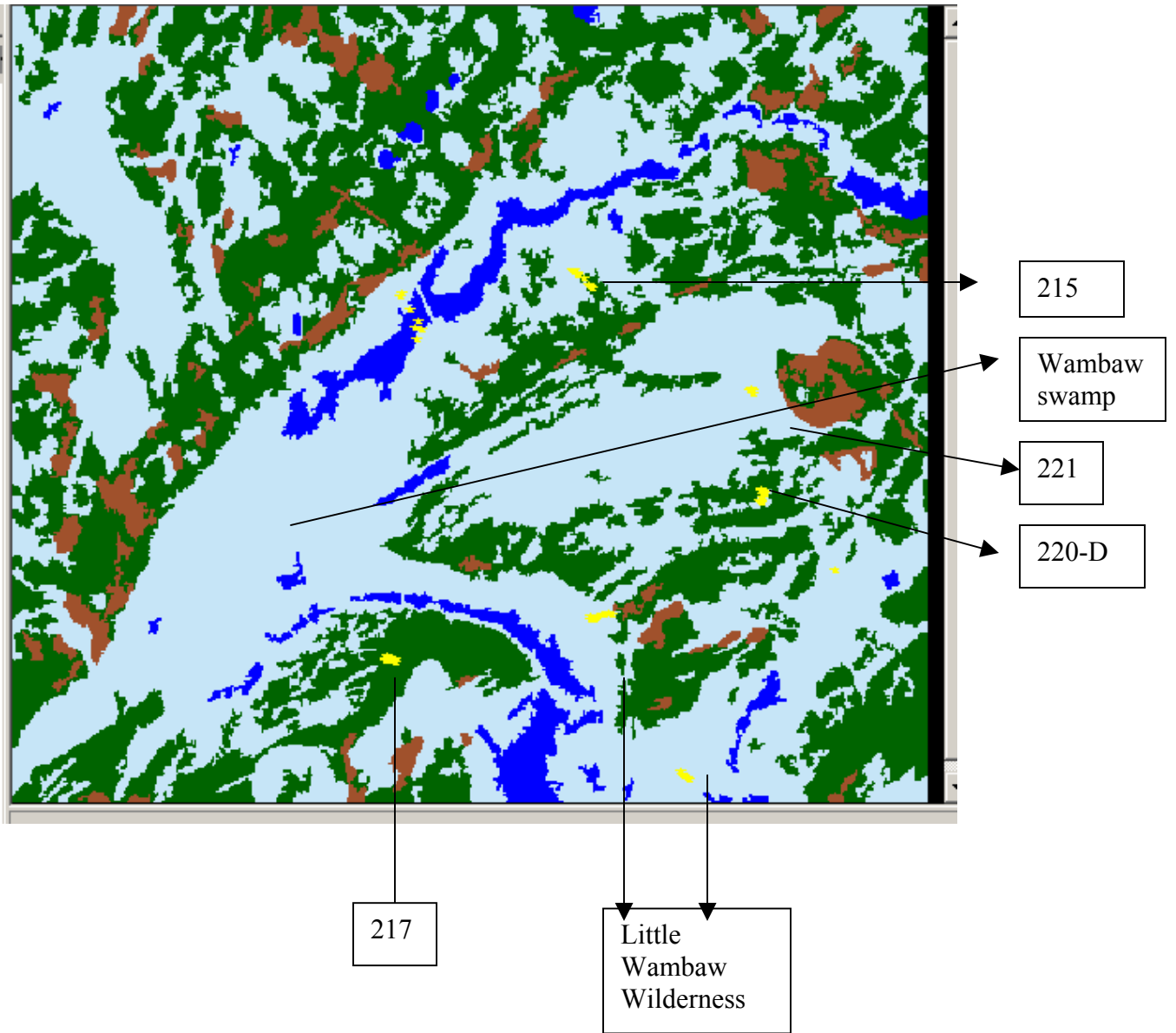


Figure 14: 56 GPS points in yellow overlaid on the 1989 classified image

Table 10: GPS point locations and class values for 1987, 1989, and 2004

GPS point id	Easting	Northing	GPS 2004 land cover classification	1987 classification	1989 classification
1	630416.793	3663555.473	Forest	Forest	Forest
2	630405.83	3663538.058	Forest	Forest	Forest
3	630432.686	3663559.997	Forest	Forest	Woody Wetland
4	630448.591	3663569.791	Forest	Forest	Forest
5	630445.675	3663588.478	Forest	Forest	C.R.C / T.B
6	630498.557	3663525.891	Forest	Woody Wetland	Forest
7	630526.959	3663518.886	Forest	Woody Wetland	Forest
8	630548.267	3663509.447	Forest	Woody Wetland	Forest
9	630546.467	3663547.896	Forest	Woody Wetland	Forest
10	633363.881	3664176.004	C.R.C / T.B	Woody Wetland	Woody Wetland
11	633354.105	3664125.405	Forest	Forest	Woody Wetland
12	633380.184	3664110.837	Forest	Forest	Forest
13	633405.734	3664126.883	Forest	Forest	Woody Wetland
14	633432.347	3664139.525	Forest	Forest	C.R.C / T.B
15	633434.223	3664152.101	Forest	Woody Wetland	Woody Wetland
16	633448.032	3664157.979	Forest	Forest	Woody Wetland
17	633540.16	3664197.83	C.R.C / T.B	Forest	Forest
18	633539.109	3664197.332	C.R.C / T.B	Forest	Forest
19	633617.011	3664210.383	C.R.C / T.B	Forest	Forest
20	633665.792	3664186.349	C.R.C / T.B	Forest	C.R.C / T.B
21	634650.424	3661944.726	Woody Wetland	Forest	Woody Wetland
22	634682.145	3661901.529	Woody Wetland	Woody Wetland	Woody Wetland
23	634682.966	3661902.005	Woody Wetland	Woody Wetland	Water
24	634718.947	3661869.668	Woody Wetland	Woody Wetland	Woody Wetland
25	634745.836	3661848.35	Woody Wetland	Forest	Water
26	634777.531	3661823.433	Woody Wetland	Forest	Woody Wetland
27	636888.121	3664832.775	C.R.C / T.B	Forest	Water
28	635841.554	3665962.827	C.R.C / T.B	Woody Wetland	Forest
29	635815.396	3665956.624	C.R.C / T.B	Forest	Woody Wetland
30	635823.901	3665982.613	C.R.C / T.B	Forest	Forest
31	635858.901	3665938.899	C.R.C / T.B	Woody Wetland	Water
32	635849.626	3665902.865	C.R.C / T.B	Woody Wetland	Woody Wetland
33	635835.94	3665869.46	C.R.C / T.B	Forest	Forest
34	635828.491	3665821.182	C.R.C / T.B	Forest	Forest
35	635818.472	3665801.337	C.R.C / T.B	Forest	Forest
36	635802.462	3665821.433	C.R.C / T.B	Forest	Forest
37	635702.082	3667364.369	C.R.C / T.B	Forest	Forest
38	635702.779	3667409.551	C.R.C / T.B	Forest	Forest
39	635669.652	3667421.753	C.R.C / T.B	Forest	Forest
40	635657.936	3667403.032	C.R.C / T.B	Forest	Forest

(table cont'd)

GPS point id	Easting	Northing	GPS 2004 land cover classification	1987 classification	1989 classification
41	633377.1	3668870.264	Woody Wetland	Woody Wetland	Woody Wetland
42	633353.855	3668890.537	Woody Wetland	Woody Wetland	Woody Wetland
43	633335.361	3668907.236	Woody Wetland	Forest	Forest
44	633270.041	3669010.497	Woody Wetland	Forest	Woody Wetland
45	633184.397	3669050.502	Woody Wetland	Woody Wetland	Woody Wetland
46	633162.349	3669085.017	Woody Wetland	Forest	Forest
47	633117.208	3669117.683	Woody Wetland	Woody Wetland	Woody Wetland
48	633107.532	3669128.611	Woody Wetland	Woody Wetland	Woody Wetland
49	633081.227	3669156.449	Woody Wetland	Woody Wetland	Forest
50	630861.265	3668126.707	Woody Wetland	Woody Wetland	Forest
51	630920.15	3668265.086	Woody Wetland	Forest	Forest
52	630884.819	3668403.464	Woody Wetland	Woody Wetland	Woody Wetland
53	630775.883	3668553.619	Woody Wetland	Woody Wetland	Water
54	630634.561	3668747.937	Woody Wetland	Woody Wetland	Water
55	630834.767	3668303.36	Woody Wetland	Woody Wetland	Woody Wetland
56	630658.114	3668797.988	Woody Wetland	Woody Wetland	Woody Wetland

N.B – C.R.C / T.B denotes cultivated row crops / transitional barren.

component with the bare patches of soil visible as bright patches of whitish hue, which may indicate cleared sections of land. The dark tones in the 1989 PC1 image denote moisture with increasing gradation i.e. the darker the tone the more is the moisture content. It is immediately clear of the decrease in vegetation for the Wambaw swamp with the increased blowdown for PC1 in the 1989 image. The sediment load in the middle of the Wambaw swamp is noticeable in the 1989 image only for PC1.

The second principal component PC2 for both the images clearly delineates the forest boundaries with some amount of topographic relief, this also seems to emphasize the big forested area between the “Mechaw” and “Thompson Corner” private holdings as a bright patch in the study area, and the cultivated row crops/transitional barren class is denoted as a dark patch. For PC2, the 1987 image contains 19.72% variance, whereas the 1989 image contains a higher variance of 33.56%. The roads are not emphasized for PC2 in both the images.

The third principal component PC3 is clearly useful only for the discrimination of the road feature, and displays large tracts of similar land cover class; the sensitivity to local height variations is decreased due to the presence of noise. The Wambaw swamp and Coffee creek swamp are both discernible for both images. The 1987 image contains 3.78% whereas the 1989 image contains a lowered variance of 2.19%.

To conclude, changes can easily be visualized with principal component analysis because PCA correctly identified the two swamps, which were a dominant feature in the study area.

4.5 Change Detection Using TCT

The TCT bands for the brightness, greenness, and wetness components are shown for the 1987 and 1989 images in Figures 21 through 26. An interesting thing to note is that the Wambaw swamp and the Coffee creek swamp is discernible in all the tasseled cap bands for both the 1987 and 1989 images, though it is more pronounced in the 1989 imagery.

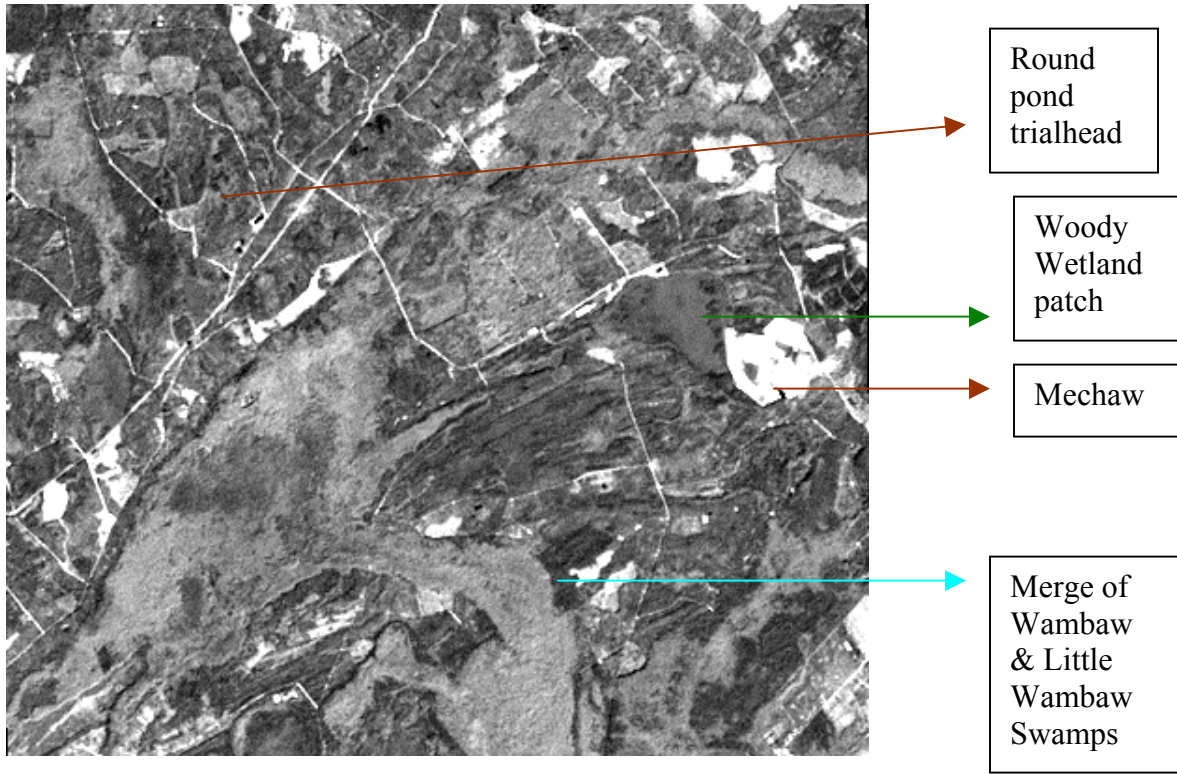


Figure 15: PC 1 for 1987

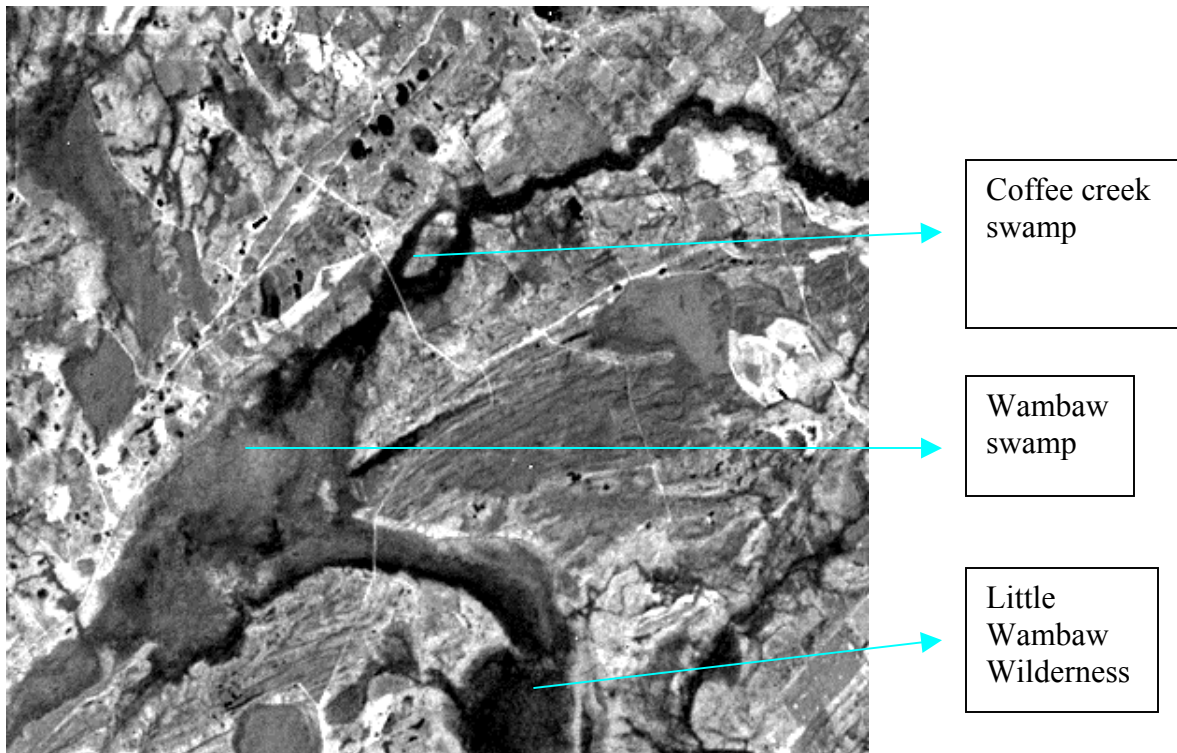


Figure 16: PC 1 for 1989

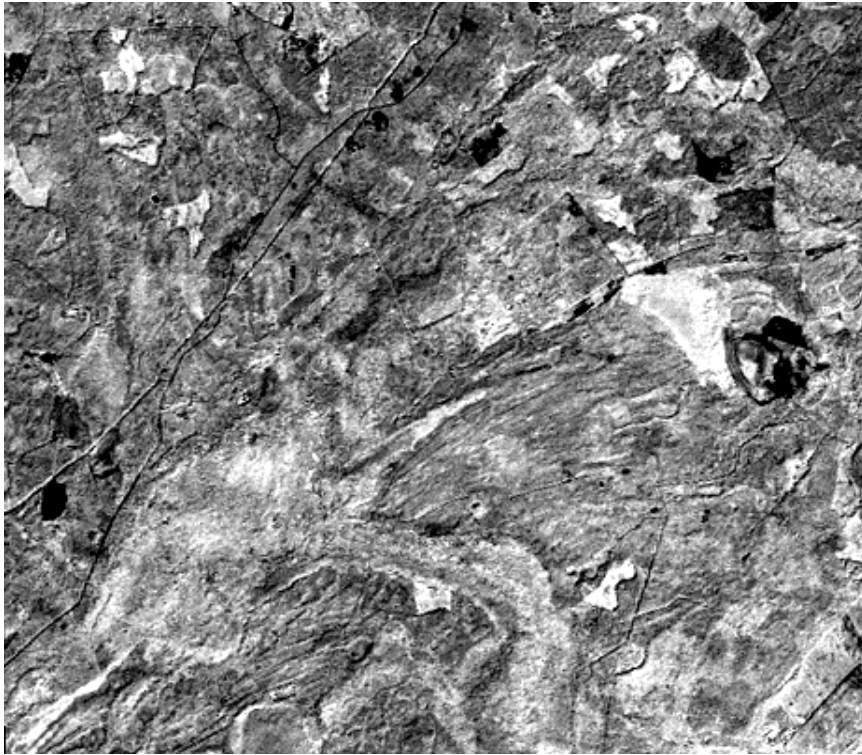


Figure 17: PC 2 for 1987

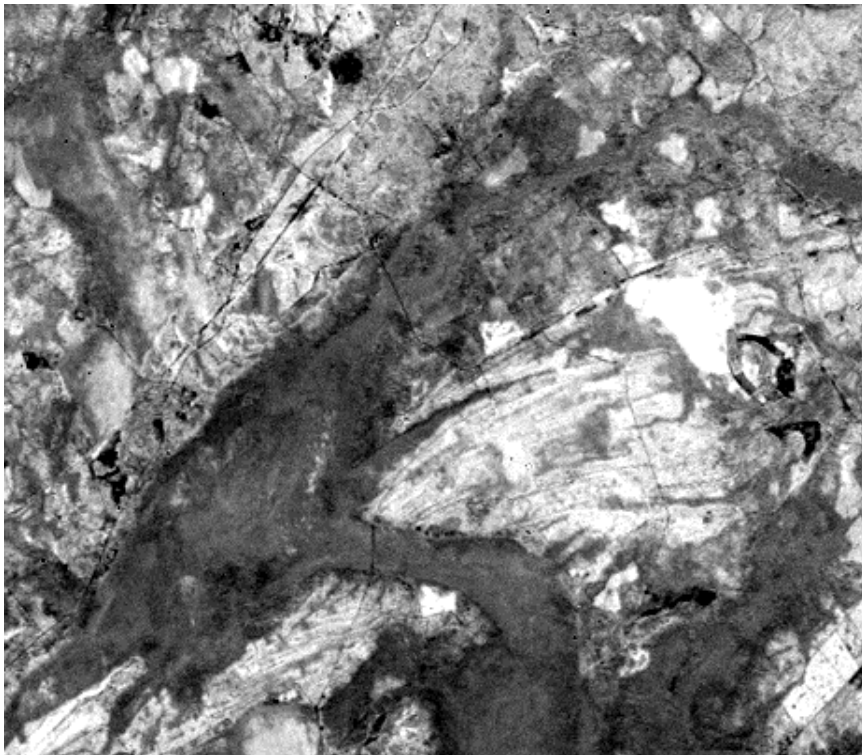


Figure 18: PC 2 for 1989

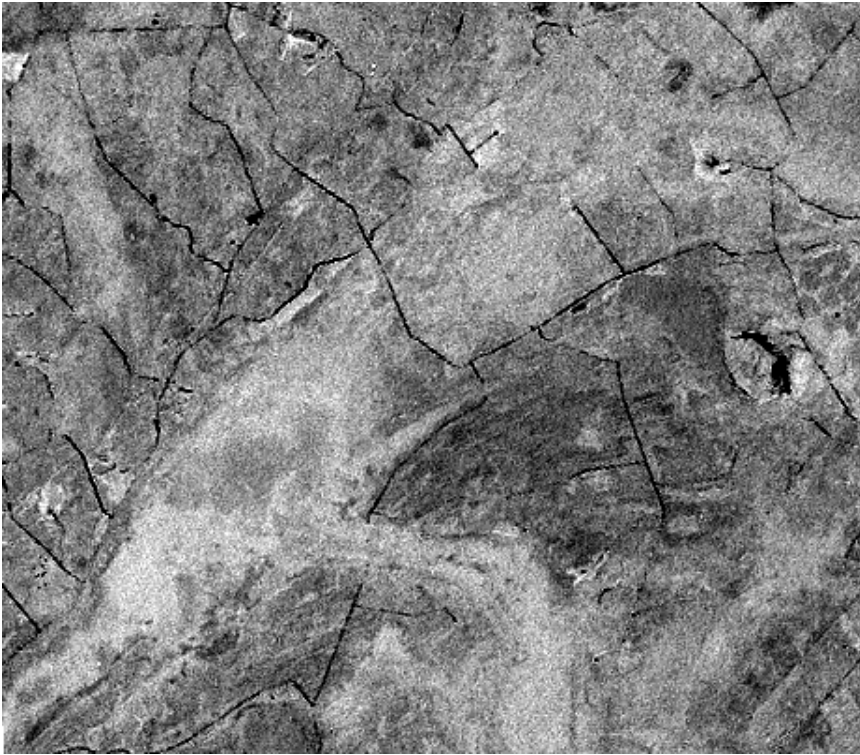


Figure 19: PC 3 for 1987

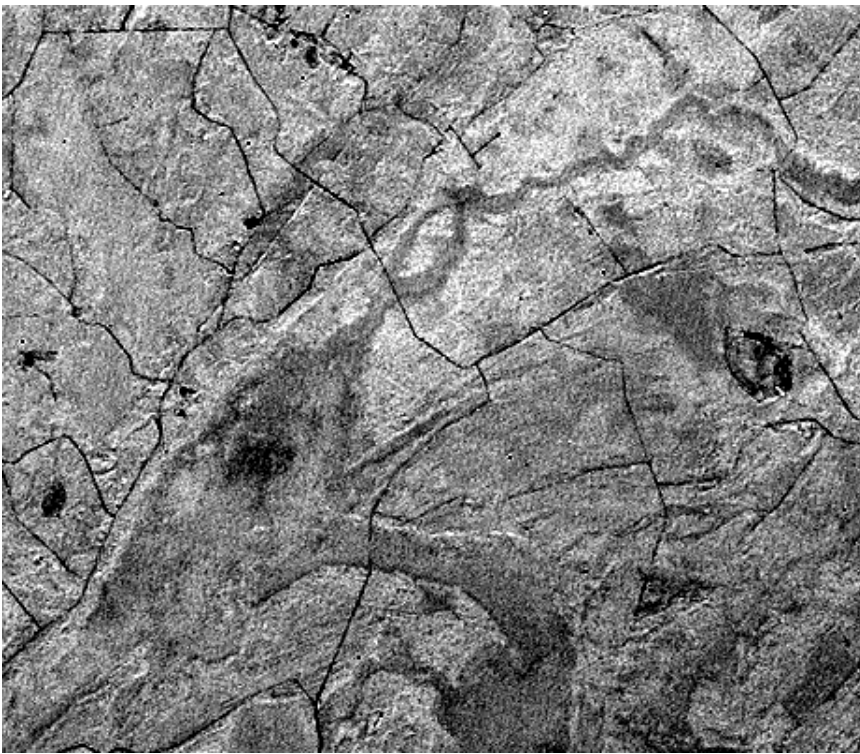


Figure 20: PC 3 for 1989

Table 11: PC component variance

Principal Component	1987 Percentage Variance	1989 Percentage Variance
PC1	74.43%	62.50%
PC2	19.72%	33.56%
PC3	3.78%	2.19%
Total	97.93%	98.25%

For the brightness component for both the 1987 and 1989 images in Figures 21 and 22, the cultivated row crops/transitional barren and the woody wetland feature classes can be clearly distinguished in the images. However, for the 1989 image in Figure 22, the water and woody wetland classes appear in darker shades. The roads and cultivated row crops areas are discernible and appear as bright patches in both the images, but they appear better in the 1987 image in Figure 21. It is difficult to detect changes in the forest feature class in this band in both Figures 21 and 22, as it appears dull and is therefore hard to distinguish. The sediment load in the middle of the Wambaw swamp is clearly discernible in Figure 22, while it appears as forested land in the 1987 image in Figure 21. It is hard to separate out water from the woody wetland class for the 1989 image in Figure 22, but it was impossible to find the water and woody wetland class in the 1987 image in Figure 21.

The greenness component displays the forested or vegetated areas as very bright for both 1987 and 1989 in Figures 23 and 24 respectively. In the 1989 image, the forest class appears brighter as confirmed from the woody wetland patch in Figure 24. The 1989 image in Figure 24 seems to emphasize the water/woody wetland class compared with the 1987 image in Figure 23 where it was faintly discernible. Both the 1987 and 1989 images as a whole appear dull for the cultivated row crops/transitional barren classes with the road areas almost completely obscured in Figures 23 and 24 respectively. The greenness band displays the sediment load in the middle of the Wambaw swamp for the 1989 image in Figure 24 better in comparison with the 1987 image in Figure 23. There is a change in the cultivated row crops feature class, which is colored dark for the 1987 image but for the 1989 image it is indistinct. A possible explanation for the disappearance of the cultivated row crops class in Figure 24 is that the storm surge might have deposited sediments and salt residues, making it hard to distinguish in this greenness band.

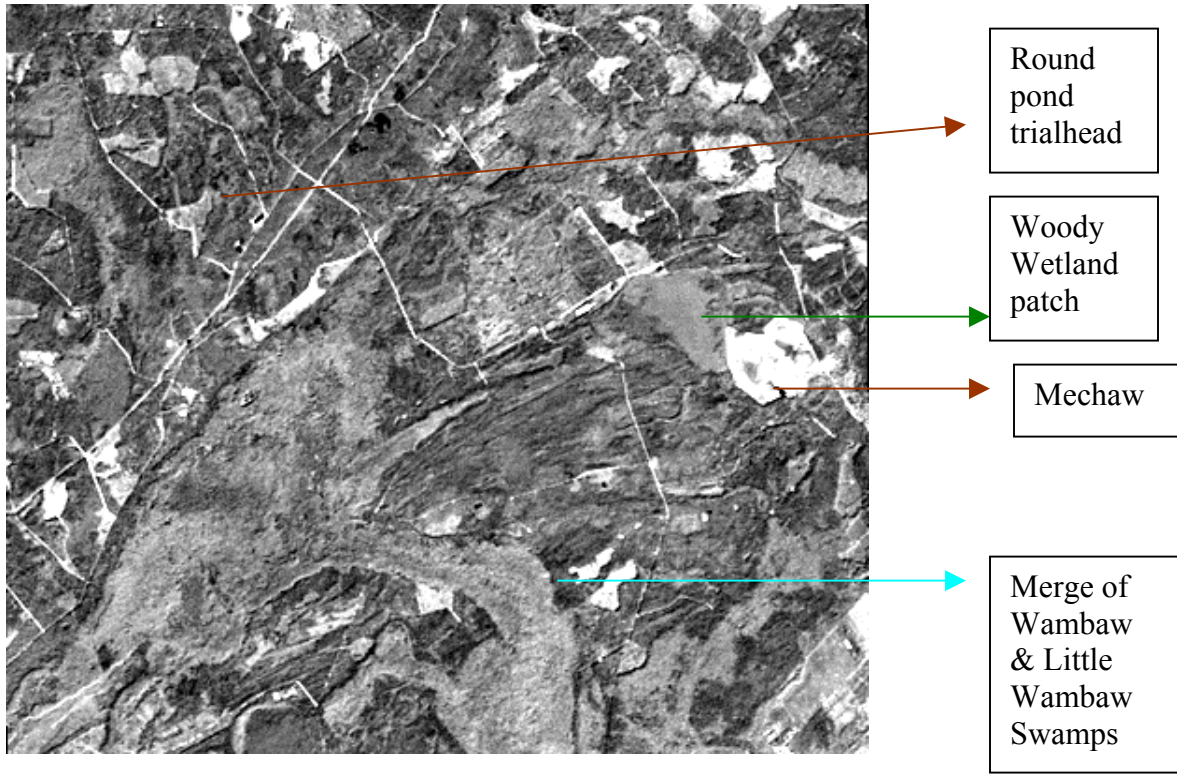


Figure 21: TCT brightness for 1987

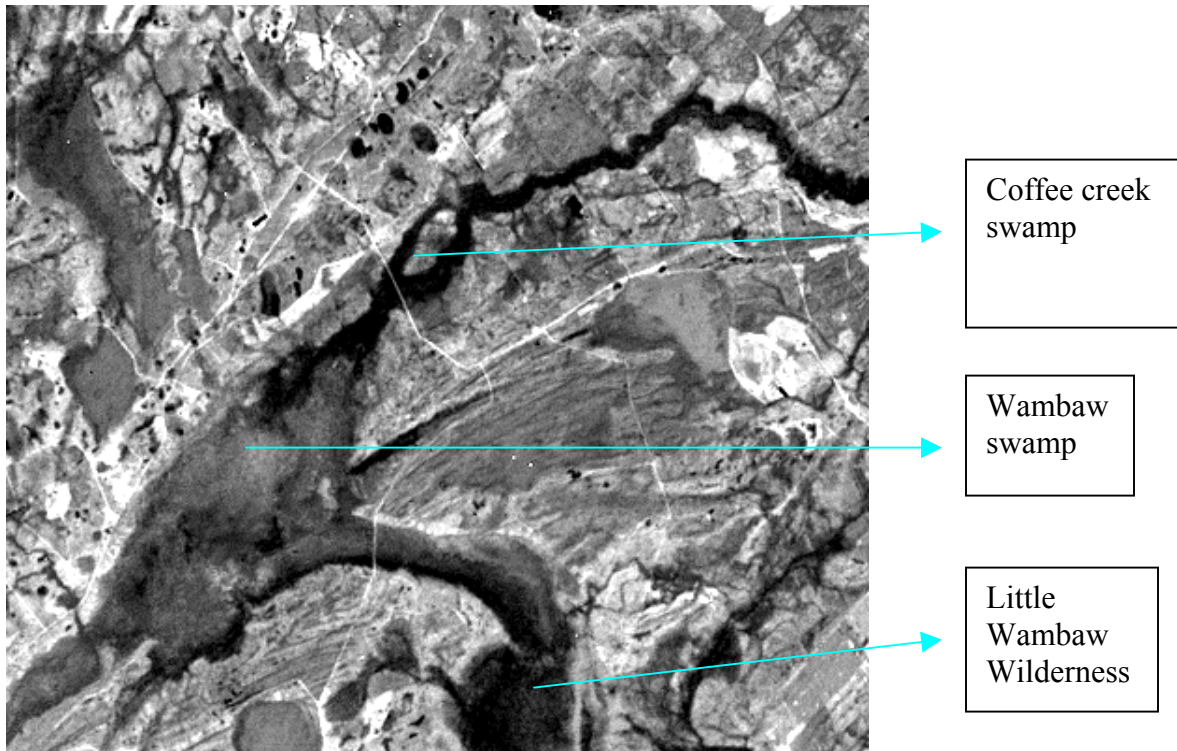


Figure 22: TCT brightness for 1989



Figure 23: TCT greenness for 1987

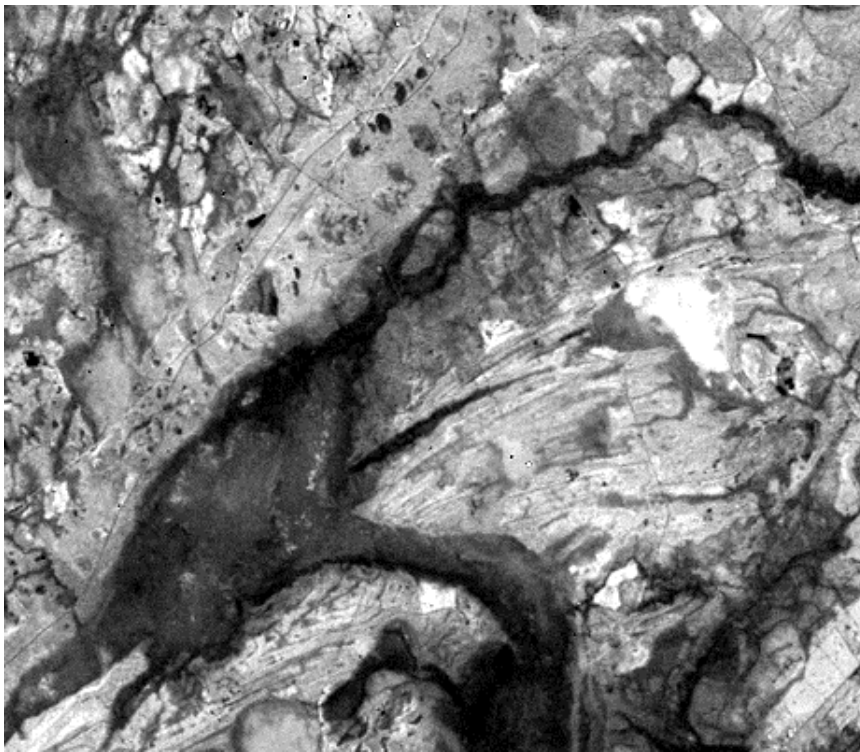


Figure 24: TCT greenness for 1989



Figure 25: TCT wetness for 1987

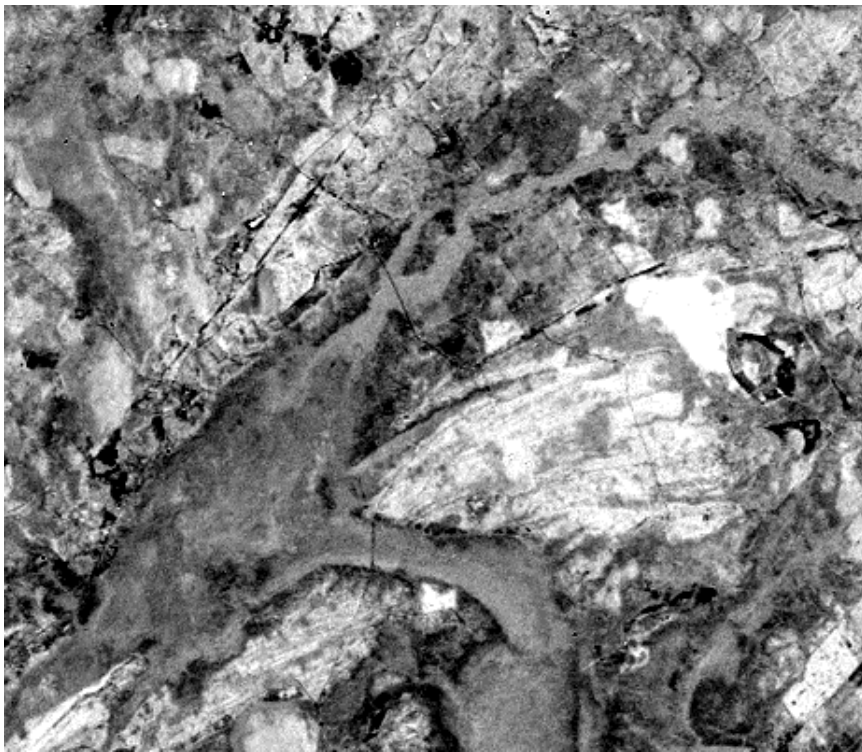


Figure 26: TCT wetness for 1989

The wetness component is the most complicated band to analyze. For the 1987 image, the cultivated row crops features are better represented as dark patches, but in the 1989 image in Figure 26, they have changed to appear indistinct from the neighboring features. The roads, which were faintly visible in Figure 25 for the 1987 image, have been obscured by the dominance of the moisture due to the woody wetland/forest classes in Figure 26 for the 1989 image. The big woody wetland patch between the “Mechaw” and “Thompson Corner” places is identified in both the images, but it is easier for the 1989 image in Figure 26. The woody wetland and forested classes are hard to distinguish in the pre-event image in Figure 25 but become easier because the forested areas appear brighter for the 1989 image in Figure 26. The sediments in the Wambaw swamp are hard to distinguish in the 1989 image but are faintly evident in the 1987 image in Figure 25. The water and woody wetland classes are hard to discriminate for the 1989 image in Figure 26 but rather they appear to be lumped together into a single class. This band is clearly useful to specifically sense moisture, either soil, plant or actual.

In general the TCT bands are easier for change analysis compared to those of the PCA because of the nature of the study area, which consists of moisture (water and woody wetland classes), and forest classes.

4.6 Change Detection Using the Local TPSA Fractal Method

The discussion below refers quite often to Figure 8, which is the printout obtained from ArcView from the FMNF Wambaw Ranger District office. A step size of five was chosen for the analysis to ensure a reliable estimate of the fractal regression line. A smaller value of step size would have less confidence and a larger value would require a larger local moving window size for computing the fractal dimensions. This step size made it possible to evaluate different moving window sizes from 9x9 pixels to 33x33 pixels with both arithmetically and geometrically increasing steps with sufficient confidence in the results.

Spatially complex/heterogeneous (heterogeneity) areas are those regions which have a relatively high D value compared to its surroundings; they are generally brighter in color.

Spatially homogeneous (homogeneity) areas are those regions which have a relatively low D value compared to its neighbors, and are generally darker in color.

4.6.1 Choice of Moving Window Size

It was found that of all the moving window sizes tested for this study the 17x17 moving window with arithmetically increasing steps was the best in representing land cover features for the 1987 and 1989 images. This moving window size produced an image with a good tradeoff between the edge effects and the identification of spatial patterns. The texture patterns begin to emerge and the actual land cover features start to blur out for this particular window size. This 17x17 moving window gives a fairly stable fractal regression with decreased noise. Based on visual examination the moving window size was found to be directly proportional to edge effects in the local TPSA outputs. The 9x9 moving window with arithmetically increasing steps had the most correlation with landcover features with least edge effects, and the 33x33 moving window with geometrically increasing steps had the opposite results i.e., least correlation with landcover features with most edge effects. The regression procedure of the TPSA algorithm therefore places a practical lower limit on the size of the moving window, decreasing the size of the window below 9 increases the amount of noise considerably and possibility of spurious D outliers. For visual comparison, the other moving window sizes are listed in Appendix A in Figures 35 through 52.

Figures 30 and 32 show the smoothed local TPSA images for 1987 and 1989 using a (convolution) low pass filter of 5x5 pixels. It is used to view the spatial patterns in the local TPSA output without the hard class transitions caused by the roads in the study area.

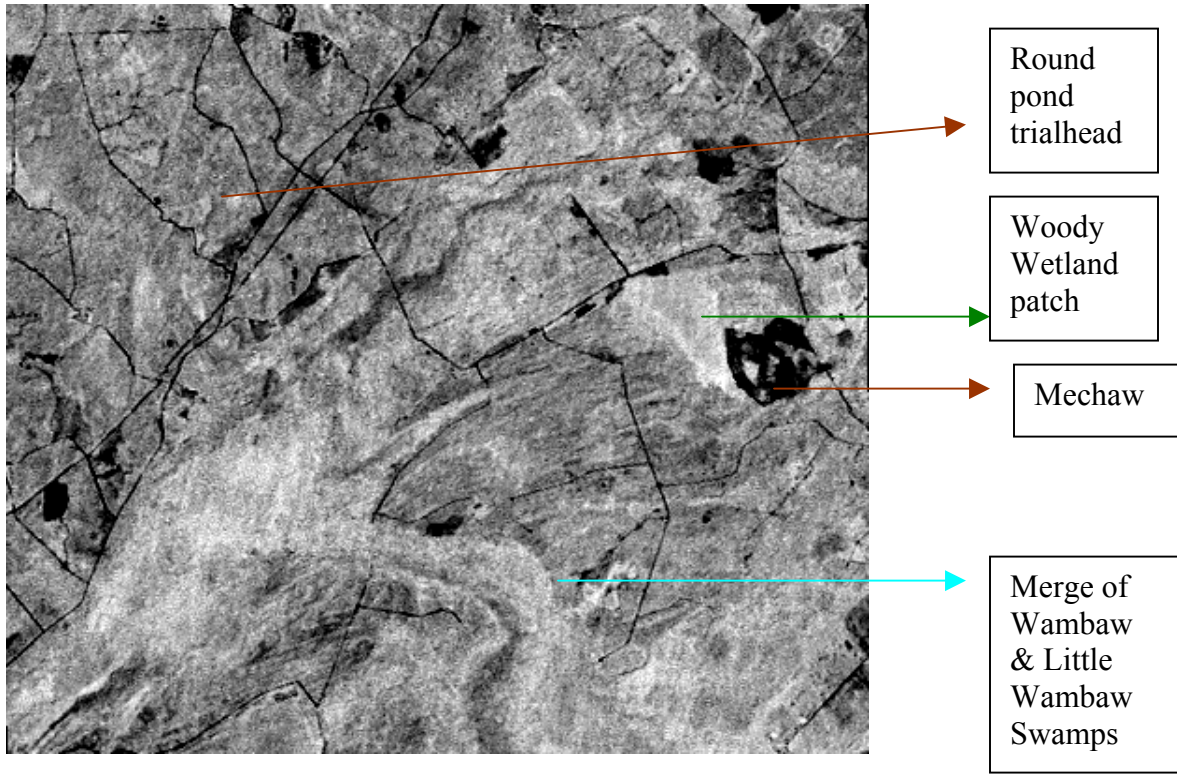


Figure 27: NDVI for 1987

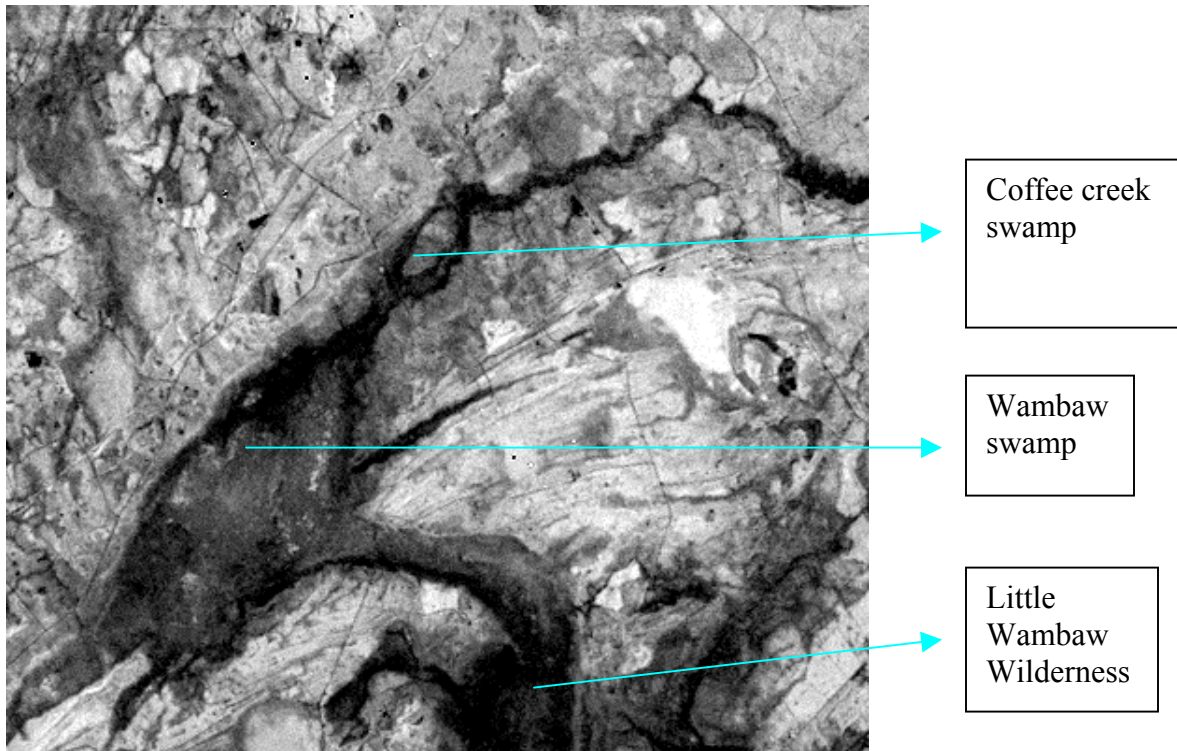


Figure 28: NDVI for 1989

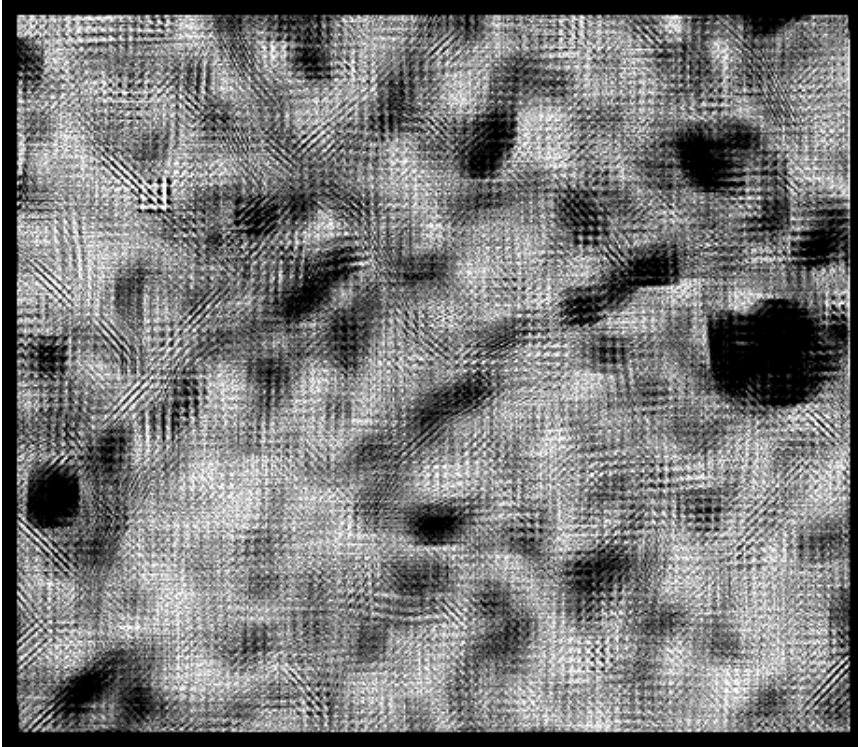


Figure 29: TPSA for 1987 with 17x17 MW with 5 Arithmetic steps

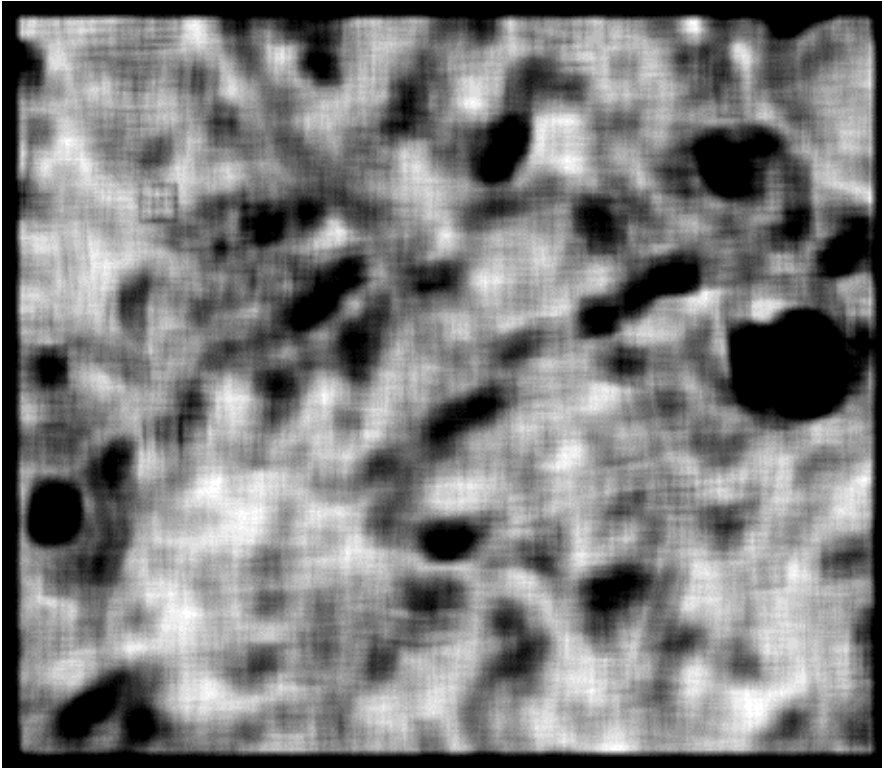


Figure 30: Same image after a 5x5 convolution low pass filter

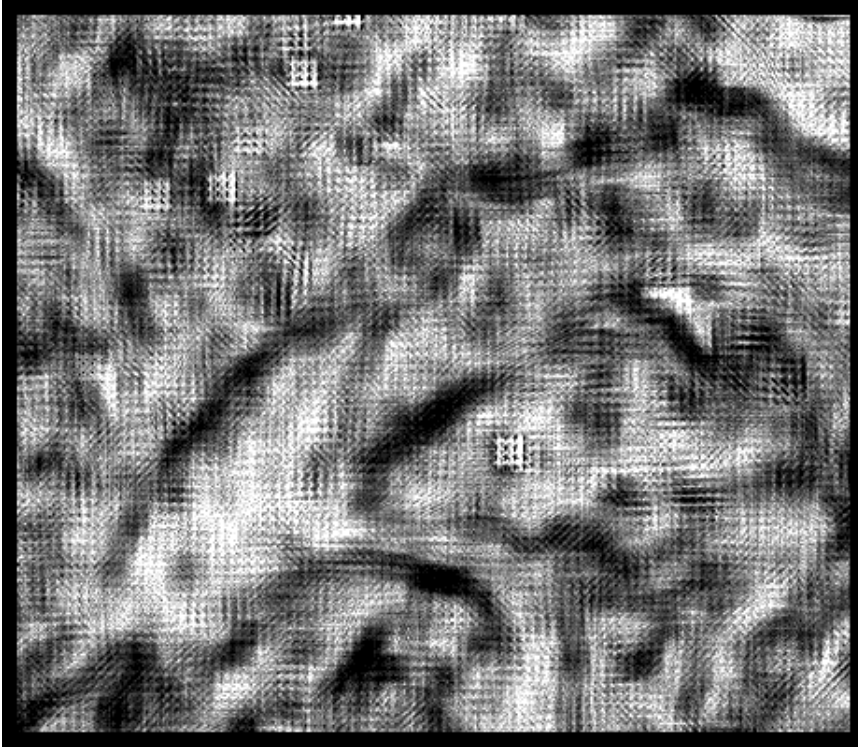


Figure 31: TPSA for 1989 with 17x17 MW with 5 Arithmetic steps

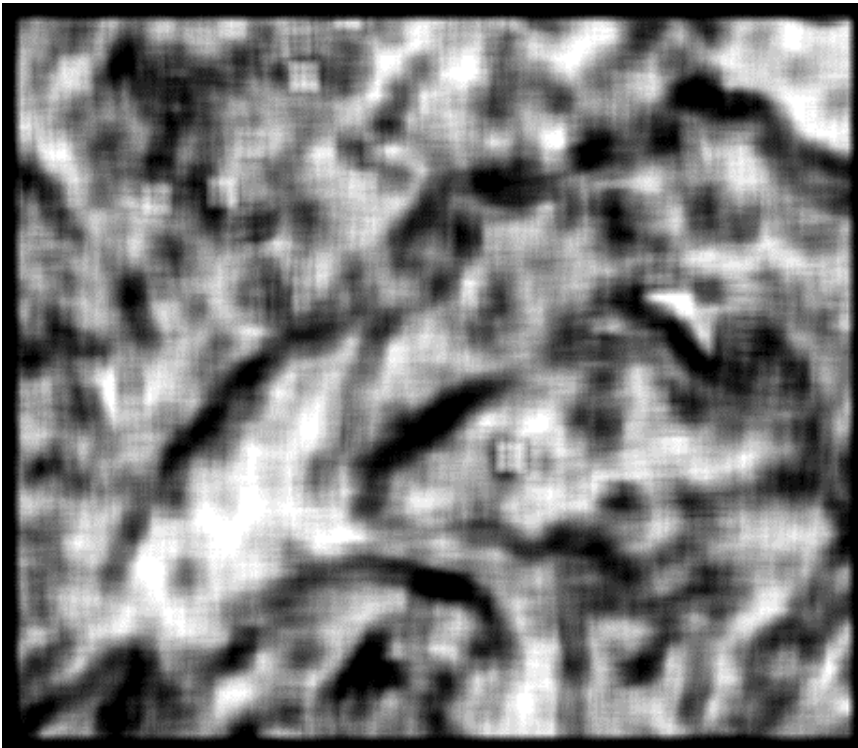


Figure 32: Same image after a 5x5 convolution low pass filter



Figure 33: Change detection TPSA with 17x17 MW with 5 arithmetic steps

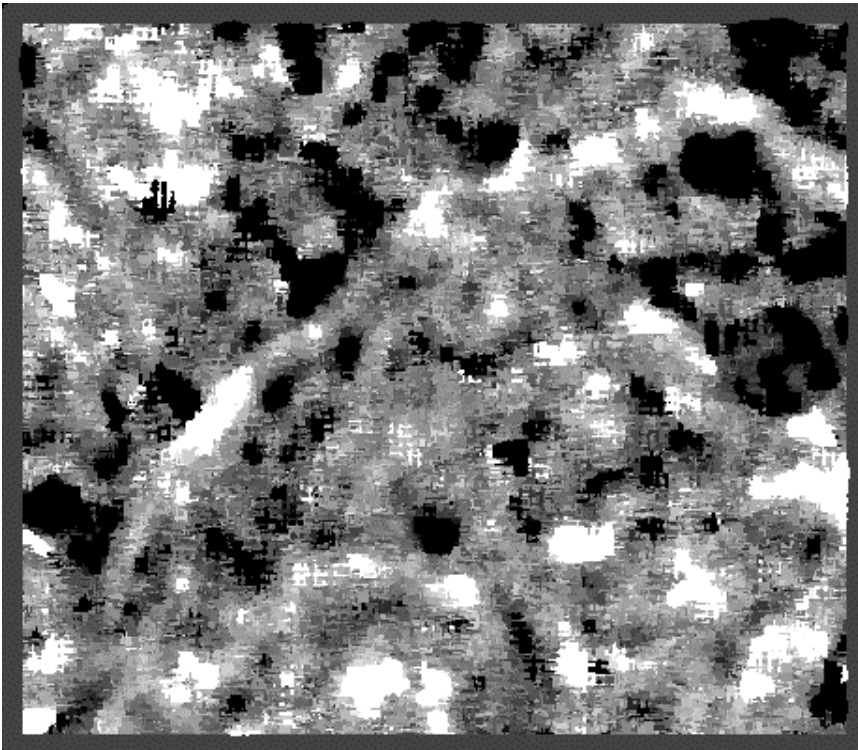


Figure 34: Same image after a 7x7 focal majority filter

4.6.2 Analysis for the 1987 and 1989 NDVI Images

The input NDVI images used in the modified triangular prism method analysis are shown in Figures 27 and 28. In general, for unscaled NDVI images the pixel values range from -1.0 to +1.0. Values less than zero indicate non-vegetated land cover features, with values close to -1.0 representative of moisture classes of water/woody wetland, and near to 0 indicative of barren features. Increasing positive values are representative of increasing density of vegetation (Lillesand and Kiefer 2004). The prominent landcover features are marked on both NDVI images for easier recognition, and for subsequent reference in the analysis.

The NDVI input image for 1987 emphasizes the roads, as the road network is prominently visible in the image; also faintly visible is the separation of the cultivated row crops/transitional barren areas from the forested area. The woody wetland is not clearly discernible but the meandering Wambaw swamp is discernible, the Coffee creek swamp is slightly obscured. The patch of forest between the “Mechaw” and the “Thompson Corner” in the center of the study area is very bright and the forest class is distinguished over the swamp. This agrees with the hybrid classification procedure. The Mechaw plantation is shown as having dark tones, along with the other cultivated row crops areas in the study area. The 1987 NDVI input image had a standard deviation of 12.36, which is low.

The 1989 NDVI image emphasizes water, woody wetland, and forested land cover classes, the road network and the cultivated row crops feature class is obscured in the image. The woody wetland class is discernible throughout the meandering Wambaw swamp and the Coffee creek swamp is clearly revealed. The big patch of forest between “Mechaw” and the “Thompson Corner” in the study area appears brighter than the 1987 image and the forest class is clearly distinguished from the swamp in the NDVI output. The overall visual impression is that the 1989 NDVI is more spatially homogeneous because of the hurricane. The NDVI input image

had a standard deviation of 16.34, which is higher than the 1987 standard deviation. It may appear that there is a disconnect, but the standard deviation is an spatial statistical measure and the fractal dimension is a spatial measure, high D values can have low standard deviation and vice versa.

4.6.3 Analysis for the 1987 Local TPSA Image

Figures 29 and 30 represent the 17x17 fractal transformed output with five arithmetically increasing step sizes, and the 5x5 convolution image with low-pass filter respectively (LPF hereafter). The most dominant feature visible in Figure 29 is a jagged image wherever there is abrupt transition between different land cover classes. This is evident throughout the image because the NDVI image for 1987 has a prominent network of roads. The dark tone patches in this image exclusively represent the cultivated row crops class which displayed high homogeneity.

Moving the mouse cursor over adjacent D values revealed that they are smooth with a maximum of 3% variation internally within the darkest and brightest tones. That is a pixel with a D of 2.7 will have adjacent pixels with D values ranging from 2.62 – 2.78. Transition zones where the colors change abruptly have fairly high D variation of approximately 10% with a pixel of $D = 2.7$ producing adjacent pixels with D values ranging from 2.43 – 2.97. The spatial variability is more when there is a complicated mix of high fractal dimensions from the sediment loadings in the Wambaw swamp, the Little Wambaw wilderness, and the road network. In the discussion below I will refer to Figure 30.

4.6.3.1 Road Network

The abrupt transitions in land cover classes due to the presence of roads i.e., the spatial heterogeneity, has diminished considerably but is still visible as dark lines on a bright

background in the 5x5 LPF image. A 3x3 box is clearly visible in the top left of the image where the “Round pond trailhead” exists. Squares start to form because the moving window size matches and captures the land cover repeatability. The relatively little change in spectral characteristic for the road area in the NDVI input image for 1987 produces consistently high D values in the range between 2.6 – 3.0 for the road features. An interesting observation is that the jagged lines appear symmetrical and parallel to the road network which causes a transition i.e., a line appears during the forest or woody wetland transition to road, and again when the road transitions into the forest or woody wetland class. Overall, the image has a bright lattice structure, which indicates that there is a repeatability of the abrupt breaks due to short area land cover class transitions.

4.6.3.2 Wambaw Swamp

The 5x5 LPF image displays the Wambaw swamp as a bright oval area with high D values surrounded with circular patches of low D values of cultivated row crops in dark tones. The spatial pattern of the Wambaw swamp looks like a pincushion. The oval surrounds an area of high albedo due to the presence of sediment load.

4.6.3.3 Little Wambaw Wilderness and Coffee Creek Swamp

The merge of the Wambaw swamp and the Little Wambaw wilderness, and the Coffee creek swamps can be spotted as a pattern with high D values sandwiched on either side by patches of dark spots representing cultivated row crops feature class with low D values. The Little Wambaw wilderness has a high amount of sediment loadings equivalent to the Wambaw swamp. The Coffee creek swamp in comparison is very tiny in size, and has a grayish tone indicating low to medium range of D values.

4.6.3.4 Woody Wetland Patch

The woody wetland patch is not emphasized at all; in fact, it is virtually masked out by the Mechaw place, indicating it is fairly homogeneous. Another thing detected for this image is the relative stable D variation of the big forested patch and the adjacent cultivated row crops class, so much that it appears to be to be the same feature. This relative homogeneity of the big patch of forest led to it being categorized along with the nearby patch of cultivated row crops area in the 1987 triangular prism output, as a mixed class.

4.6.3.5 Cultivated Row Crops

The cultivated row crops class influence is more pronounced as the edge effects are increased with increase in the moving window size. The cultivated row crops features appear dark in color and are emphasized throughout the image, as there is uniformity in spatial variation for the cultivated row crops area, there is not much visible class transitions, i.e. it displays homogeneity.

4.6.4 Analysis for 1989 Local TPSA Image

For the 1989 fractal transformed output in Figures 31 and 32, the most obvious feature is the dominance of the water feature class. The plume of water as it meanders through the Wambaw swamp and Coffee creek is clearly visible in dark tones, which has a D value ranging from 2.4 to 2.6, from moving the mouse cursor in ICAMS, denoting a less complicated and uniform spatial variation for the water/woody wetland feature classes. The dark tone patches in this image exclusively represented the water and woody wetland classes, which displayed high homogeneity.

Overall, the 1989 image in Figure 31 has less overlap between the forested and woody wetland classes and appears darker, which denotes a gain in homogeneity. The spatial variability

for the sediment loadings in the Wambaw swamp has increased compared to the 1987 image with a complicated mix of high fractal dimensions. Transition zones where the colors change abruptly have fairly reduced D variation of approximately 5% with a pixel of $D = 2.7$ producing adjacent pixels with D values ranging from 2.56 – 2.84, except for areas surrounding the Wambaw swamp where the adjacent pixels vary by as much as 20%. The edge transitions for the water and woody wetland classes is prominently displayed i.e., a transition from a zone of low or high moisture like woody wetland to cultivated row crops or vice versa is detected. In the following discussion I will refer to Figure 32 which represents the 5x5 convolution image with low-pass filter (LPF hereafter).

4.6.4.1 Road Network

The road feature class is now obscured in this image with the presence of a lot of noise. The abrupt land cover feature transitions so clearly evident in the 1987 image are smoothed out due to the relatively low D values. The lattice framework appearance of the image makes it fairly difficult to fix the occurrence of the road network in the study area.

4.6.4.2 Wambaw Swamp

The sediment load in the middle of the Wambaw swamp has been emphasized a lot ; the swamp displays sediments with high D values and the surrounding vegetation on top of the water surface with relatively low D values. The shape of the Wambaw swamp, which was unclear in 1987, is now very clear in 1989 due to the sediment loadings and the reduction of the trees over the Wambaw swamp as reported in Hook *et al.* (1991).

4.6.4.3 Little Wambaw Wilderness and Coffee Creek Swamp

The Little Wambaw wilderness and the Coffee creek swamp are clearly visible. An interesting finding is that for the 1989 image, the dark tones representing water/woody wetland

classes surround the bright tones of sediments for both areas. This indicates that the underlying spatial patterns are altered considerably which is explained due to the residual storm surge surrounding the swamps. A small bright 3x3 square is formed above the bend where Wambaw swamp merges with the Little Wambaw wilderness. This square is important because it is discernible with the larger moving window sizes but the other squares in the image disappear.

4.6.4.4 Woody Wetland Patch

The woody wetland near “Mechaw” appears to be divided into two distinct areas. One area has very low range of D values from 2.3 – 2.6, obtained by moving the mouse cursor in ICAMS, and the other smaller zone has consistently high D values ranging from a minimum of 2.75 to 3.05.

4.6.4.5 Cultivated Row Crops

In this image the cultivated row crops class is obscured which is a very big change from the 1987 image where it formed the most dominant spatial patterns. In this 1989 image the most dominant class is the woody wetland in the Wambaw swamp with consistently high local fractal dimensions.

4.6.5 Change Detection of Local TPSA Image

Figure 33 is the change detection output and Figure 34 shows the change detection figure passed through the focal (neighborhood) majority function with a 7x7 pixel filter accessed through the viewer (Raster ==> Filtering ==> Statistical Filtering). The difference image was produced with the ICAMS Difference option by subtracting the 1987 image from the 1989 image. Since this is a difference image, a positive difference in D values shows up as bright tones and a negative difference shows up as dark tones in the image. The positive difference implies that the 1989 image had a higher fractal dimension for a pixel than the 1987 image, and

vice versa. Therefore, a positive value in the change image denotes an increase in spatial complexity, and a negative value implies a drop in spatial complexity. For change detection, we are interested in areas that have the largest difference in D values in both positive and negative directions. Therefore, the 7×7 focal majority function image in Figure 34 is used in the analysis to enhance the largest positive and negative changes in spatial patterns due to the hurricane.

A first glance at the change detection image shows that the cultivated row crops feature class, which includes the Mechaw plantation, shows a noticeable decrease in spatial complexity due to its dark tones. The white tones, which denote increased spatial complexity is present where either the sediments were deposited over the Wambaw or Coffee creek swamps, in top left corner near the “Round pond trailhead” area and near the southeastern corner of the study area. Most of the change detection image has a gain of homogeneity because the overall tone of the study area is dark, with the presence of low to moderate negative D difference values.

Most of the area covered by the Wambaw swamp, Coffee creek swamp, and the Little Wambaw wilderness has shown a gain in homogeneity due to its low to moderate negative D difference values. A small part of the woody wetland patch between Mechaw and the “Thompson corner” has a spatial complexity increase, but the major forested area has a low to moderate negative D difference values. It is interesting to note that the abrupt feature class transitions, which followed the road feature class, are completely obscured in the 7×7 focal majority image. As in the 1987 and 1989 images, the squares with low to moderate D difference values are formed in the original change detection image over the cultivated row crops areas, but are transformed into high negative D difference values because of the 7×7 majority filter.

4.6.6 Zonal Statistics for Correlation of Classified Land Cover Areas to D Values

Tables 12 and 13 give the fractal dimension distribution as generated by the modified local TPSA method shown with the associated land cover classes. The fractal dimension values

generated in the Summary operation were divided by 100 to produce the actual results shown in the table. One thing which immediately stands out from the tables is that the 1987 *D* distribution is more spatially complex. This is indicated by the *D* value where the mean and median for the 1987 correlation are all higher compared to the 1989 correlation. For both 1987 and 1989, the woody wetland and forest classes, which have the highest majority count are almost similar when comparing their fractal dimension values. The woody wetland class has a mean of 2.66 and median of 2.82 for 1987 which then drops to a mean of 2.5 and a median of 2.64 for the 1989 correlation. The forest class has a mean of 2.61 and a median of 2.83 for 1987 which then drops to a mean of 2.42 and a median of 2.64 for the 1989 correlation.

Table 12: Classification to Fractal Dimension Zonal Statistics for 1987

Zone Name	Majority	Mean	Median	Min.	Max.	Range	Diversity	Std. Dev	Majority Count	Majority %
Water	2.73	2.74	2.75	2.5	2.99	0.5	0.36	0.10	7	10.61%
Woody wetland	0	2.66	2.82	0	3.41	3.42	1.14	0.68	5451	5.93%
Forest	0	2.61	2.83	0	3.45	3.46	1.15	0.77	6534	7.85%
C.R.C/T.B	0	2.38	2.61	0	3.23	3.24	0.94	0.79	856	9.74%

Table 13: Classification to Fractal Dimension Zonal Statistics for 1989

Zone Name	Majority	Mean	Median	Min.	Max.	Range	Diversity	Std. Dev	Majority Count	Majority %
Water	0	2.45	2.6	0	3.15	3.16	0.81	0.65	485	6.45%
Woody wetland	0	2.5	2.64	0	3.38	3.39	1.05	0.62	5747	5.67%
Forest	0	2.42	2.64	0	3.28	3.29	1.04	0.76	5882	8.89%
C.R.C/T.B	0	2.44	2.62	0	3.19	3.2	0.85	0.68	622	6.95%

CHAPTER 5: CONCLUSION

The three objectives for the study were all met successfully as I was able to

- identify the impacts on land cover changes for the study area from 1987 to 1989.
- identify the spatial patterns of the impacts.
- identify the local fractal method as the most effective method used in the study.

For the post-classification comparison, the hybrid method was chosen for analysis. For the hybrid classification, the accuracy was found to be 81.44% and 85.71% for the 1987 and the 1989 images. In evaluating classification accuracy, the rule of a minimum 50 random points per feature class was followed with the exception of the water class. Fewer points were used due to the small area of coverage for the water feature class in the 1987 image (Congalton 2001). The results of land cover change due to the hurricane are summarized as follows (from Table 8)

- a gain in water class of 4.03%
- a gain of woody wetland areas of 5.09%
- a loss of forest cover of 9.24%

The forested area over the Wambaw swamp, Coffee creek swamp, and the Little Wambaw wilderness was converted into water and woody wetland classes. Forest cover was gained near the edge of the Wambaw swamp. Due to this, the woody wetland became more homogeneous around the three swamps. The storm surge from the hurricane caused some of the low lying flooded areas to be classified as water and woody wetlands, and the areas above the banks of the low lying woody wetlands to be classified as forest.

The PCA and TCT were used to validate the results of the classification procedure and to see if the hybrid algorithm missed any important changes, which occurred due to the hurricane. PC1 and PC2 bands had a very good correlation with the TCT brightness and greenness bands, with the visual appearance almost similar. PC1 and the TCT brightness band emphasized the

changes in the water and woody wetland classes with an increase in spatial homogeneity of the three swamp areas clearly revealed. Changes in the cultivated row crops/transitional barren areas were detected in both PC1 and TCT brightness, and it was clear that the cultivated row crops area coverage had increased in 1989. Both PC1 and TCT brightness revealed the substantial change caused by the Hurricane in the Wambaw swamp sediments. PC2 and the TCT greenness bands emphasized the changes in the forested areas and to a lesser extent for the woody wetland areas. These bands clearly revealed the increase in spatial homogeneity of the forested areas. The TCT greenness band revealed the increase in homogeneity from 1987 to 1989 better than PC2 band. PC3 faintly revealed the changes for the woody wetland areas and to a lesser extent for the cultivated row crops area from 1987 to 1989. The TCT wetness band emphasized the homogeneity increase for the forested areas, and was the only band that revealed the spatial heterogeneity increase for the woody wetland and cultivated row crops classes.

For the local fractal TPSA method the 17x17 moving window with an arithmetic step increase of 5 steps was found to be the best moving window size for this study with a good tradeoff between the edge effects and the identification of spatial patterns. For the local fractal method the most dominant spatial patterns identified for the 1987 transformed image were the dark tones representing the cultivated row crops/transitional barren feature class. For 1989, the local TPSA method identified spatial patterns which were again dark tones representing the water/woody wetland feature classes. The dark tones represent high spatial homogeneity. Both of the 1987 and 1989 local TPSA outputs identified the sediment loadings with their high heterogeneity in the Wambaw swamp with the brightest tones in the images. The texture in the 1987 image was found to have large variation in D values and an overall high spatial complexity. This was confirmed in the Zonal statistics correlation of classification vs fractal dimension values where the mean and median D values for the dominant woody wetland and the forest classes have both decreased for 1989 compared to the values in 1987.

The local fractal TPSA method identified the cultivated row crops/transitional barren class as having the biggest drop in spatial complexity from 1987 to 1989 in the change detection image. The post-classification comparison did not have a spatial complexity change result for the cultivated row crops areas. A majority of the area covered by the Wambaw swamp, the Coffee creek swamp, and the Little Wambaw wilderness displayed low to moderate negative and uniform D difference values, which meant a gain in homogeneity, and a consequent reduction in the spatial complexity. This was also confirmed by the PC1, PC2 and the TCT brightness and greenness bands. The local fractal TPSA method identified the areas with the highest gain and the highest loss in spatial complexity in the change detection image. Highest gain in areas of spatial complexity were found to be situated near the intersections of the dirt roads or running parallel between the dirt roads, for example, the bright spots near the “Round pond trailhead” and “Bark Island”. Highest loss in areas of spatial complexity was the cultivated row crops feature classes. It was not possible to find out the areas with maximum spatial complexity change with the TCT wetness band.

The biggest advantage of the local TPSA fractal method is to identify the locations of largest spatial homogeneity and spatial heterogeneity changes in an automated manner. This will be very useful for forest service staff in directing their field work towards the areas with the highest gain and highest loss in spatial complexity, because we expect they would be the most “affected” areas.

REFERENCES

- South Carolina Climate Summary. 2004. National Climatic Data Center, Asheville, North Carolina. 27 August. <http://lwf.ncdc.noaa.gov/oa/climate/research/cag3/SC.html> (last accessed 27 August 2004)
- USDC-NWS, North Atlantic Hurricane Tracking Chart. 2003. US Department of Commerce, National Weather Service, North Atlantic Hurricane Tracking Chart. 29 October. <http://www.publicaffairs.noaa.gov/tracks/1989.gif> (last accessed 29 October 2003)
- USDA Publication: Monitoring and Evaluation Annual Reports: 2002 Francis Marion National Forest. 29 January. <http://www.fs.fed.us/r8/fms/forest/publications/FM2002.pdf> (last accessed 29 January 2004)
- USDA Publication: Revised Land and Resource Management Plan. 1996. FMS National Forest - USDA Forest service. 29 January. [http://www.fs.fed.us/r8/fms/forest/aboutus/fm copy.pdf](http://www.fs.fed.us/r8/fms/forest/aboutus/fm%20copy.pdf) (last accessed 29 January 2004)
- National Land Cover Characterization. 2004. US Department of the Interior, U.S Geological Survey. 22 August. <http://landcover.usgs.gov/natl/landcover.asp> (last accessed 22 August 2004)
- Anderson, J.R., E.T. Hardy, J.T. Roach, and R.E. Witmer. 1976. *A land use and land cover classification system for use with remote sensor data*. Geological Survey Professional Paper 964. Washington D.C.
- Angeles, G.R., G.M.E. Perillo, M.C. Piccolo, and J.O. Pierini. 2004. Fractal analysis of tidal channels in the Bahia Blanca Estuary (Argentina). *Geomorphology* 57 (3-4): 263-274.
- Arzandeh, S., and J.F. Wang. 2003. Monitoring the change of Phragmites distribution using satellite data. *Canadian Journal of Remote Sensing* 29 (1): 24-35.
- Bourgeau-Chavez, L.L., E.S. Kasischke, S.M. Brunzell, J.P. Mudd, K.B. Smith, and A.L. Frick. 2001. Analysis of space-borne SAR data for wetland mapping in Virginia riparian ecosystems. *International Journal of Remote Sensing* 22 (18): 3665-3687.
- Brinson, M.M., and A.I. Malvarez. 2002. Temperate freshwater wetlands: types, status, and threats. *Environmental Conservation* 29 (2): 115-133.
- Cablk, M.E., W.K. Michener, B. Kjerfve, and J.R. Jensen. 1994. Impacts of Hurricane Hugo on Coastal Forest Assessment Using Landsat TM Data. *Geocarto International: A Multidisciplinary Journal of Remote Sensing* 9 (2): 15-24.

- Chan, J.C.W., K.P. Chan, and A.G.O. Yeh. 2001. Detecting the nature of change in an urban environment: A comparison of machine learning algorithms. *Photogrammetric Engineering and Remote Sensing* 67 (2): 213-225.
- Chander, G., and B. Markham. 2003. Revised Landsat 5 TM Radiometric Calibration Procedures and Post-Calibration Dynamic Ranges. *USGS Publication*.
- Coch, N.K. 1994. Geologic Effects of Hurricanes. *Geomorphology* 10 (1-4): 37-63.
- Collins, J.B., and C.E. Woodcock. 1996. An assessment of several linear change detection techniques for mapping forest mortality using multitemporal landsat TM data. *Remote Sensing of Environment* 56 (1): 66-77.
- Congalton, R.G. 2001. Accuracy assessment and validation of remotely sensed and other spatial information. *International Journal of Wildland Fire* 10 (3-4): 321-328.
- Conner, W.H. 1998. Impact of hurricanes on forests of the Atlantic and Gulf Coasts. In *Coastally restricted forests*, ed. Laderman, A.D., pp. 271-277. New York: Oxford University Press.
- Cox, D.D., and S.A. Peron. 2002. *A naturalist's guide to wetland plants : an ecology for eastern North America*. 1st ed. Syracuse, N.Y.: Syracuse University Press.
- Crist, E.P., and R.C. Cicone. 1984a. A Physically-Based Transformation of Thematic Mapper Data - the Tm Tasseled Cap. *Ieee Transactions on Geoscience and Remote Sensing* 22 (3): 256-263.
- Crist, E.P., and R.C. Cicone. 1984b. Application of the Tasseled Cap Concept to Simulated Thematic Mapper Data. *Photogrammetric Engineering and Remote Sensing* 50 (3): 343-352.
- Crist, E.P., and R.J. Kauth. 1986. The Tasseled Cap De-Mystified. *Photogrammetric Engineering and Remote Sensing* 52 (1): 81-86.
- Dai, X.L., and S. Khorram. 1999. Remotely sensed change detection based on artificial neural networks. *Photogrammetric Engineering and Remote Sensing* 65 (10): 1187-1194.
- Dale, M.R., P. Dixon, M.J. Fortin, P. Legendre, D.E. Myers, and M.S. Rosenberg. 2002. Conceptual and mathematical relationships among methods for spatial analysis. *Ecography* 25 (5): 558-577.
- Day, J.W., D. Pont, P.F. Hensel, and C. Ibanez. 1995. Impacts of Sea-Level Rise on Deltas in the Gulf-of-Mexico and the Mediterranean - the Importance of Pulsing Events to Sustainability. *Estuaries* 18 (4): 636-647.

- De Cola, L. 1989. Fractal Analysis of a Classified Landsat Scene. *Photogrammetric Engineering and Remote Sensing* 55 (5): 601-610.
- De Jong, S.M., and P.A. Burrough. 1995. A Fractal Approach to the Classification of Mediterranean Vegetation Types in Remotely-Sensed Images. *Photogrammetric Engineering and Remote Sensing* 61 (8): 1041-1053.
- Dobson, M.C., F.T. Ulaby, and L.E. Pierce. 1995. Land-Cover Classification and Estimation of Terrain Attributes Using Synthetic-Aperture Radar. *Remote Sensing of Environment* 51 (1): 199-214.
- Emerson, C.W., N.S.N. Lam, and D.A. Quattrochi. 1999. Multi-scale fractal analysis of image texture and pattern. *Photogrammetric Engineering and Remote Sensing* 65 (1): 51-61.
- Feral, L., and H. Sauvageot. 2002. Fractal identification of supercell storms. *Geophysical Research Letters* 29 (14): -.
- Foody, G.M. 2002. Status of land cover classification accuracy assessment. *Remote Sensing of Environment* 80 (1): 185-201.
- Franklin, S.E., M.B. Lavigne, M.A. Wulder, and T.M. McCaffrey. 2002. Large-area forest structure change detection: An example. *Canadian Journal of Remote Sensing* 28 (4): 588-592.
- Friedl, M.A., and C.E. Brodley. 1997. Decision tree classification of land cover from remotely sensed data. *Remote Sensing of Environment* 61 (3): 399-409.
- Fung, T., and E. Ledrew. 1987. Application of Principal Components-Analysis to Change Detection. *Photogrammetric Engineering and Remote Sensing* 53 (12): 1649-1658.
- Goodchild, M.F. 1980. Fractals and the Accuracy of Geographical Measures. *Journal of the International Association for Mathematical Geology* 12 (2): 85-98.
- Goodchild, M.F., and D.M. Mark. 1987. The Fractal Nature of Geographic Phenomena. *Annals of the Association of American Geographers* 77 (2): 265-278.
- Goodchild, M.F. 2003. Bits of Geography. Louisiana State University, Baton Rouge.
- Grover, K., S. Quegan, and C.D. Freitas. 1999. Quantitative estimation of tropical forest cover by SAR. *Ieee Transactions on Geoscience and Remote Sensing* 37 (1): 479-490.
- Hammitt, W.E., R.D. Bixler, and T.A. Herrick. 1996. Assessing the forest-based recreation impacts of Hurricane Hugo in South Carolina. *USDA Forest Service Southern Research Station General Technical Report SRS-005*: 336-346.

- Hayes, D.J., and S.A. Sader. 2001. Comparison of change-detection techniques for monitoring tropical forest clearing and vegetation regrowth in a time series. *Photogrammetric Engineering and Remote Sensing* 67 (9): 1067-1075.
- Hook, D.D., M.A. Buford, and T.M. Williams. 1991. Impact of Hurricane Hugo on the South Carolina coastal plain forest. *Journal of Coastal Research* SI8: 291-300.
- Houhoulis, P.F., and W.K. Michener. 2000. Detecting wetland change: A rule-based approach using NWI and SPOT-XS data. *Photogrammetric Engineering and Remote Sensing* 66 (2): 205-211.
- Jaggi, S., D.A. Quattrochi, and N.S.N. Lam. 1993. Implementation and Operation of 3 Fractal Measurement Algorithms for Analysis of Remote-Sensing Data. *Computers & Geosciences* 19 (6): 745-767.
- Kolibal, J., and J. Monde. 1998. Fractal image error analysis. *Computers & Geosciences* 24 (8): 785-795.
- Krzanowski, W.J. 1984. Sensitivity of Principal Components. *Journal of the Royal Statistical Society Series B-Methodological* 46 (3): 558-563.
- Lam, N.S.N. 1990. Description and Measurement of Landsat Tm Images Using Fractals. *Photogrammetric Engineering and Remote Sensing* 56 (2): 187-195.
- Lam, N.S.N., and D.A. Quattrochi. 1992. On the Issues of Scale, Resolution, and Fractal Analysis in the Mapping Sciences. *Professional Geographer* 44 (1): 88-98.
- Lam, N.S.N., and L. De Cola. 1993. *Fractals in geography*. Englewood Cliffs, N.J.: PTR Prentice Hall.
- Lam, N.S.N., H.L. Qiu, and D.A. Quattrochi. 1997. An evaluation of fractal surface measurement methods using ICAMS (Image Characterization and Modeling System). Paper read at ACSM/ASPRS Annual Convention, at Seattle, WA.
- Lam, N.S.N., D.A. Quattrochi, H.L. Qiu, and W. Zhao. 1998. Environmental assessment and monitoring with image characterization and modeling system using multiscale remote sensing data. *Applied Geographic Studies* 2: 77-93.
- Lam, N.S.N., H.L. Qiu, D.A. Quattrochi, and C.W. Emerson. 2002. An Evaluation of Fractal Methods for Characterizing Image Complexity. *Cartography and Geographic Information Science* 29 (1): 25-35.
- Li, X., and A.G.O. Yeh. 1998. Principal component analysis of stacked multi-temporal images for the monitoring of rapid urban expansion in the Pearl River Delta. *International Journal of Remote Sensing* 19 (8): 1501-1518.

- Lillesand, T.M., and R.W. Kiefer. 2004. *Remote sensing and image interpretation*. 5th ed. New York: John Wiley & Sons.
- Lugo, A.E. 2000. Effects and outcomes of Caribbean hurricanes in a climate change scenario. *Science of the Total Environment* 262 (3): 243-251.
- Maeder, J., S. Narumalani, D.C. Rundquist, R.L. Perk, J. Schalles, K. Hutchins, and J. Keck. 2002. Classifying and mapping general coral-reef structure using Ikonos data. *Photogrammetric Engineering and Remote Sensing* 68 (12): 1297-1305.
- Mas, J.F. 1999. Monitoring land-cover changes: a comparison of change detection techniques. *International Journal of Remote Sensing* 20 (1): 139-152.
- Mather, P., and S. Openshaw. 1974. Multivariate Methods and Geographical Data. *Statistician* 23 (3-4): 283-308.
- Mertens, K.C., L.P.C. Verbeke, E.I. Ducheyne, and R.R. De Wulf. 2003. Using genetic algorithms in sub-pixel mapping. *International Journal of Remote Sensing* 24 (21): 4241-4247.
- Mesev, T.V., P.A. Longley, M. Batty, and Y. Xie. 1995. Morphology from Imagery - Detecting and Measuring the Density of Urban Land-Use. *Environment and Planning A* 27 (5): 759-780.
- Michener, W.K., E.R. Blood, K.L. Bildstein, M.M. Brinson, and L.R. Gardner. 1997. Climate change, hurricanes and tropical storms, and rising sea level in coastal wetlands. *Ecological Applications* 7 (3): 770-801.
- Nath, S.K., and P. Dewangan. 2002. Detection of seismic reflections from seismic attributes through fractal analysis. *Geophysical Prospecting* 50 (3): 341-360.
- National Weather Service, Tropical Prediction Center. Costliest US Hurricanes 1900-2000 (unadjusted). 2004. <http://www.nhc.noaa.gov/pastcost.shtml> (last accessed 5/10/2004)
- Peterson, C.J. 2000. Catastrophic wind damage to North American forests and the potential impact of climate change. *Science of the Total Environment* 262 (3): 287-311.
- Qiu, H.L., N.S.N. Lam, D.A. Quattrochi, and J.A. Gamon. 1999. Fractal characterization of hyperspectral imagery. *Photogrammetric Engineering and Remote Sensing* 65 (1): 63-71.
- Quattrochi, D.A., N.S.N. Lam, H.L. Qiu, and W. Zhao. 1997. Image Characterization and Modeling System (ICAMS): A geographic information system for the characterization and modeling of multi-scale remote sensing data. In *Scale in Remote Sensing and GIS*,

ed. Quattrochi, D.A., and M.F. Goodchild, pp. 295-307. Boca Raton, FL: CRC Lewis Publishers.

Ramsey, E.W., D.K. Chappell, and D.G. Baldwin. 1997. AVHRR imagery used to identify hurricane damage in a forested wetland of Louisiana. *Photogrammetric Engineering and Remote Sensing* 63 (3): 293-297.

Ramsey, E.W., and S.C. Laine. 1997. Comparison of landsat thematic mapper and high resolution photography to identify change in complex coastal wetlands. *Journal of Coastal Research* 13 (2): 281-292.

Ramsey, E.W., D.K. Chappell, D.M. Jacobs, S.K. Sapkota, and D.G. Baldwin. 1998. Resource management of forested wetlands: Hurricane impact and recovery mapped by combining Landsat TM and NOAA AVHRR data. *Photogrammetric Engineering and Remote Sensing* 64 (7): 733-738.

Ramsey, E.W., M.E. Hodgson, S.K. Sapkota, and G.A. Nelson. 2001a. Forest impact estimated with NOAA AVHRR and Landsat TM data related to an empirical hurricane wind-field distribution. *Remote Sensing of Environment* 77 (3): 279-292.

Ramsey, E.W., G.A. Nelson, and S.K. Sapkota. 2001b. Coastal change analysis program implemented in Louisiana. *Journal of Coastal Research* 17 (1): 53-71.

Read, J.M. 1999. *Land-cover change detection for the tropics using remote sensing and geographic information systems*. Dissertation, Department of Geography and Anthropology, Louisiana State University, Baton Rouge.

Read, J.M., and N.S.N. Lam. 2002. Spatial methods for characterising land cover and detecting land-cover changes for the tropics. *International Journal of Remote Sensing* 23 (12): 2457-2474.

Rees, W.G. 1992. Measurement of the Fractal Dimension of Ice-Sheet Surfaces Using Landsat Data. *International Journal of Remote Sensing* 13 (4): 663-671.

Ridd, M., N.S.N. Lam, V. Mesev, and others. Mapping and monitoring land cover/land use dynamic of human settlement. In *Remote Sensing of Human Settlements*, ed. Ridd, M., and others, pp. --: John Wiley & Sons.

Roy, D.P., P.E. Lewis, and C.O. Justice. 2002. Burned area mapping using multi-temporal moderate spatial resolution data - a bi-directional reflectance model-based expectation approach. *Remote Sensing of Environment* 83 (1-2): 263-286.

Schmalzer, P.A. 1995. Biodiversity of Saline and Brackish Marshes of the Indian-River Lagoon - Historic and Current Patterns. *Bulletin of Marine Science* 57 (1): 37-48.

Serra, P., X. Pons, and D. Sauri. 2003. Post-classification change detection with data from different sensors: some accuracy considerations. *International Journal of Remote Sensing* 24 (16): 3311-3340.

Shaw, G., and D. Wheeler. 1994. *Statistical techniques in geographical analysis*. 2nd ed. London ; [New York]: David Fulton Publishers.

Singh, A. 1989. Digital Change Detection Techniques Using Remotely-Sensed Data. *International Journal of Remote Sensing* 10 (6): 989-1003.

Sommerfeld, R.A., J.E. Lundquist, and J. Smith. 2000. Characterizing the canopy gap structure of a disturbed forest using the Fourier transform. *Forest Ecology and Management* 128 (1-2): 101-108.

Space Imaging: satellites. <http://www.spaceimaging.com/corporate/sats.htm> (last accessed 05/10/2004)

StOnge, B.A., and F. Cavayas. 1997. Automated forest structure mapping from high resolution imagery based on directional semivariogram estimates. *Remote Sensing of Environment* 61 (1): 82-95.

Thomson, A.G., R.M. Fuller, and J.A. Eastwood. 1998. Supervised versus unsupervised methods for classification of coasts and river corridors from airborne remote sensing. *International Journal of Remote Sensing* 19 (17): 3423-3431.

Tobler, W.R. 1970. Computer Movie Simulating Urban Growth in Detroit Region. *Economic Geography* 46 (2): 234-240.

Townsend, P.A., and S.J. Walsh. 1998. Modeling floodplain inundation using an integrated GIS with radar and optical remote sensing. *Geomorphology* 21 (3-4): 295-312.

Turner, R.K., S. Georgiou, R. Brouwer, I.J. Bateman, and I.J. Langford. 2003. Towards an integrated environmental assessment for wetland and catchment management. *Geographical Journal* 169: 99-116.

USGS Landsat Project. <http://landsat7.usgs.gov/updates.php> (last accessed 5/10/2004)

van den Bos, R. 2003. Restoration of former wetlands in the Netherlands; effect on the balance between CO₂ sink and CH₄ source. *Netherlands Journal of Geosciences-Geologie En Mijnbouw* 82 (4): 325-331.

Weishampel, J.F., J.R. Godin, and G.M. Henebry. 2001. Pantropical dynamics of 'intact' rain forest canopy texture. *Global Ecology and Biogeography* 10 (4): 389-397.

Xiao, K. 2000. *Fractal Compression and Analysis on Remotely Sensed Imagery*. Dissertation, Department of Geography and Anthropology, Louisiana State University, Baton Rouge.

Zhang, Y. 1999. Optimisation of building detection in satellite images by combining multispectral classification and texture filtering. *Isprs Journal of Photogrammetry and Remote Sensing* 54 (1): 50-60.

Zhu, Z.L., L.M. Yang, S.V. Stehman, and R.L. Czaplewski. 2000. Accuracy assessment for the US Geological Survey Regional Land-Cover Mapping Program: New York and New Jersey region. *Photogrammetric Engineering and Remote Sensing* 66 (12): 1425-1435.

Zukowskyj, P.M., M.A. Bussell, C. Power, and R.M. Teeuw. 2001. Quantitative accuracy assessment of contextually filtered classified images. *International Journal of Remote Sensing* 22 (16): 3203-3222.

APPENDIX A: LOCAL FRACTAL OUTPUT FOR DIFFERENT MW SIZES

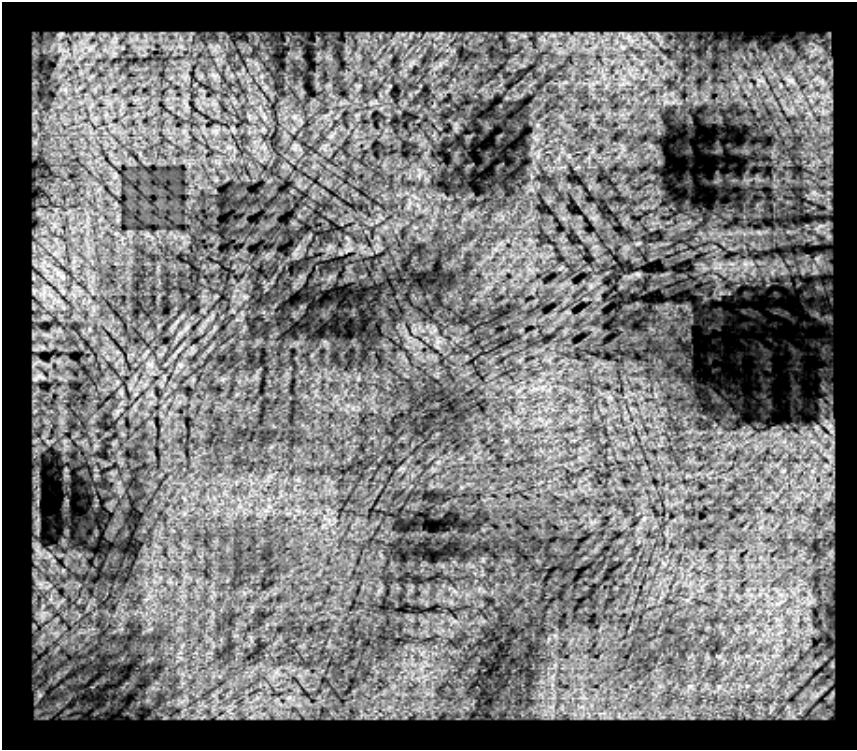


Figure 35: TPSA for 1987 with 33x33 MW with 5 Geometric steps

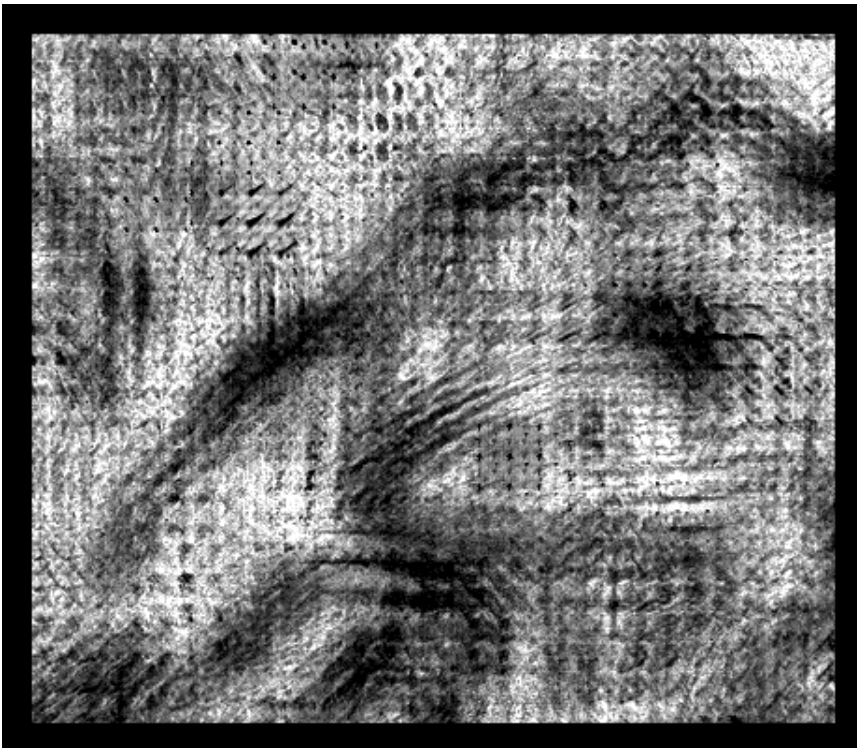


Figure 36: TPSA for 1989 with 33x33 MW with 5 Geometric steps

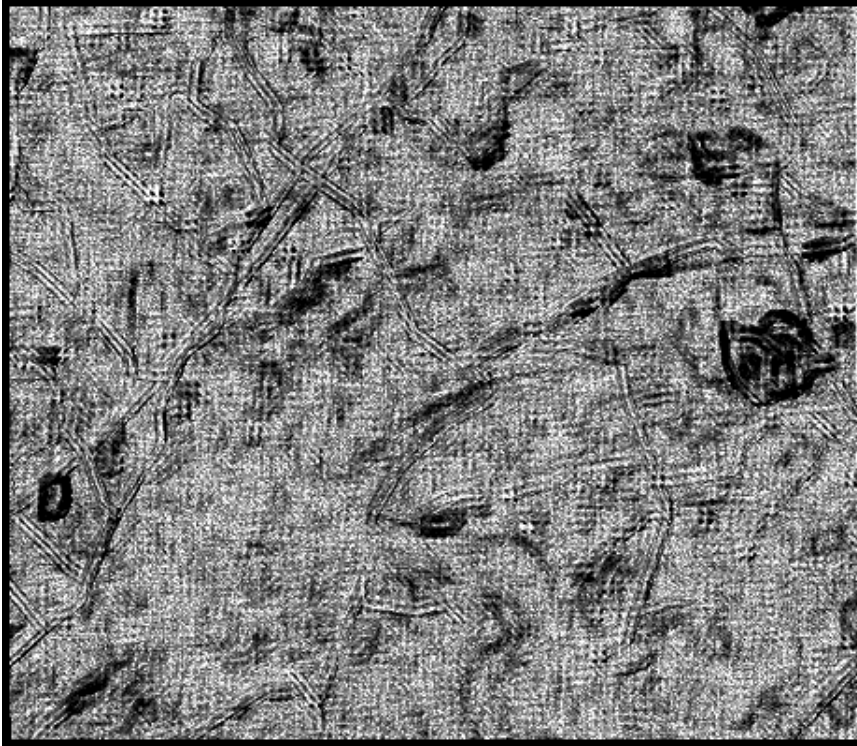


Figure 37: TPSA for 1987 with 9x9 MW with 5 Arithmetic steps

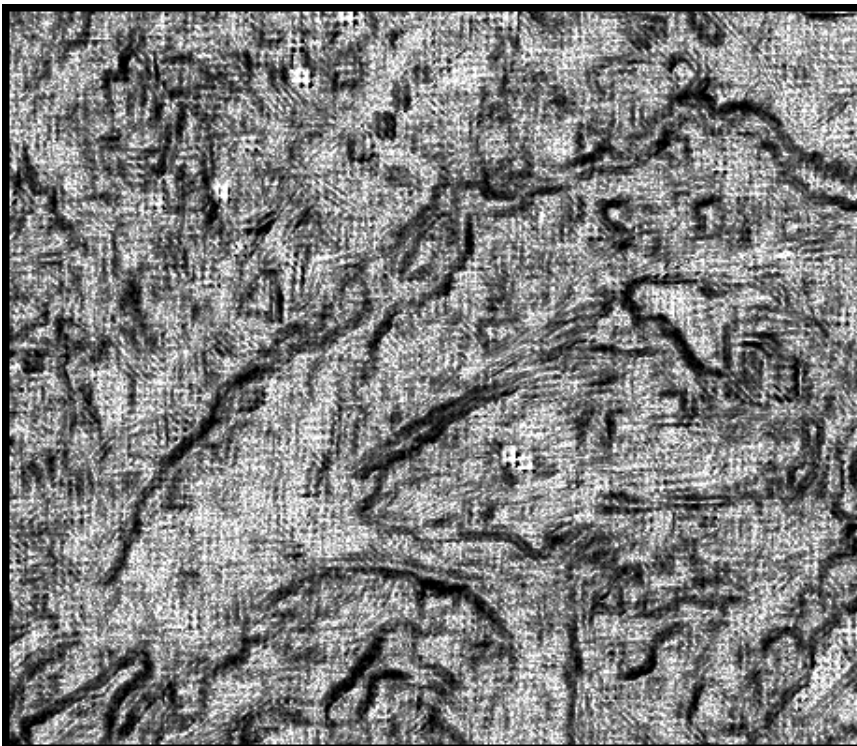


Figure 38: TPSA for 1989 with 9x9 MW with 5 Arithmetic steps

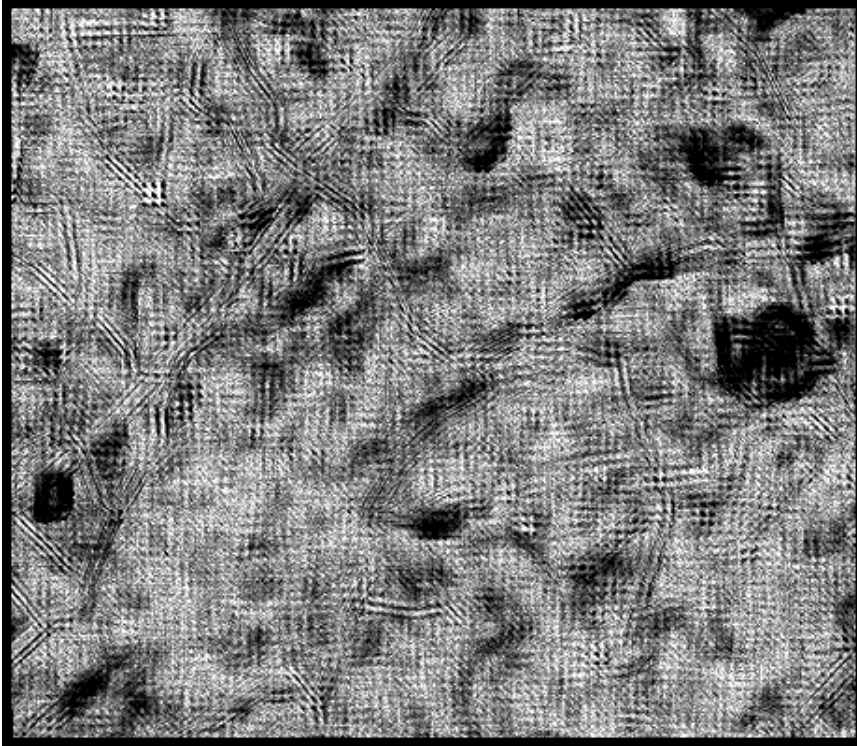


Figure 39: TPSA for 1987 with 11x11 MW with 5 Arithmetic steps

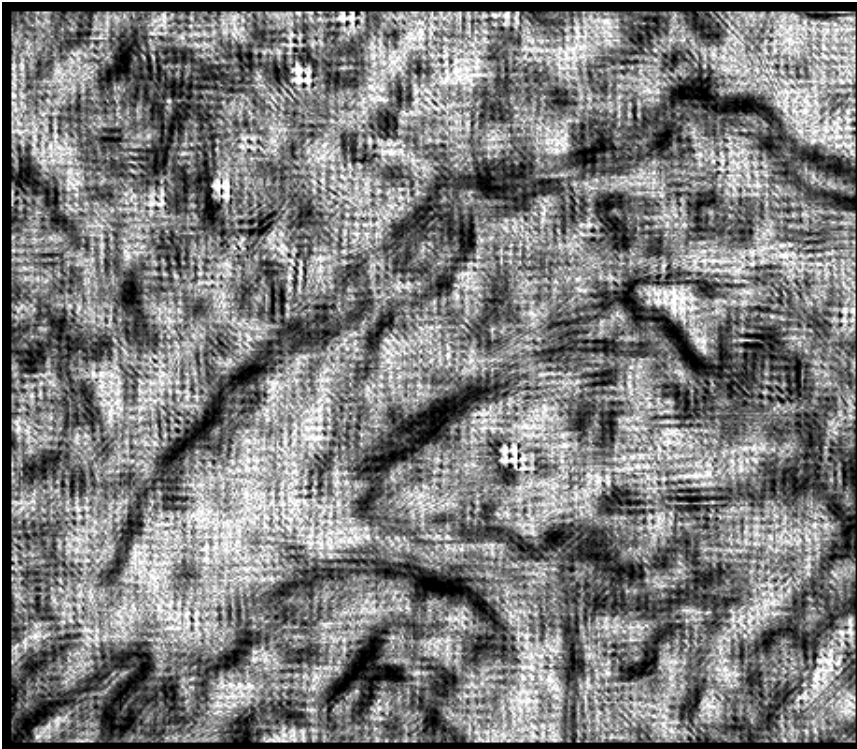


Figure 40: TPSA for 1989 with 11x11 MW with 5 Arithmetic steps

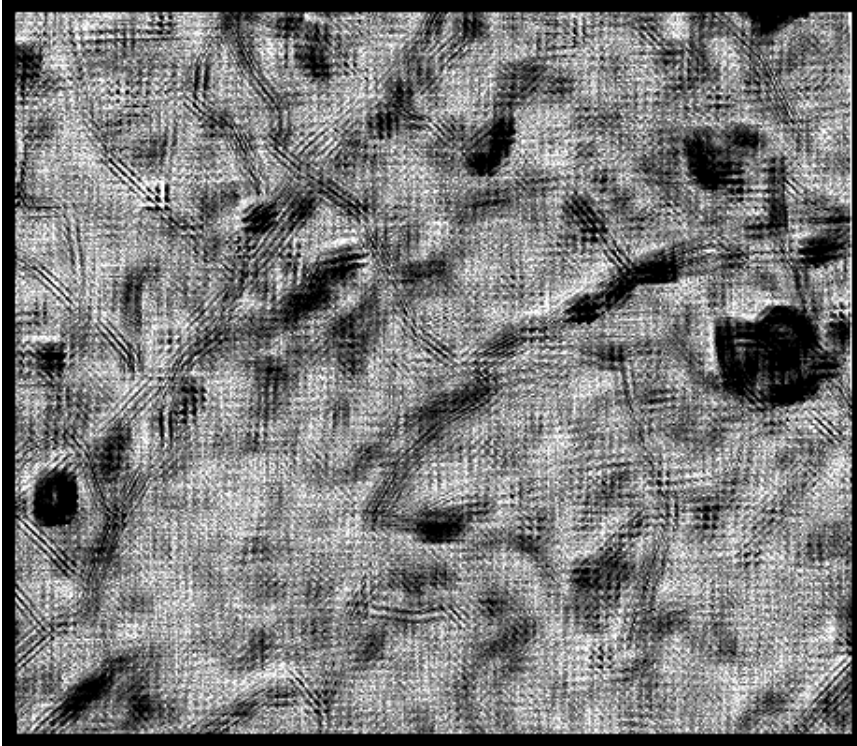


Figure 41: TPSA for 1987 with 15x15 MW with 5 Arithmetic steps

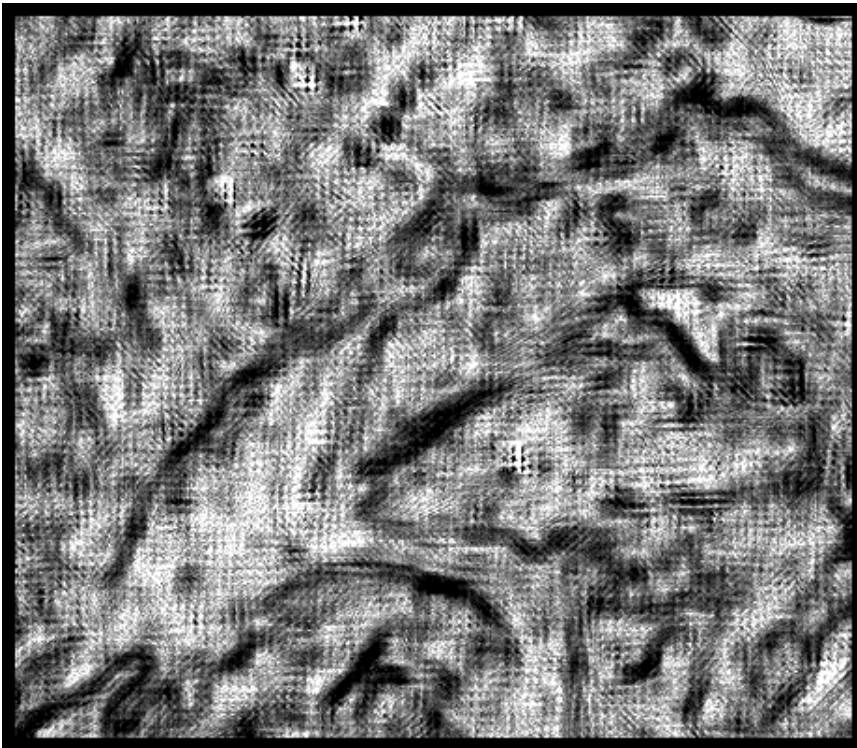


Figure 42: TPSA for 1989 with 15x15 MW with 5 Arithmetic steps

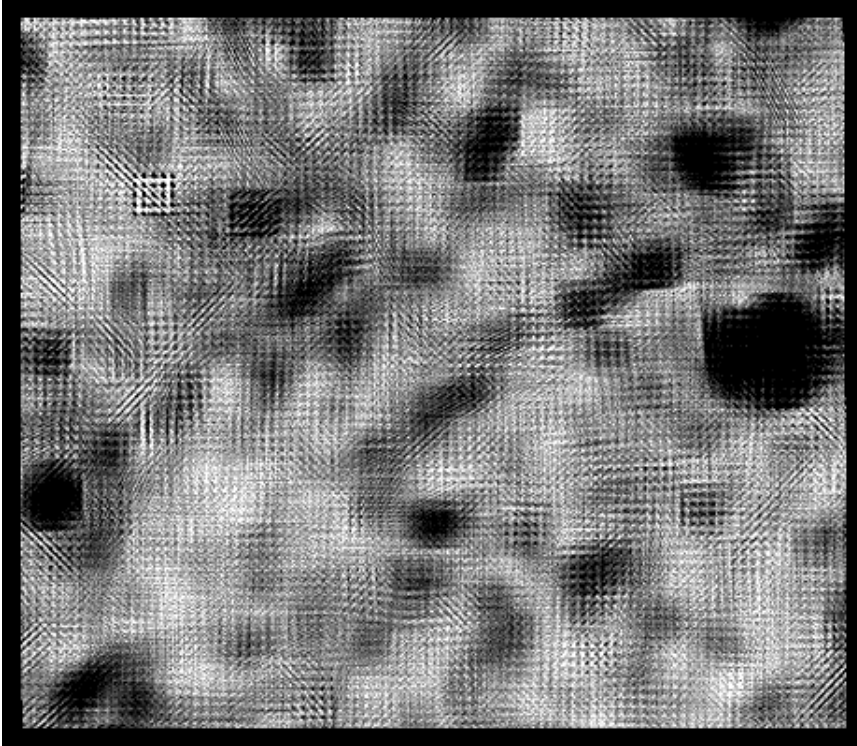


Figure 43: TPSA for 1987 with 21x21 MW with 5 Arithmetic steps

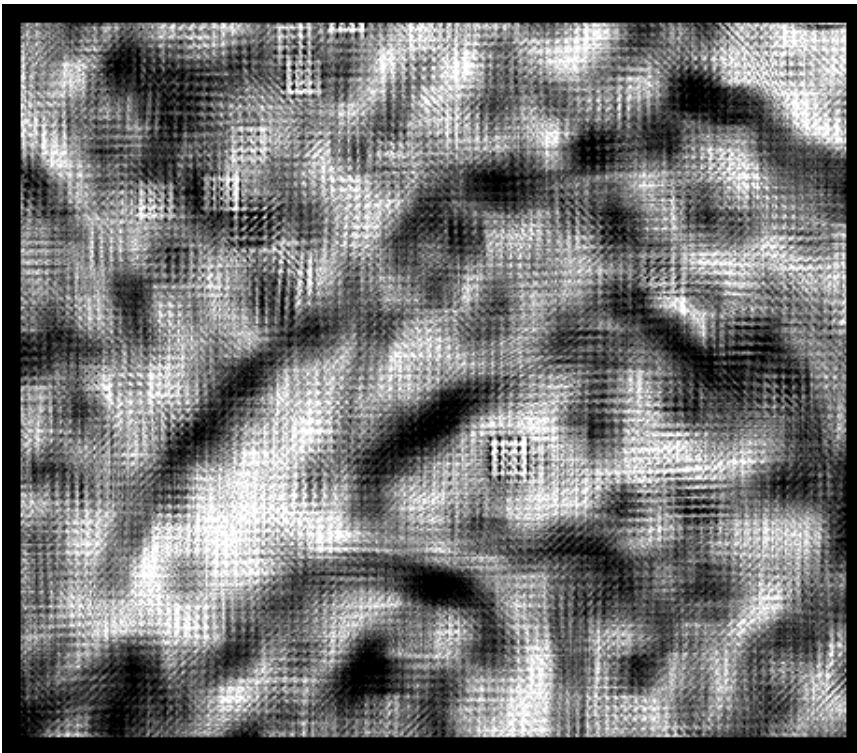


Figure 44: TPSA for 1989 with 21x21 MW with 5 Arithmetic steps

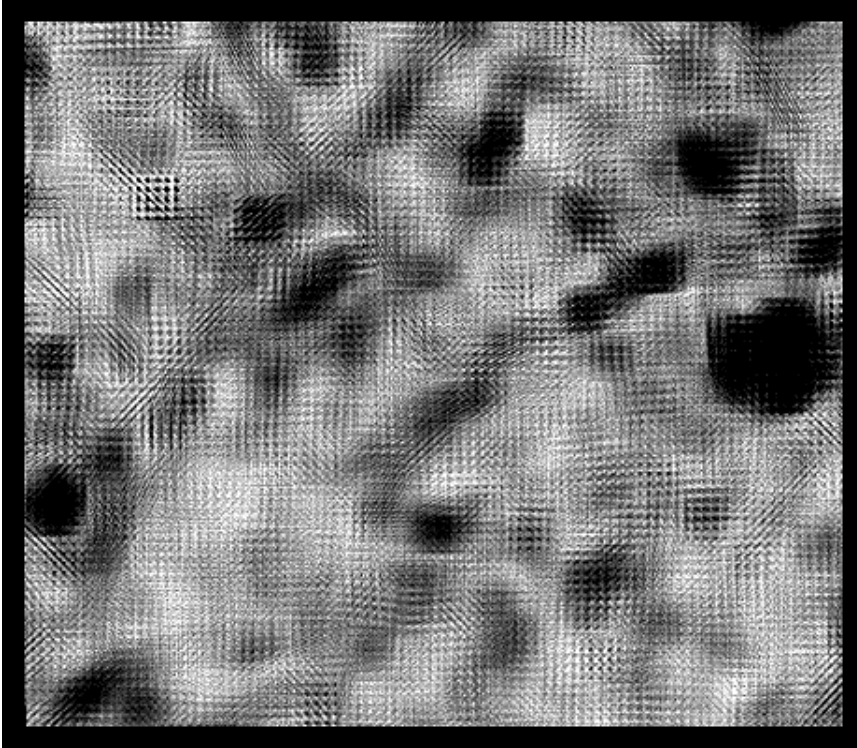


Figure 45: TPSA for 1987 with 25x25 MW with 5 Arithmetic steps

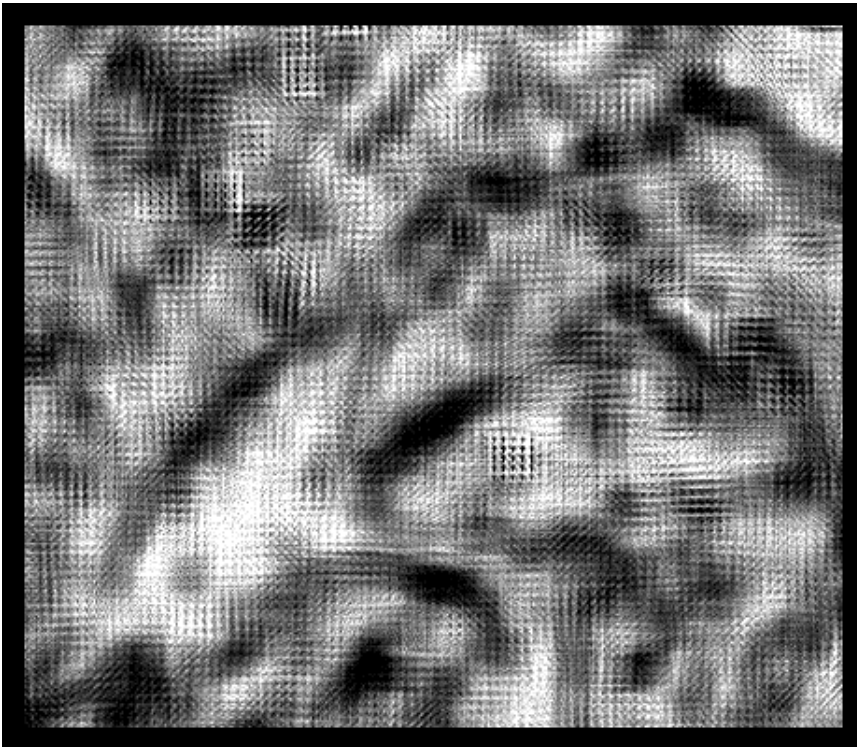


Figure 46: TPSA for 1989 with 25x25 MW with 5 Arithmetic steps

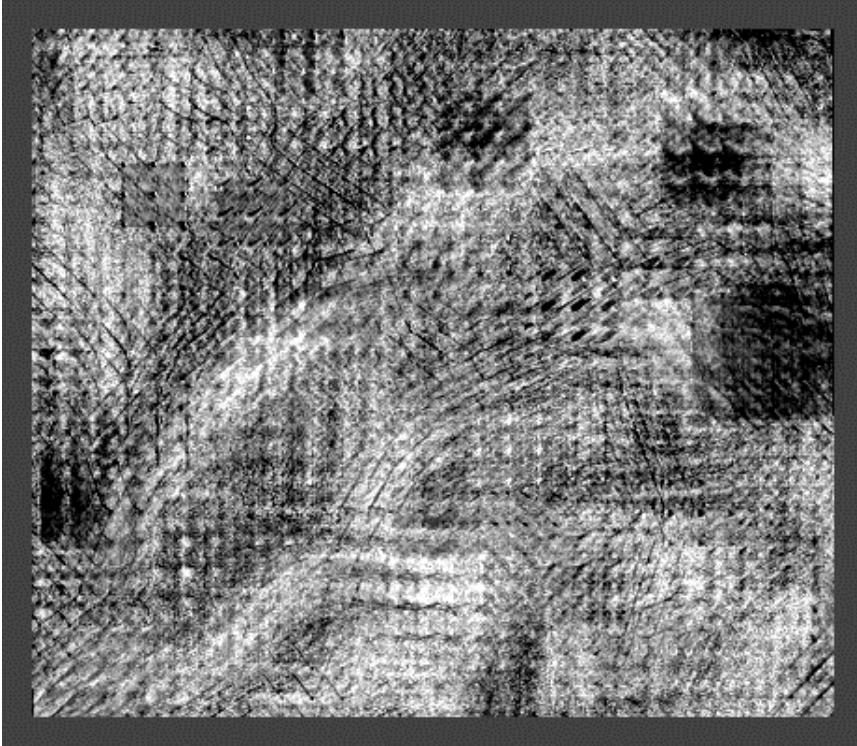


Figure 47: Change detection TPSA with 33x33 MW with 5 Geometric steps

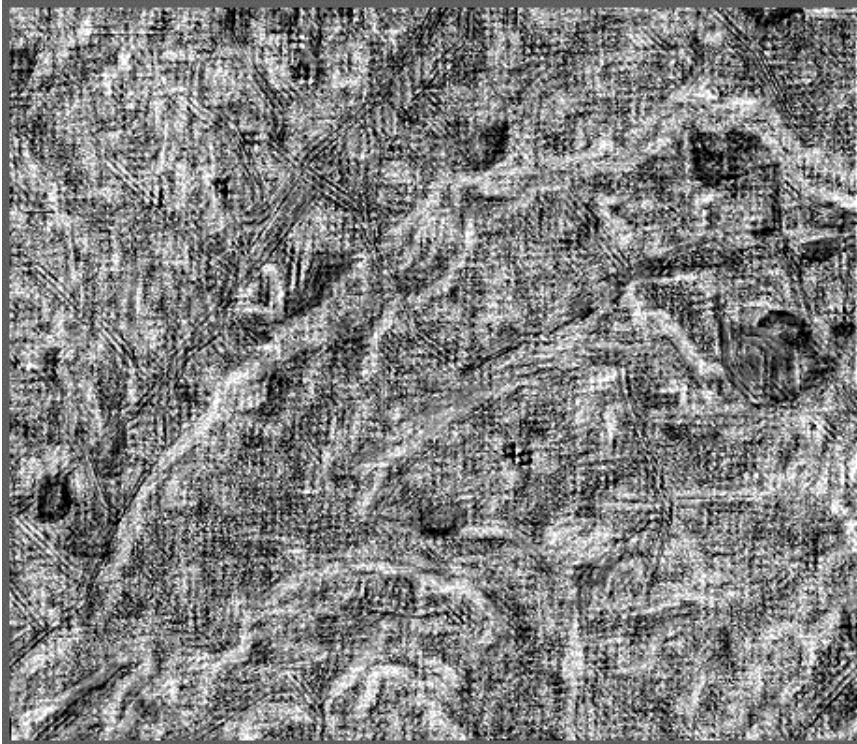


Figure 48: Change detection TPSA with 9x9 MW with 5 Arithmetic steps

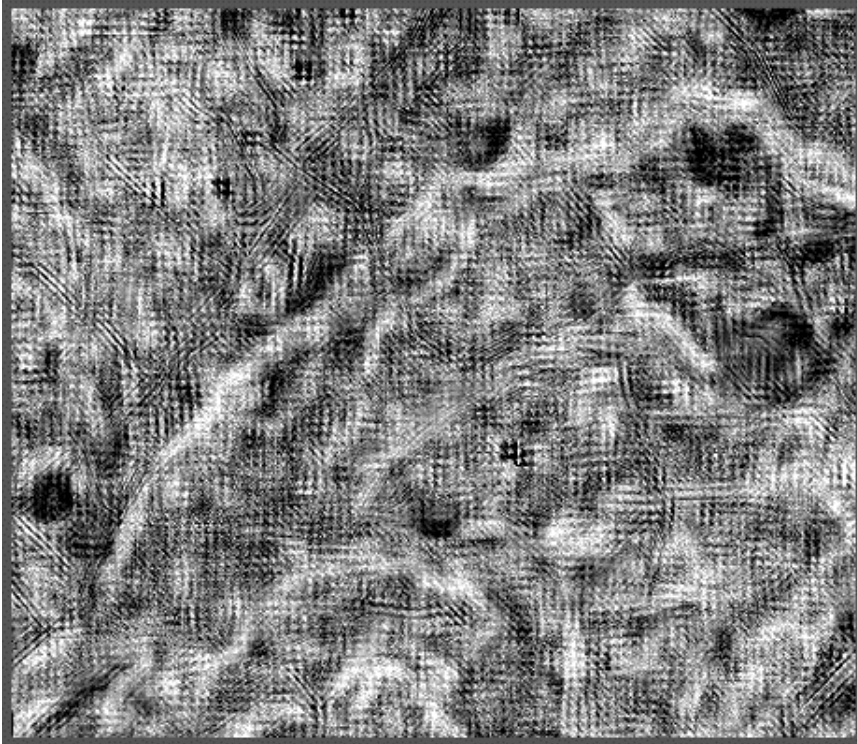


Figure 49: Change detection TPSA with 11x11 MW with 5 Arithmetic steps

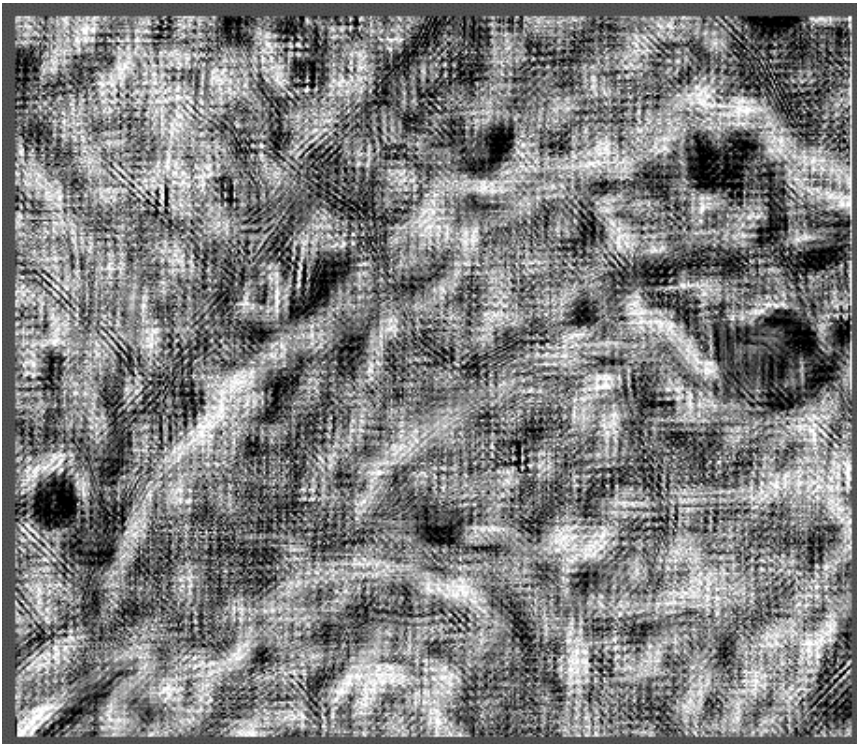


Figure 50: Change detection TPSA with 15x15 MW with 5 Arithmetic steps

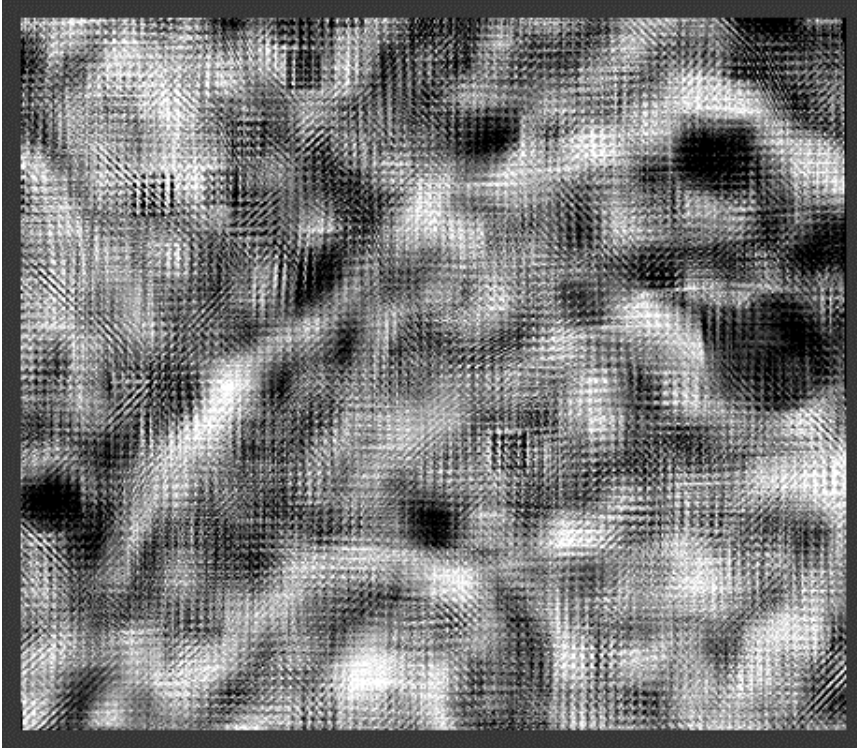


Figure 51: Change detection TPSA with 21x21 MW with 5 Arithmetic steps



Figure 52: Change detection TPSA with 25x25 MW with 5 Arithmetic steps

Table 14: Local fractal dimension D values for the 1987 and 1989 images

Year	Moving window size	Step size	Step increase method	Min D	Max D	Mean D	Std Dev
1987	33x33	5	Geometric	1.95	3.25	2.79	0.12
1987	9x9	5	Arithmetic	2.01	4.6	3.24	0.25
1987	11x11	5	Arithmetic	1.97	3.81	2.92	0.18
1987	15x15	5	Arithmetic	2.09	4.15	3.16	0.18
1987	17x17	5	Arithmetic	2.1	3.45	2.82	0.14
1987	21x21	5	Arithmetic	2.12	3.27	2.77	0.12
1987	25x25	5	Arithmetic	2.25	3.35	2.9	0.12
1989	33x33	5	Geometric	2.01	3.11	2.64	0.11
1989	9x9	5	Arithmetic	1.88	4.57	3.07	0.26
1989	11x11	5	Arithmetic	1.97	4.01	2.75	0.19
1989	15x15	5	Arithmetic	2.18	4	2.99	0.18
1989	17x17	5	Arithmetic	2.16	3.38	2.66	0.13
1989	21x21	5	Arithmetic	2.18	3.13	2.61	0.11
1989	25x25	5	Arithmetic	2.28	3.24	2.73	0.11
1989 - 1987	33x33	5	Geometric	-0.79	0.87	0.15	0.15
1989 - 1987	9x9	5	Arithmetic	-1.68	1.88	0.17	0.35
1989 - 1987	11x11	5	Arithmetic	-1.21	1.27	0.17	0.25
1989 - 1987	15x15	5	Arithmetic	-1.11	1.44	0.17	0.23
1989 - 1987	17x17	5	Arithmetic	-0.71	0.88	0.17	0.18
1989 - 1987	21x21	5	Arithmetic	-0.63	0.77	0.17	0.15
1989 - 1987	25x25	5	Arithmetic	-0.57	0.73	0.17	0.14

Explanation for abnormal low and high D values in the table

The erroneous low and high fractal dimension values i.e., below 2.0 and above 4.0 are caused due to outliers.

APPENDIX B: TABLES USED FOR TASSELED CAP TRANSFORM

Table.1								
L-5 TM Post-Calibration Dynamic Ranges for U.S. Processed NLAPS Data								
Spectral Radiances, Lmin and Lmax in $W/(m^2 \cdot sr \cdot \mu m)$								
Processing Date	From March 1st 1984				After May 5th 2003			
	To May 4th 2003							
Band	Lmin	Lmax	G_{rescale}	B_{rescale}	Lmin	Lmax	G_{rescale}	B_{rescale}
1	-1.52	152.10	0.602431	-1.52	-1.52	193.0	0.762824	-1.52
2	-2.84	296.81	1.175100	-2.84	-2.84	365.0	1.442510	-2.84
3	-1.17	204.30	0.805765	-1.17	-1.17	264.0	1.039880	-1.17
4	-1.51	206.20	0.814549	-1.51	-1.51	221.0	0.872588	-1.51
5	-0.37	27.19	0.108078	-0.37	-0.37	30.2	0.119882	-0.37
6	1.2378	15.303	0.055158	1.2378	1.2378	15.303	0.055158	1.2378
7	-0.15	14.38	0.056980	-0.15	-0.15	16.5	0.065294	-0.15

(Source: Chander and Markham 2003)

Table-2				
TM Solar Exoatmospheric Spectral Irradiances				
Units:	ESUN = W/(m ² .um)			
Model :	Neckel and Labs		Chance Spectrum CHKUR	
Band	Landsat 4	Landsat 5	Landsat 4	Landsat 5
1	1958	1957	1957	1957
2	1828	1829	1825	1826
3	1559	1557	1557	1554
4	1045	1047	1033	1036
5	219.1	219.3	214.9	215.0
7	74.57	74.52	80.72	80.67

(Source: Chander and Markham 2003)

Table-3					
Earth-Sun Distance in Astronomical Units					
DOY	Distance	DOY	Distance	DOY	Distance
1	0.9832	121	1.0076	242	1.0092
15	0.9836	135	1.0109	258	1.0057
32	0.9853	152	1.014	274	1.0011
46	0.9878	166	1.0158	288	0.9972
60	0.9909	182	1.0167	305	0.9925
74	0.9945	196	1.0165	319	0.9892
91	0.9993	213	1.0149	335	0.986
106	1.0033	227	1.0128	349	0.9843
DOY- Day of Year (Julian Day)				365	0.9833

(Source: Chander and Markham 2003)

Table 4		
TM Thermal Band Calibration Constants		
Units	W/(m².sr.um)	Kelvin
Constant	K1	K2
Landsat 4	671.62	1284.30
Landsat 5	607.76	1280.58

(Source: Chander and Markham 2003)

APPENDIX C: TASSELED CAP TRANSFORM EQUATIONS

Tasseled Cap transformation equations for Landsat 4

$$\text{Brightness} = 0.3037 * \text{TM1} + 0.2793 * \text{TM2} + 0.4743 * \text{TM3} + 0.5585 * \text{TM4} + 0.5082 * \text{TM5} + 0.1863 * \text{TM7}$$

$$\text{Greenness} = -0.2848 * \text{TM1} - 0.2435 * \text{TM2} - 0.5436 * \text{TM3} + 0.7243 * \text{TM4} + 0.0840 * \text{TM5} - 0.1800 * \text{TM7}$$

$$\text{Wetness} = 0.1509 * \text{TM1} + 0.1973 * \text{TM2} + 0.3279 * \text{TM3} + 0.3406 * \text{TM4} - 0.7112 * \text{TM5} - 0.4572 * \text{TM7}$$

Tasseled Cap transformation equations for Landsat 5

$$\text{Brightness} = 0.2909 * \text{TM1} + 0.2493 * \text{TM2} + 0.4806 * \text{TM3} + 0.5568 * \text{TM4} + 0.4438 * \text{TM5} + 0.1706 * \text{TM7}$$

$$\text{Greenness} = -0.2728 * \text{TM1} - 0.2174 * \text{TM2} - 0.5508 * \text{TM3} + 0.7221 * \text{TM4} + 0.0733 * \text{TM5} - 0.1648 * \text{TM7}$$

$$\text{Wetness} = 0.1446 * \text{TM1} + 0.1761 * \text{TM2} + 0.3322 * \text{TM3} + 0.3396 * \text{TM4} - 0.6210 * \text{TM5} - 0.4186 * \text{TM7}$$

(Source: ERDAS Imagine 8.7 software, 2004)

VITA

Amit Kulkarni was born in Thane, India. His parents were refreshingly different and forced him to think independently from a very young age, which has helped him whenever he has been up the creek without a paddle. After a very disturbing period in school, he attended St. Xavier's Technical Institute where he managed to learn how to get along with people. He then wormed his way into the College of Engineering, Pune, for a Bachelor degree of Engineering in Electronics and Telecommunication where he learnt all about Jackie Chan, Jet Li, and developed a passion for Chinese styles of self-defense techniques.

After he was threatened to be kicked out from home, he finally got a series of programming jobs each more interesting than the previous one. Finally, he decided to pursue his dream of earning the degree of Master of Science in an earth science field by enrolling in geography at Louisiana State University. After a painful adjustment to an academic life from a professional one and some more unmentionable pitfalls he is glad he is in one piece and about to graduate. He would like to remind people about this quote from Louis L'Amour:

“No one can get an education, for of necessity education is a continuing process.”